Joana Formigal Tavares

Study of the factors that influence proteotoxic stress in yeast

Estudo dos factores que influenciam o stress proteotóxico em levedura

Universidade de Aveiro Secção Autónoma de Ciências da Saúde
2012

Joana Formigal Tavares

Study of the factors that influence proteotoxic stress in yeast

Estudo dos factores que influenciam o stress proteotóxico em levedura

Dissertação apresentada à Universidade de Aveiro para cumprimento dos requisitos necessários à obtenção do grau de Mestre em Biomedicina Molecular, realizada sob a orientação científica da Doutora Gabriela Maria Ferreira Ribeiro de Moura, Investigadora Auxiliar do CESAM, Universidade de Aveiro, e a co-orientação científica do Doutor Manuel António da Silva Santos, Professor Associado da Universidade de Aveiro

Apoio financeiro da FCT e do Programa Operacional Temático Factores de Competitividade (COMPETE), comparticipado pelo fundo comunitário europeu FEDER

o júri / the jury

presidente / president

Professor Doutor Nélson Fernando Pacheco da Rocha
Professor Catedrático, Universidade de Aveiro

vogais / examiners committee

Professora Doutora Margarida Alexandra Vaz Caldeira
Professora Auxiliar Convidada, Centro de Neurociências e Biologia Celular da Universidade de Coimbra

Doutora Gabriela Maria Ferreira Ribeiro de Moura
Investigadora Auxiliar, CESAM - Centro de Estudos do Ambiente e do Mar da Universidade de Aveiro

Professor Doutor Manuel António da Silva Santos
Professor Associado, Universidade de Aveiro

agradecimentos /
acknowledgements

À Doutora Gabriela e ao Professor Manuel por me terem dado a oportunidade de trabalhar no laboratório de Biologia do RNA, pelo acompanhamento, pela partilha do saber e pela motivação.

A todos os elementos do laboratório de Biologia do RNA, que tão bem me acolheram, em especial ao João, Violeta e Laura. À Sofia e à Rita Araújo pela amizade e pela partilha dos bons e maus momentos dentro e fora do laboratório.

Aos responsáveis e professores dos cursos de Ciências Biomédicas e Biomedicina Molecular da Universidade de Aveiro pela partilha de conhecimentos e envolvimento com os alunos.

Aos biomédicos por todos os momentos de trabalho e diversão passados em Aveiro, em especial à Carina, ao Pimpas, ao Roberto e à Maria.

À Sofia, ao Renato, ao Luís, ao Ilan, ao Boss e à Daniela pela amizade ao longo destes anos, mesmo com a distância.

À Catarina, à Inês, à Chita, à Andreia Luís e ao Badaró pela amizade, pelo apoio e pelos momentos mais marcantes vividos em Aveiro.

Aos meus pais pelo amor, apoio e exemplo. A eles agradeço tudo o que sou hoje.

Palavras Chave

arrays de células, erros de tradução, tRNA, agregação proteica, resposta ao stress, stress proteotóxico.

Resumo

O stress proteotóxico resulta da acumulação de proteínas agregadas que destabilizam a homeostase do proteoma (proteostase). As células respondem à agregação de proteínas, induzindo e aumentando a expressão de chaperones moleculares, que auxiliam as proteínas a re-adquirir o seu estado nativo, do sistema ubiquitina-proteassoma e autofagia, que degradam estas proteínas. Disfunção destas respostas celulares conduz frequentemente a doença.

Para clarificar a biologia do stress proteotóxico, expusemos células de levedura a 32 condições fisiológicas diferentes e, utilizámos uma metodologia que destabiliza o proteoma através da indução de erros de tradução do mRNA. Estes estudos demonstraram que várias substâncias químicas (como cloreto de cálcio, cloreto de cádmio, cloreto de lítio, cloreto de magnésio, trióxido de crómio, geneticina, menadiona e temperatura elevada) e erros ribossomais (incorporação incorrecta de serina nos codões dos restantes aminoácidos) induzem a formação de agregados proteicos.

Os estudos mencionados acima foram realizados recorrendo a *arrays* de células. Os *arrays* de células são uma nova tecnologia com um número crescente de aplicações, nomeadamente na identificação de determinantes genéticos de doenças e nas relações dinâmicas entre células e o ambiente que as rodeia. São também uma ferramenta valiosa em estudos de análise de fenomas. Neste estudo, otimizámos esta nova técnica no nosso laboratório, de modo a facilitar os estudos do stress proteotóxico em curso no nosso laboratório.

Keywords cell-arrays, mistranslation, tRNA, protein aggregation, stress response, proteotoxic stress.

Abstract

Proteotoxic stress is associated with the accumulation of aggregated proteins in the cell. Cells respond to protein aggregation by inducting and up-regulating the expression of molecular chaperones, which help refold other proteins back into their native state, the ubiquitin-proteasome system and autophagy that lead to their degradation. Malfunction of these cellular responses leads frequently to disease.

In order to clarify the biology of proteotoxic stress, we have exposed yeast cells to 32 physiological conditions and destabilized the proteome through ribosomal errors. The data show that many chemical stressors (namely, calcium chloride, cadmium chloride, chromium trioxide, geneticine, lithium chloride, magnesium chloride, menadione, and high temperature) and protein synthesis errors (misincorporation of serine at 19 non-cognate codons) induce the formation of protein aggregation.

The above studies were carried out using cell-arrays. This new type of arrays has an increasing number of applications, namely in the identification of genetic determinants of disease and in the study of the dynamic relationship between cells and environment. It also has important advantages to study the phenome. In order to advance our knowledge of proteotoxic stress we have optimized this new technique in our laboratory during this MsC thesis project.

Contents

Abbreviations

A: Adenine

aaRS: Aminoacyl tRNA synthetase

aa-tRNA: Aminoacyl-tRNA

A-site: Aminoacyl-tRNA site

ATP: Adenosine 5'-triphosphate

bp: Base pair

C: Cytosine

cDNA: Complementary DNA

DNA: Deoxyribonucleic acid

DTT: Dithiothreitol

EF: Elongation factor

ER: Endoplasmatic reticulum

E-site: Exit-tRNA site

G: Guanine

GDP: Guanosine diphosphate

GFP: Green fluorescent protein

GTP: Guanosine triphosphate

HSF: Heat shock factor

HSP: Heat shock protein

HSR: Heat shock response

IF: Initiation factor

LeuRS: Leucyl tRNA synthetase

MM: Minimal medium

mQ: MilliQ

mRNA: Messenger RNA

OD: Optical density

PBS: Phosphate buffered saline

PCR: Polymerase chain reaction

PQC: Protein quality control

P-site: Peptidyl-tRNA site

RNA: Ribonucleic acid

RNAi: RNA interference

ROS: Reactive oxygen species

rpm: Revolutions per minute

rRNA: Ribosomal RNA

SDM: Site directed mutagenesis

SDS: Sodium dodecyl sulfate

SerRS: Seryl tRNA synthetase

siRNA: Small interfering RNA

T: Thymine

TF: Transcription factor

tRNA: Transfer RNA

tRNAi: Initiator transfer tRNA

U: Uracil

UPS: Ubiquitin proteasome system

UTR: Untranslated region

YPD: Rich medium

List of Figures

List of Tables

Chapter 1

Introduction

This introduction is divided in three main topics, namely protein biosynthesis, protein folding and misfolding and cell-arrays technology. It provides an overview of the main processes involved in proteotoxic stress with a particular emphasis on protein biosynthesis. Protein misfolding and aggregation is generally considered as being a post-translational process, but it may also result from errors that occur during protein synthesis and we provide an overview of the types of translational errors that may result in increased protein aggregation.

1.1 Biosynthesis of proteins

Translation is divided into four main steps: initiation, elongation, termination and recycling. The goal of initiation is to position the ribosome at the start of the coding region, i. e., at the initiation codon of the mRNA with a methionyl initiator tRNA bound in the peptidyl (P) site. Elongation of the peptide chain then begins with the selection of tRNAs in the acceptor (A) site, and then the ribosome catalyzes the formation of a peptide bond. The tRNAs and mRNA are translocated, so that the next codon can be moved into the A-site. Termination occurs when a stop codon (UAA, UAG, or UGA) arrives at the active ribosomal A-site and the finished peptide is then released from the ribosome. Finally, recycling involves the separation of the ribosomal subunits, releasing the mRNA and the deacylated tRNA [38, 39]. These fundamental events sometimes differ between bacteria, eukaryote, and archaea [39].

The ribosomes are critical for protein synthesis. They consist of two subunits: the small subunit (40S) and the large subunit (60S) (in eukaryotes) [70], and have three decoding sites, namely A-, P- and E- (exit) sites. The A- and P-sites participate in aminoacyl-tRNA (aa-tRNA) selection and translocation. The E-site is an exit site for deacylated tRNA. Additionally, the occupation of the E-site can change allosterically the affinity of the A-site during selection of in-coming aa-tRNAs, so it influences decoding fidelity [58, 88]. The ribosome experiments two conformational states during translation: pre-translocational state and post-translocational state. The first one is characterized by high affinity for tRNA in A- and P-sites and low affinity in the E-site, while in the second step the P- and E-sites have high affinity for tRNA and the A-site has low affinity. Interestingly, transitions from one state to the other occur when the previous low affinity binding site is occupied [23].

Gene expression is regulated at different levels, namely transcription of the gene into mRNA, processing of the mRNA, transport of the mRNA from the nucleus to the cytoplasm, binding of the mRNA to ribosomes, initiation, elongation and termination of translation,

and processing of proteins to their final and functional conformation [50]. At the translation level, the main control points is the initiation step, but elongation and termination are also important.

1.1.1 Translation

Initiation

During transcription in the nucleus, mRNA looses its introns and acquires a cap structure at its 5'-end and a poly(A)-tail at the 3'-end. The mature strand of RNA can be divided into three domains, namely the 5'-untranslated region (5'-UTR), the region encoding the protein (ORF − open reading frame), and the 3'-UTR or 3'-tail [38].

The initiation pathway begins when the eIF2·GTP·Met-tRNAi ternary complex is assembled. The formation of this complex is assisted by eIF2B, in order to recycle the eIF2·GDP complex after each initiation cycle: eIF2 is a G protein and has higher affinity for GDP than GTP [39]. After the formation of eIF2·GTP·Met-tRNAi ternary complex, it binds to the small ribosomal subunit (40S), forming the 43S complex. The formation of this complex is mainly assisted by eIF1, eIF1A and eIF3 [12, 39]. The Met-tRNAi binds to the P-site of the ribosome, in contrast to the delivery of specific aa-tRNA to the A-site of the ribosome during elongation [13].

On the 5'-cap of the mRNA is assembled the eIF4F complex that opens secondary structures present in the 5'-UTR. Additionally, eIF4F, together with the poly(A)-binding protein (PAB) bound to the 3'-poly(A) tail and eIF3, bring mRNA onto the 43S complex. This complex scans the message in the 5' to 3' direction until the initiation codon is found, with the help of eIF1 and eIF1A. As soon as the 43S complex finds the proper start AUG codon on the mRNA it stops due to the interaction of the AUG codon with the anticodon of the initiator tRNA in the ternary complex. This leads to the hydrolysis of GTP by eIF2, facilitated by the GTPase-activating protein (GAP) eIF5. Then, eIF2·GDP releases the Met-tRNAi into the P-site of the 40S subunit and dissociates from the complex, as well as eIF1, eIF1A, eIF3 and eIF5 [39]. Simultaneously, eIF5B·GTP binds to the complex, and facilitates the binding of the large ribosomal subunit (60S) (containing the peptidyl-transferase active site) to the 40S·Met-tRNAi·mRNA complex, generating a translationally competent ribosome (Figure 1.1) [13, 39]. This event is the signal for GTP hydrolysis by eIF5B, followed by its dissociation from the complex, due to the low affinity of the GDP-bound form for the ribosome [39].

Elongation

Translation elongation uses a highly conserved machinery across the three kingdoms of life. The elongation of the peptide chain begins with a peptidyl-tRNA in the P-site of the ribosome. An aminoacyl-tRNA is transferred from a ternary complex to the elongation factor (eEF1A) [39]. This eEF1A·GTP·aa-tRNA ternary complex binds to the A-site of the ribosome [1, 39]. In order to ensure that only the cognate tRNA is selected for the next stage of elongation the codon-anticodon base pairing between the mRNA and the tRNA are checked and conformational changes in the decoding center of the small ribosomal subunit and GTP hydrolysis by eEF1A provide additional proofreading of that interaction. In the first step, codon-anticodon base pairing induces a change in the conformation of three bases in the 40S subunit in order to interact with the mRNA-tRNA duplex. This interaction is likely to activate eEF1A's GTPase activity, resulting in the release of the aminoacyl-tRNA into de A-site by

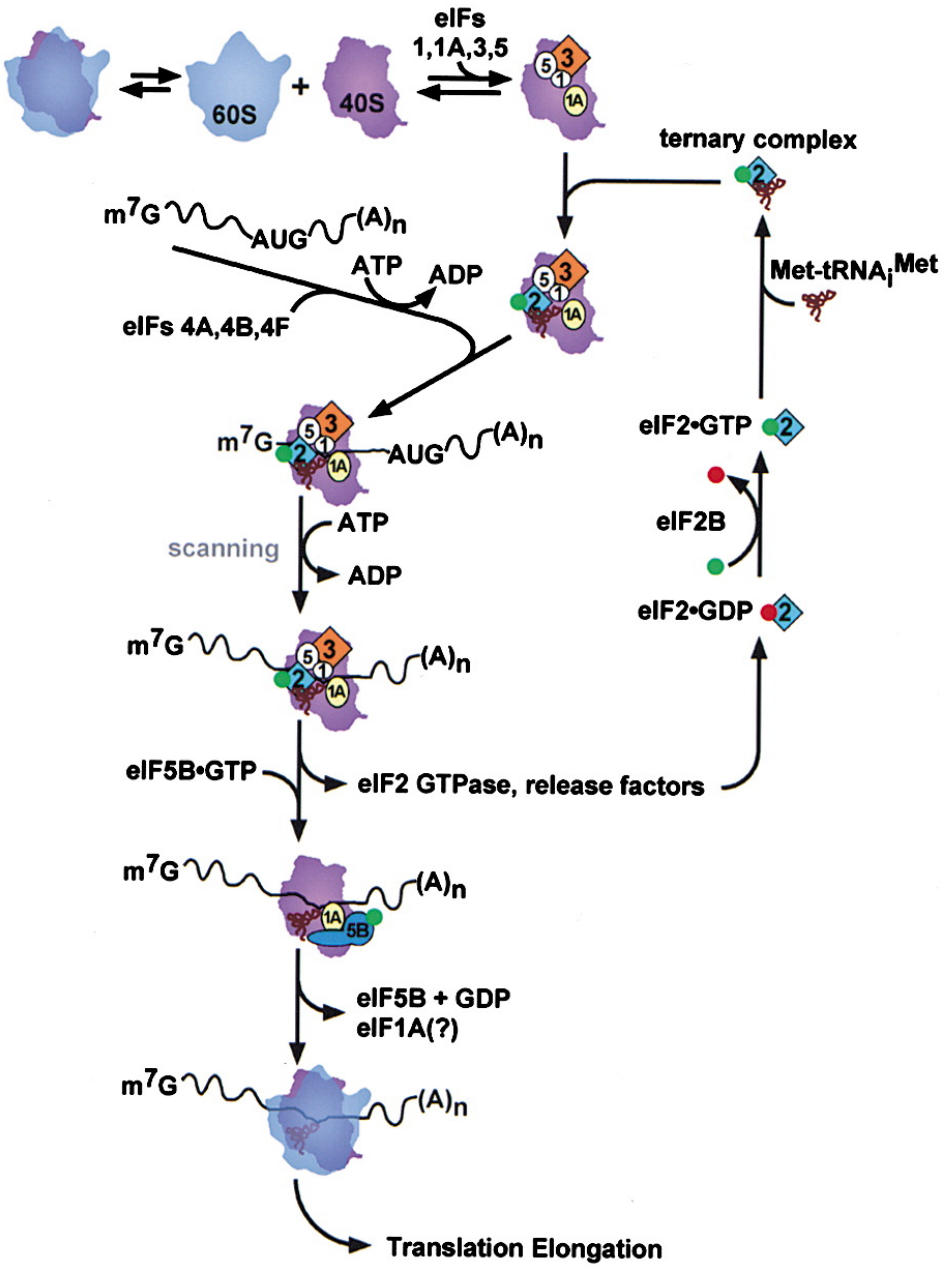

Figure 1.1: **Pathway of translation initiation in eukaryotes.** Red dots represent GDP and green dots are GTP. More details described in the text. Adapted from [13].

eEF1A·GDP [1, 39]. Then, the formation of a peptide bond between the incoming amino acid and the peptidyl-tRNA is catalysed by the ribosomal peptidyl transferase center of the 60S subunit. As a result a deacylated tRNA in a hybrid state is formed with its anticodon in the P-site of the 40S subunit and its acceptor terminal in the E-site of the 60S subunit of the ribosome. At the same time, the peptidyl-tRNA is in a similar hybrid conformation with its anticodon in the A-site of the small subunit and its acceptor terminal in the P-site of the large subunit. For progression of elongation, this complex is translocated so that the

deacylated tRNA is in the E-site only, the peptidyl-tRNA in the P-site only, and the mRNA moves three nucleotides downstream to place the next codon of the mRNA into the A-site. These steps require elongation factor 2, which is responsible for the hydrolysis of GTP that facilitates translocation. After the hydrolysis of GTP and the discharge of aminoacyl-tRNA from the ribosome, eEF1A·GDP is also released and recycled to its GTP-bound form, mediated by eEF1B (a multifactor complex), in order to participate in further cycles of polypeptide elongation. This process is repeated until a stop codon enters the A-site, leading to the beginning of the termination factors [39].

Termination

As referred above, the presence of a stop codon in the ribosomal A-site leads to the termination of translation. Stop codons presented in the A-site are decoded by class 1 release factors (eRF1, in eukaryotes). Class 2 release factors (eRF3, in eukaryotes) are GTPases that stimulate the activity of eRF1 bound to the stop codon. In response to the activity of class 1 release factors, the peptidyl transferase center of the ribosome catalyses the hydrolysis of the ester bond, linking the polypeptide chain to the P-site tRNA, which results in the release of the completed polypeptide [39].

Recycling

The last stage of translation is the recycling of the ribosomal subunits, for another cycle of translation. In eukaryotes, ribosome recycling requires eIF3, which binds to the small ribosomal subunit opposite to the interface. In this way, eIF3 induces a conformational change in the 40S subunit, increasing the rate of subunit dissociation and lowering the rate of association. Another model for ribosomal recycling posits that termination and recycling may not discharge the 40S subunit back into the cytoplasm, instead this subunit may be transferred over or across the poly(A)-tail back to the 5'-end of the mRNA, mediated by the interaction of eRF3 and PAB with initiation factor eIF4G. These events facilitate the reinitiation of translation eliminating the need of the first initiation event [39].

1.1.2 tRNA and aminoacyl-tRNA synthetases

Transfer RNAs molecules have a fundamental role in protein synthesis. Indeed, tRNAs decode codons (interact with mRNAs) and carry amino acids into the ribosome. Structurally, tRNAs can be subdivided into families, according to the amino acid that they carry. The tRNA species that are charged with the amino acid are called isoacceptor tRNAs [25, 41].

The secondary structure of tRNAs is highly conserved and form a cloverleaf structure (Figure 1.2) [25, 41]. It consists of an acceptor stem, three stem-loops (or arms) and a variable-loop, that are stabilized by hydrogen bonds between the stems. The stem-loops are the dihydrouridine (D) loop, the anticodon-loop, and the TΨC-loop. Additionally, there are specific nucleotides that are conserved in most tRNA species, and serve to stabilize tertiary interactions that originate a three-dimensional structure, similar in all tRNA species. The 3'-end of tRNAs always ends up with the sequence CCA. The acceptor stem is formed by the 5'- and 3'-ends of the molecule, with seven base pairs followed by an overhanging unpaired nucleotide at position 73 and the CCA. In protein synthesis, the amino acid is attached to the ribose of the 3'-terminal A residue. The D-loop (8-11 bases) is on the left side, following a stem of 3-4 base pairs. On the right side of the cloverleaf there's the 7-base TΨC-loop or T-loop,

following a 5 base pair stem. Below the T-loop there is the variable-loop, which is the main source of variability in tRNA structure and may contain 4 to 21 (or even more) bases. Finally, at the bottom of the cloverleaf, following a 5 bp stem, is the anticodon-loop with 7 bases. The anticodon, i. e. a 3-base sequence complementary to the codon that it decodes, is located in the middle of the loop. The pairing of codon-anticodon occurs in an antiparallel fashion, meaning that the 5'-anticodon base in the tRNA (nucleotide 34) pairs with the 3'-codon base in the mRNA, and the 3'-anticodon base (nucleotide 36) with the 5'-codon base [25, 75].

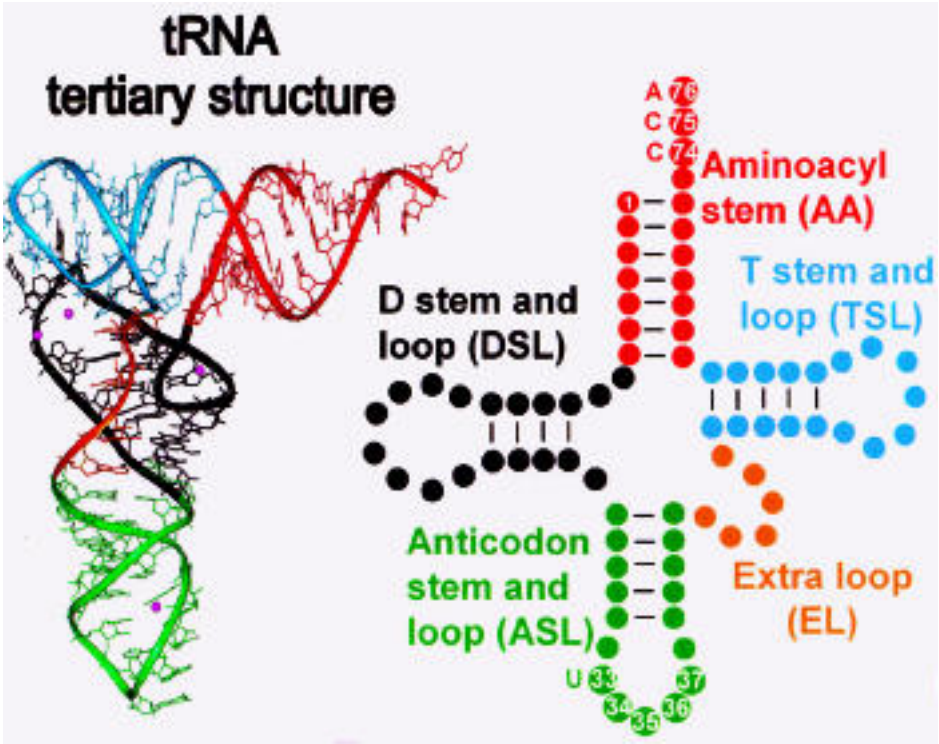

Figure 1.2: **tRNA structure.** On the left, the crystallographic structure of yeast $tRNA^{Phe}$ represents the global three-dimensional structure of tRNAs. The right panel shows the cloverleaf secondary structure of tRNA. In red: amino acid accepting stem or aminoacyl-stem (AA); in black: dihydrouridine stem and loop domain (DSL); in green: anticodon stem and loop domain (ASL); in gold: extra-loop (EL); and, in blue, the ribothymidine, or TΨC, stem and loop (TSL). Adapted from [1].

There are two ways of producing aminoacyl-tRNAs: the direct acylation of tRNA by aminoacyl-tRNA synthetases (aaRSs) and an indirect pathway of aminoacyl-tRNA synthesis. The first one is an ATP-dependent reaction carried out by aaRSs that are very specific in selecting amino acids and tRNAs. Each family of tRNA isoacceptors is recognized by an aaRS. So, each of the 20 amino acids is recognized and activated by a specific synthetase [25, 68, 75]. These enzymes catalyze the first step in protein biosynthesis: the specific aminoacylation of tRNAs, linking anticodons of tRNAs with specific amino acids [68, 75]. In this reaction, each amino acid is attached to the 3'-end of its tRNA, forming an ester bond between the amino acid and one of the hydroxyl groups of the terminal adenosine of the CCA end [75]. Alternatively, tRNA-dependent amino acid modification, where the acylation of tRNA involves acylation by a 'precursor' amino acid by a nondiscriminating aaRS, and then, this 'precursor' amino acid

is converted to the correct amino acid. This conversion of the 'precursor' amino acid to the correct one, matching the tRNA specificity, is mediated by a non-aaRS [89].

The aaRS can be divided in two distinct families: class I and class II (Figure 1.3) [68]. Class I enzymes contain a Rossmann nucleotide-binding fold in the active site domain, composed of alternating β-strands and α-helices. This class can be split into three subgroups (Ia, Ib, and Ic), whose enzymes have a tendency to recognize amino acids that are chemically related. Class II enzymes have in their active sites a seven-stranded β-sheet with flaking α-helices. These enzymes can also be split into three subclasses (IIa, IIb, and IIc). Apart from the biochemistry of the aminoacylation reaction both classes differ in several aspects. For example, proteins of these two classes show little or no structural similarity, they have almost no structural motifs in common, they acylate the amino acid to different hydroxyl groups of the terminal ribose of the tRNA, and face the tRNA from different angles [68, 89].

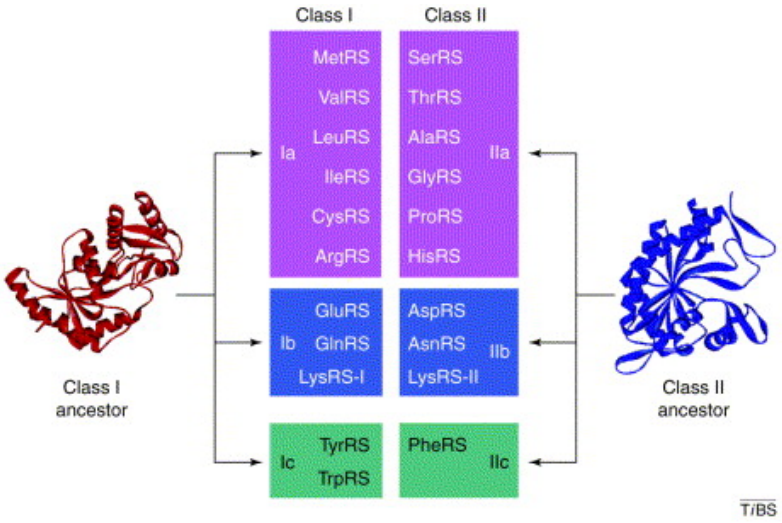

Figure 1.3: **The two subclasses of aminoacyl-tRNA synthetases.** The ancestor of the class I enzyme is GlnRS, whereas the ancestor of the class II enzyme is AspRS. Adapted from [68].

1.1.3 Translation fidelity

Translation errors can emerge during tRNA charging by aaRSs and when the mRNA is decoded by the ribosome. At the ribosome level, mRNA decoding can be affected by four major types or errors: missence errors, which cause incorrect amino acid incorporation into polypeptide chains, resulting in the synthesis of mutant proteins; nonsense errors, which cause readthrough of stop codon, producing proteins with extended C-termini; frameshifting errors that alter the mRNA reading frame, resulting in out-of-frame truncated proteins; and, processivity errors that terminate translation prematurely, producing truncated proteins. In terms of aminoacylation errors, these are mostly caused by the incorrect recognition of cognate tRNAs by aaRSs or by inability of the aaRSs to differentiate between similar amino acids. These errors are minimized by aaRSs editing mechanisms, responsible to reject incorrectly bound amino acids, and by specific tRNA-aaRS interaction networks [57].

Aminoacyl-tRNA synthetase editing activities can occur either before and/or after the

misactivated amino acid is attached to tRNA, known as pretransfer editing and posttransfer editing, respectively. This editing activity, namely posttransfer editing, was first demonstrated by Eldred and Schimmel and by Yarus [18, 48, 93]. In pretansfer editing, the hydrolysis of misactivated aminoacyl adenylate (aa-AMP) occur before the aminoacyl moiety is transfered to the 3'–end of tRNA. There are three main models to explain the mechanisms of pretransfer editing: translocation, selective release, and active site hydrolysis models (Figure 1.4). In the translocation model, near-cognate aa-AMP is synthesized at the active site but hydrolyzed at the editing site. In the two other models, pretransfer editing involves selective release of misactivated amino acids, which then undergoes spontaneous hydrolysis in solution, and/or their hydrolysis in the active site, respectively [48]. Pretransfer editing is utilized for the clearance of misactivated Ile by LeuRS, Ala by ProRS, Val by IleRS, and Ser by ThrRS [37]. In posttransfer editing, the 3'–end of mischarged aa-tRNAs moves from the active site to the editing site, while the rest of the tRNA molecule remain attached to the aaRS (Figure 1.4). In the editing site, the aminoacyl ester bond between non-cognate amino acid and tRNA is deacylated. Posttransfer editing activities are associated with both class I and II aaRSs, IleRS, ValRS, LeuRS, PheRS, ThrRS, ProRS, and AlaRS to eliminate non-cognate aminoacyl-tRNAs [37, 48, 91].

As mentioned above, protein synthesis errors (mistranslation) can occur during initiation, elongation and termination and have a major impact on yeast biology (Table 1.1), and most likely in the biology of all organisms, but its relevance for protein misfolding/aggregation and proteotoxic stress is still poorly understood.

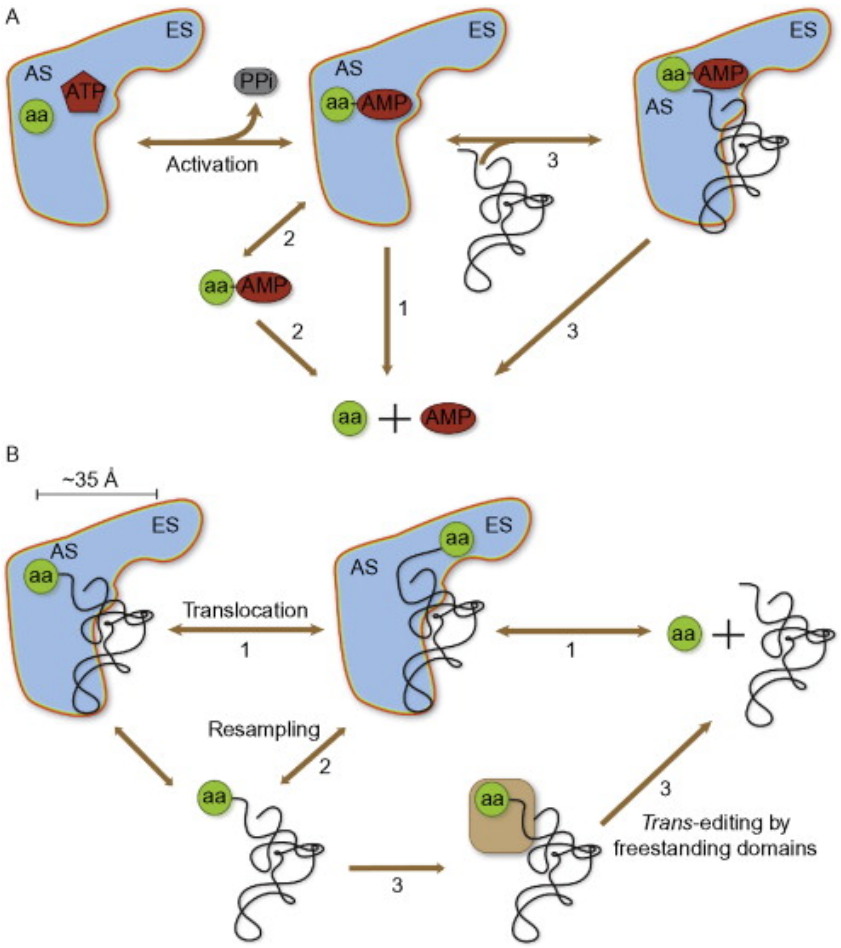

Figure 1.4: **Editing mechanisms in aaRSs.** (A) Pretransfer editing pathways in aaRSs. The misactivated aa-AMP can be hydrolyzed in a tRNA-independent manner either through the direct catalysis of aa-AMP hydrolysis by the aminoacylation active site (AS) before release (pathway 1 − active site hydrolysis) or through selective release of non-cognate aa-AMP followed by spontaneous hydrolysis in solution (pathway 2 − selective release). tRNA-dependent pretransfer hydrolysis (pathway 3 − translocation of aa-AMP) can occur within the aminoacylation AS in some aaRSs, or in the editing site (ES) presumably via translocation of aa-AMP through a channel between AS and ES. (B) Posttransfer editing pathways in aaRSs. Mischarged aminoacyl-tRNA (aa-tRNA) can be hydrolyzed via translocation of the 3'-terminal CCA of tRNA from the aminoacylation AS to the distal ES (pathway 1). Alternatively in class II aaRSs, the mischarged aa-tRNA may be released into solution, then either resampled by the aaRS (pathway 2) or hydrolyzed by an accessory *trans*-editing factor (pathway 3). Adapted from [91].

Table 1.1: **Major effects of mistranslation in *S. cerevisiae*** [55, 59, 73, 78].

Effects of CUG mistranslation in *S. cerevisiae*
- increased ploidy (up to 4N); - large chromosomal rearrangements; - blocking mating and sexual reproduction; - altered sporulation; - altered expression of molecular chaperones and carbohydrate metabolism; - increased proteasome activity; - up-regulation of cell wall structural proteins; - down-regulation of protein synthesis and amino acid metabolism; - alterations in genome and gene expression $\longrightarrow$ phenotypic alterations: - morphology and cell shape and size heterogeneous; - formation of pseudohyphae and hyphae; - increased resistance to several agents (e.g. nutrient starvation, cadmium, H_2O_2); - accumulation of glycogen and trehalose; - increased secretion of extracellular hydrolases: lipases and proteases; - strong effect on cell adhesion.

1.2 Protein folding and misfolding

After biosynthesis and in order to become functional newly synthesized polypeptide chains are folded into compact structures, based on the information encoded in their amino acids sequence [4, 15]. The term protein folding is universally recognized as the process responsible for the acquisition of the native structure, starting from a completely or partially unfolded state. This folding process, occurring within the cells of living organisms, is assisted by a large number of auxiliary factors, including molecular chaperones and folding catalysts. These auxiliary factors do not contribute with conformational information to the folding process or form a part of the final biologically active structure, instead they enable polypeptide chains to fold efficiently [4, 15, 66]. The idea that there is a unidirectional relationship between the primary amino acid sequence of a protein and its final conformation was suggested by Anfinsen with their work with the enzyme ribonuclease [3, 66]. These authors concluded that the information encoded in the primary sequence of proteins is an important factor in the folding process. There are various forces involved in the folding process, such as Van der Waals force, electrostatic force, hydrogen bonding, and hydrophobic force, but there are evidences that the hydrophobic force is the dominant one, determining the overall folded structure of the protein [15, 66]. Protein folding is now considered a stochastic process and involves the concept of an 'energy landscape' for each protein, with a finite number of possibilities for proteins to misfold and adopt non-native states, still being transiently stable (kinetic traps) [15, 66].

In vivo, some proteins fold while still attached to the ribosome. While other proteins fold in the cytoplasm after release from the ribosome, or when they enter specific compartments, such as the endoplasmatic reticulum (ER). Depending on the environment in which protein folding takes place, the details of the folding process vary, although the basic principles are maintained [14].

The term misfolding describes processes that result in the acquisition of a number of persistent non-native interactions that affect protein's architecture and/or its properties, leading many times to the formation of insoluble protein aggregates [15, 71]. As a result of the accumulation of misfolded proteins in cells, proteotoxic stress is produced. This subtype of stress can occur under a variety of conditions, including hypoxia, hyperthermia, and exposure to denaturing agents or drugs that inhibit chaperone or proteasome activities. If misfolded proteins accumulate and aggregate above a certain threshold, proteotoxic stress can be toxic, likely because of the presence of oligomeric species that interfere with cellular processes [64, 71, 86]. Fortunately, living systems have elaborated strategies to prevent interactions of proteins with other molecules prior to folding completion [15, 86]. One of these strategies is the use of molecular chaperones that associate with unfolded protein chains, avoiding aggregation and supporting a more efficient folding in an ATP-dependent manner [86]. Additionally, there are folding catalysts, whose function is to accelerate potentially slow steps in the folding process. Peptidylprolyl isomerases (PPI) and protein disulphide isomerases (PDI) are the most important folding catalysts. The first ones amplify the rate of *cis*/*trans* isomerisation of peptide bonds involving proline residues, and the second ones improve the rate of formation and reorganization of disulphide bonds within proteins [14, 15]. Additionally, in cases of proteotoxic stress, cells also activate an adaptive response, known as the heat shock response (HSR) [64].

1.2.1 Protein aggregation

Protein aggregates are oligomeric complexes that arise from non-native interactions among structured intermediates in protein folding or assembly. They have poor solubility in aqueous or detergent solvents, aberrant sub-cellular or extracellular localization and non-native secondary structure [43]. There are different types of protein aggregates: ordered (or structured) aggregates as amyloid fibrils, and disordered (or amorphous) aggregates as inclusion bodies [21, 43]. In both cases, aggregates are insoluble and metabolically stable under physiological conditions [43].

The formation and structure of protein aggregates imply specific intermolecular interactions between hydrophobic surfaces of structural subunits in partially folded intermediates. Thus, initial stages of aggregation involve the interaction between specific surface elements of one molecule and hydrophobic surface areas of structural subunits of neighboring molecules. When a high number of interactions occur, the formation of large aggregates is likely. It is possible that these aggregates (dimmers and tetramers) are soluble initially, but the formation of larger aggregates will tend to exceed the solubility limit [21].

Environmental stressors are not the only agents that lead to the formation of partially folded intermediates and aggregation. Rather, mutations, RNA modifications and ribosomal errors can also lead to differential destabilization of the native state relative to the partially folded intermediate [21, 43]. So, the main factors that determine if a truly synthesized protein will aggregate, and the rate and extent of the aggregation, are the amino acid sequence, pH, temperature and ionic strength, concentration of the protein, presence of co-solutes (for instance, denaturants), and the presence/absence of molecular chaperones [21].

Since protein aggregates are more stable than the intermediate conformers from which they originate the destiny of misfolded proteins will be determined by kinetic competition for the aggregated substrates between proteasomal degradation and aggregation into high molecular weight oligomers [43].

1.2.2 Cellular quality control mechanisms

The production of aberrant proteins is common and cells require protein quality control mechanisms (PQC) to handle aberrant proteins. Physiological and environmental factors can also denature proteins and cells use PQC systems to recover them [71]. Therefore, protein aggregates do not accumulate in unstressed cells, due in part to the PQC system which is able to destroy aberrant proteins arriving from transcription and translation [43].

Aberrant or misfolded proteins are marked by PQC systems and targeted for degradation via the ubiquitin-proteasome system (UPS) [71]. The nascent polypeptide chain in the ribosome needs help to reach its translation end, and many proteins (20-30%) also need assistance to reach their folding state. Thus, the PQC network evolved to maintain cellular protein homeostasis or proteostasis, maximizing cellular protein folding capacity (by the chaperone system and folding catalysts), minimizing intrinsic and extrinsic attacks and degradation of misfolded proteins by proteases, the ubiquitin-proteasome (UPS), and the lysosome-autophagy systems, in order to avoid any potential harmful effects in the cell [9, 47, 66].

The first evidence for the existence and function of molecular chaperones came from exposure of cells to heat-shock. For this reason, many chaperones are known as Hsps (heat shock proteins) [15, 47, 86]. Chaperones do not serve as template or code for misfolded proteins, but help to avoid and reverse non-functional conformations; to facilitate co- and post-translational

folding; and, to assist in assembly and disassembly of protein complexes [47, 56]. They often support the folding process *via* cycles of substrate binding and release, regulated by ATPase activity [4]. Transcriptional regulation of Hsps is controlled by specific transcription factors (TF), namely RpoH and heat shock factor (HSF). Under non-stress conditions, these TF are present in the cytoplasm as monomers bound to chaperones. Under stress, the presence of unfolded proteins titrate chaperones that release the TF to trimerize, translocate to the nucleus and bind their *cis*-regulatory elements [47]. Chaperones can act together and in synergy within the chaperone network and with other PQC systems, namely the proteasome and lysosomal degradation pathways [47]. And, interact momentarily with unfolded or partially folded intermediates, covering hydrophobic surfaces from forming inappropriate intra- or intermolecular contacts [43]. They are also involved in other cellular processes, including protein targeting, regulation of translocation, degradation and signal transduction [4, 56].

Chaperones are divided into different families or classes, classified by size and function: small hsp (sHSP), Hsp60 chaperones, Hsp70 chaperones, the ATP-dependent Hsp90 family, and the ATPase Associated with diverse Activities (AAA+) family [47, 86].

Members of the sHSP family have a molecular mass <43 kDa and the capacity to maintain the solubility of partially folded proteins through binding to protect their exposed hydrophobic surface. The sHSP destabilize protein aggregates and ease their solubilisation, refolding, or degradation, mediated by Hsp104 and Hsp70/40 chaperones.

The hsp60 chaperones facilitate protein folding using an isolated cavity, known as the 'Anfinsen cage' and are present in the mitochondria.

The Hsp70 chaperones are cytosolic but, in eukaryotes, are also present in organelles such as mitochondria and the endoplasmatic reticulum. These chaperones need numerous co-factors to work efficiently in the folding of nascent polypeptides and their assembly, refolding of misfolded proteins, translocation of proteins through membranes into organelles and for secretion, and controlling the function and life-time of signaling and regulatory proteins.

The ATP-dependent Hsp90 family has similar functions to the Hsp70 family avoiding non-specific aggregation of generic proteins. Besides that, Hsp90 are involved in signal transduction, cell cycle, meiosis, transport, secretion and chromatin remodeling, epigenetic gene regulation and viral replication, together with several co-factors. Moreover, Hsp90 can mediate conformational changes of folded proteins, in order to achieve their stabilization, activation or degradation.

The Hsp104 proteins are members of the AAA+ family and are highly induced in response to stress conditions, conferring tolerance to it. Their functions are to prevent misfolding and, mainly, to disaggregate proteins [47].

The transition of folding intermediates to the native state is highly regulated by Hsp70 and ATP hydrolysis [56]. Interestingly, the different classes of molecular chaperones cooperate in the cell, and all chaperones can suppress the aggregation of folding proteins. In this way, all chaperones are overproduced simultaneously under stress conditions [86].

The ubiquitin-proteasome system is the other main PQC system and is involved in degradation of proteins (including short-lived, misfolded and damaged polypeptides) in an ubiquitin-dependent manner. Ubiquitinated proteins (with at least four ubiquitin moieties) selectively bind to the proteasome, which in turn unfolds and translocates them into a proteolytic chamber where proteins are hydrolyzed into short peptide fragments. Deubiquitination enzymes present in the proteasome convert ubiquitin chains into monomers that can be used in new ubiquitination reactions. Beyond, its proteolytic function, ubiquitination may be involved in membrane trafficking, cell-cycle progression, differentiation, synaptic plasticity, apoptosis,

endocytosis, DNA repair and transcriptional regulation [6, 71].

At a level of higher complexity, there is a connection between the ubiquitin-proteasome system and molecular chaperones. Indeed, some molecular chaperones are linked to the UPS, bind to non-native proteins and mediate their refolding or degradation [6].

Additionally, protein degradation can occur in the vacuole of yeasts and in the lysosome of mammalian cells, known as the lysosome-autophagy system. The vacuole/lysosome are suitable for degrading larger and more complex substrates, including protein complexes and organelles, extending protein degradation capacity of the proteasome. Particles destined for autophagic degradation are engulfed by membrane to form autophagosomes, where proteases can access their substrates for degradation [35, 43, 47].

1.2.3 Protein misfolding and disease

It is not surprising that the presence of unfolded or misfolded proteins will lead to diseases [15]. Under stress, genes related to chaperones and the autophagy and ubiquitin proteasome system (UPS) are abundantly expressed. However, this machinery capacity to deal with protein aggregation is limited and saturation of these PQC systems allows for accumulation of protein aggregates [56].

Misfolding and aggregation are identified as common molecular events for a large number of human diseases. These diseases are known as conformational diseases and they are characterized by proteotoxic stress which disrupts various cellular functions [56]. Additionally, the most typical feature of many of the aggregation diseases is the final deposition of aggregation-prone proteins in the form of amyloid fibrils and plaques. Such deposits can form in vital organs, such as brain, liver and spleen, or in the skeletal tissue, depending on the disease involved [15]. Conformational diseases include CAG-repeat/polyglutamine (polyQ) expansion disease (Huntington's disease, HD; Kennedy's disease; spinocerebellar ataxias, SCAs) and non-CAG diseases (Parkinson's disease, PD; prion diseases, such as Creutzfeldt-Jakob disease, CJD; amyotrophic lateral sclerosis, ALS; and, Alzheimer's disease, AD) [4, 56]. Each of these diseases has the typical characteristic of an age-dependent onset and a progressive fatal clinical course [56]. The appearance of self-associated folded states together with aggregation and fibril formation can be toxic (but not always), and is often caused by mutations in the disease proteins, resulting in cellular dysfunction and pathology [56].

Other examples of diseases associated to aberrant proteins are cystic fibrosis and hypertrophic cardiomyophaty [4]. There are also several protein deposition diseases that involve non-ordered proteins deposits, such as inclusion body myositis, light-chain deposition disease and cataracts [21]. A summary of the main diseases associated to protein aggregation is shown in Table 1.2.

As referred before, the symptoms of many diseases associated with the expression of aggregation-prone proteins begin later in life and this suggests that aged cells are more susceptible to proteotoxic stress. On the one hand, with aging protein oxidation increases, leading to the formation of protein aggregates. Also the functionality of the chaperone and proteasome networks declines during aging. In this situation, there is an imbalance between the ever growing production of toxic misfolded species and the decreased protective capacity of the PQC machinery [79, 85]. So, even in the absence of mutations in genes encoding aggregation-prone proteins, cell aging and oxidative stress are sufficient to increase protein aggregates.

Table 1.2: **A summary of the main diseases associated to protein aggregation** [4, 14, 80].

Clinical syndrome	**Proteins/peptides involved**
Alzheimer's disease	APP β-peptide
Scrapie/Creutzfeldt-Jakob's disease	Prion protein
Polyglutamine expansion disease:	Various polyQ proteins:
Huntington's disease	Huntingtin
Dentatorubro-pallido-Luysian atrophy	Atrophin 1
Cerebellar ataxias	Ataxins
Kennedy disease	Androgen receptor
Spino cerebellar ataxia 17	TATA box-binding protein
Familial amyloidosis	Transthyretin/lysozyme
Cystic fibrosis	CFTR
Familial hypercholesterolemia	LDL receptor
Phenylketonuria	Phenylalanine hydroxylase
MCAD deficiency	Medium-chain acyl-CoA dehydrogenase
Hypertrophic cardiomyopathy	Various sarcometric proteins
Osteogenesis imperfecta	Collagens
Epidermolysis bullosa simplex	Keratins
Hereditary spastic paraplegia	Mitochondrial Hsp60
Desmin-related myopathy	αB-Crystallin
Sanjad-Sakati and Kenny-Caffrey	TBCE
Marfan syndrome	Fibrillin

1.3 Cell-arrays technology

Microarrays technology was developed in the early 1990's as a way to measure the transcription levels of a set of genes simultaneously and became an effective tool for gene expression or transcriptional analysis [65, 87]. This technique consists in arrayed nucleotide probes printed onto the surface of glass slides for testing their degree of hybridization to the investigated cell-derived cDNA [65, 67]. Some variants of DNA microarrays have been developed, namely complementary DNA (cDNA) microarrays − double-stranded cDNA or PCR products spotted on glass slides, and oligonucleotide microarrays [65]. This technology was expanded to protein arrays for probing protein-protein or protein-small molecule interactions, in which pure proteins are immobilized on the surface of a glass slide [87, 95]. Further developments expanded the technology to carbohydrates, tissues, small-molecules and drug-like molecules [60, 87]. The principle in all cases is the same: reactive molecules are fixed onto a mapped solid surface grid and exposed to a multi-competent analyte mixture. There is diversity of arrayed molecules and array formats as well as diversity of detection techniques, such as fluorescence, luminescence, electrochemical detection, mass spectrometry, surface plasmon resonance and others [5, 60]. As a consequence, array technologies can be used in a large number of applications in medicine, biology, toxicology, drug screening, etc. [5]. In combination with bioinformatics tools to process and analyse array data, this technology is widely used in systems biology, genomics, transcriptomics and proteomics [60].

However, DNA arrays have limitations due to artifacts from RNA isolation and cross hybridization, and protein arrays are difficult to produce because large numbers of individually purified proteins are required, and it is unclear for how long the proteins remain stable once the array is printed [95]. Additionally, to understand the role of genes with unknown function, it is better to analyse phenotypes resulting from either gain or loss of function of each gene in a global manner [10]. To address this problem, whole-cell arrays have been developed, namely the LuxArray. This technology used a collection of 689 non-redundant functional promoter fusions to *Photorhabdus luminescens lux*CDABE in live *E. coli* strains that were used to build the array [5, 16]. Another cell-based microarray system for identifying the cellular functions of gene products was described by Ziauddin and Sabatini. In this system, the array spots are clusters of mammalian cells expressing defined DNA constructs, whose decrease or increase is indicative of the function of specific gene products [95, 90]. So, cell arrays allow investigators to identify genes implicated in various cellular processes, such as cell adhesion, apoptosis and signal transduction [90].

Taking into account the usual cell-assaying methods (based in micro-well plate format), cell microarrays also bring some additional advantages: they can hold at least 5000-6000 spots in one slide (enabling a genome-wide screen on only a few slides); need small quantities of expensive reagents, use limited biological samples, and allow for a larger range of detection methods to be used [10, 20, 90]. However, this technology has some limitations, such as cell stress, efficiency of transfection, flexibility of detection, etc. [10]. For instance, some treatments used during production of cell arrays can be toxic to live cells, leading to stress. Additionally, collection of high-content images of each spot, automated analysis of each image and organization of the resulting data are issues that still need special attention in cell-microarrays analysis [87].

1.3.1 Types of cell-arrays

Cell-arrays technology can be divided in subtypes, namely positional cell microarrays and batch or non-positional cell microarrays. In positional cell microarrays, cells are printed directly onto a surface, in an arranged way, and preferentially attach to the arrayed substrates (such as polymers, carbohydrates, antibodies, proteins from the extracellular matrix, etc.); clusters of cells are physically separated and characterized by specific x and y coordinates. On the other hand, batch arrays are non-positional arrays, and do not rely on x and y coordinates to deconvolute the data. In this case, cells are encoded (ranging from a color code to a radio frequencies code), phenotypes are assayed in batch and cells of interest are retrieved through decoding [10].

There are also transfected cell-arrays, small interfering RNA (siRNA) cell-arrays and spotted cell-arrays. In general, for constructing transfected-cell microarrays nanoliter quantities of nucleic acids (cDNA in plasmid expressing vectors or linear PCR products designed to express proteins of interest) are printed in defined locations onto the surfaces of glass slides, using a robotic microarrayer. Before cells are added to the printed array, it can be treated with a transfection reagent or a stable transfection reagent may be printed along with the nucleic acid. In order to initiate transfection, cultured cells in medium are added to printed arrays disposed in tissue culture dishes (few days in culture). The printed material is internalized as cells adhere to the spots and become transfected. Cells that do not adhere to the spots form a non-transfected lawn between spots. At the end of an experiment, the microarrays are fixed and prepared for immunofluorescence, staining for DNA and F-actin, *in situ* hybridization, chemiluminescence, autoradiography, apoptosis detection or other visualization methods. The arrays are then covered with a cover slip and visualized with a microarray scanner or fluorescence microscope to provide a view of the entire array area (Figure 1.5) [65, 87, 90]. Ziauddin and Sabatini called this method 'reverse transfection' because cells are added on top of the nucleic acid instead of the opposite [87, 95]. This technique came as a great promise for high-throughput characterization of cellular phenotypes, identification of small molecule targets (for drug screening, for instance), and large-scale functional genomic studies [29, 65, 95]. Nevertheless, transfected cell arrays still have some limitations, such as the difficulty in obtaining high transfection efficiency in some cell lines, and getting the genomic cDNA expression constructs [8, 29, 65]. Despite this, transfected cell arrays have already been used to identify genes involved in chromosome maintenance, measuring response of neural precursor cells to a multiplicity of extracellular matrix components, finding ubiquitin targets, and detecting protein-protein interactions [29].

siRNA cell-arrays take advantage of RNAi's potential to silence genes selectively, producing loss-of-function phenotypes for genetic studies. RNAi is a post-transcriptional gene silencing process, in which double-stranded RNA triggers sequence-specific degradation of target mRNAs [87, 90]. The chemically synthesized small interfering RNAs are RNA duplexes containing 21 bp and 3' dinucleotide overhangs that are cleavage products of the Dicer enzyme. This enzyme cleaves double stranded RNA precursor molecules into short interfering RNAs and small temporal RNAs [90]. Cell microarrays using siRNA can considerably reduce the amount of RNAi reagents and cells and improves the speed of high-throughput studies with RNAi libraries [10, 87]. This technology is a subtype of transfected cell-microarrays, since mixtures of siRNA-plasmid constructs, polymer and transfection reagent are arrayed onto a glass slide, followed by deposition of cells onto the array and transfection of cells (Figure 1.5) [10, 53, 90].

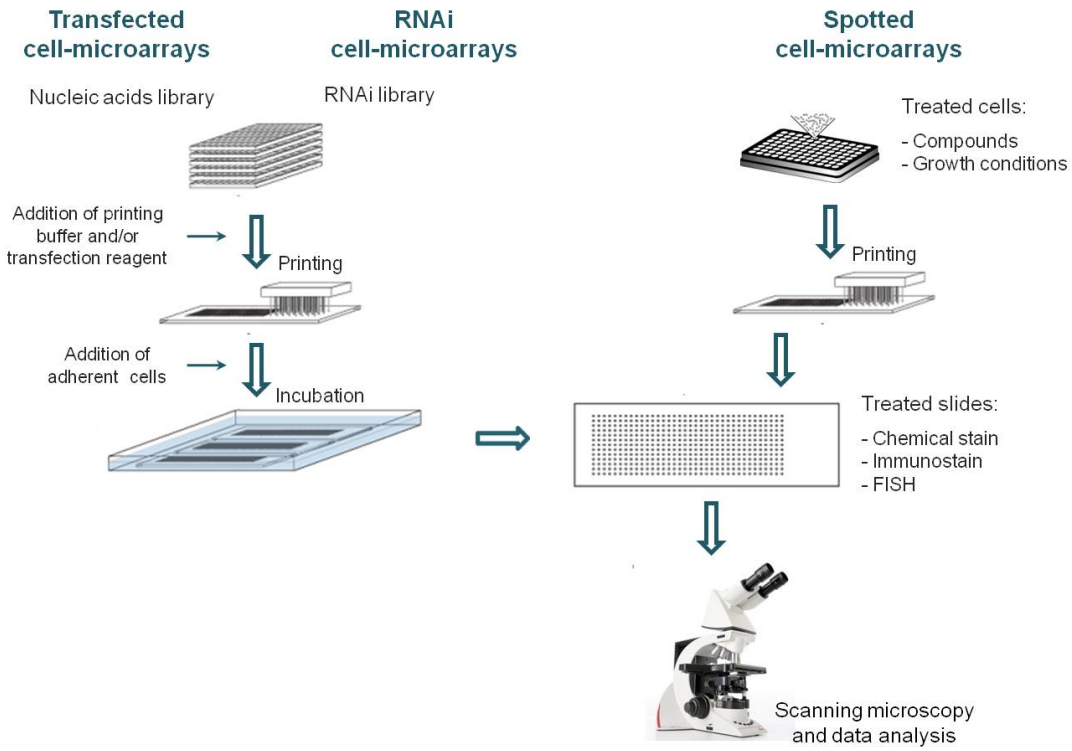

Figure 1.5: **Schematic model of the three types of cell microarrays.** Transfected cell-microarrays: nucleic acids (such as expression plasmid or RNA) are printed on a standard glass microarray and used to transfect cells with the addition of a transfection reagent. Cultured cells in medium are added to the array, adhere to the spots and become transfected by internalising the nucleic acids. RNAi cell-microarrays: is a subtype of transfected cell-microarrays, differing in the printing of RNAi onto glass slides to transfect cells. Spotted cell-microarrays: a suspension of cells is printed onto coated glass slides by contact deposition, in an organized manner. After printing, in the three types of cell-arrays, slides are treated to an efficient screening of the arrayed cell population.

The numerous phenotypes that result from specific gene knock-downs can be analyzed either in living cells using gene expression reporters, labeled proteins or calcium fluxes with calcium-sensitive fluorophores, or in fixed cells by *in situ* hybridization or immunostaining [10]. Another advantage of this technique is that, as siRNA microarrays are a subtype of transfected cell microarrays, these two categories of cell microarray can co-exist on the same array, and the two species of constructs can be co-transfected, resulting in cell clusters that overexpress and underexpress any genes of interest [90].

Finally, spotted cell microarrays (also named cell chips) are made by contact deposition of suspensions of cells onto coated glass slides using a printing arrayer and imaging the stained subcellular features (Figure 1.5). Importantly, cells from a wide variety of cell types, growth conditions, and treatments can be arrayed on a single slide. Spotted cell microarrays are a high-throughput technology used for measuring cellular phenotypes, including cell morphology, protein and RNA localization. This technique has some advantages in comparison with the two deviations of cell arrays presented before, namely it avoids the laborious cDNA expression or RNAi construct procedure and it is not limited to high-efficient transfections [29, 62, 65]. Spotted cell microarrays were first developed and applied for *Saccharomyces cerevisiae* and bacteria to set up functional genomic screens [62, 94]. Protocols to print human cells have also been described by Hart and colleagues [29].

1.3.2 Imaging cell-arrays

Analysis of cell microarrays requires automation: high-throughput image acquisition and automated image analysis. To achieve this, there are two different types of systems: microarray scanners (low-resolution image of an entire slide), and motorized microscopes (high-resolution readout). Depending on the resolution required to visualize phenotypes of interest, an appropriated system must be selected. For instance, when a low-resolution assay for phenotypes (such as cell growth, death or total amount of protein) is intended, it may be reasonable to acquire an image with a high-resolution microarrays scanner. On the other hand, in order to visualize the phenotype of interest, at a subcellular level, high-resolution images are often required, using, in this case, microscopes outfitted with motorized components. However, these microscope-derived instruments have been designed to acquire images from multi-well plates rather than cell microarrays, which poses a challenge to imaging cell microarrays [87].

1.3.3 Potential uses of cell-arrays

Cell microarrays have advantages over traditional methods, being an expressing-cloning system for the high-throughput identification of genes of biological interest. For this purpose, Ziauddin and Sabatini made a screen of 192 epitope-tagged cDNA clones in expression vectors, which were printed and transfected without knowing the identities of each gene. Then, the identification of genes that can affect specific cellular processes is made by probing the resulting cell arrays. In fact, through the analysis of cell clusters, they identified genes involved in apoptosis (cell fragmentation), cell adhesion (by close juxtaposition of cell membranes), phosphorylation, and nuclear and cytosolic subcellular locations of epitope-tagged protein. This study illustrated the diversity of cellular phenomena that becomes accessible to investigation through cell arrays. Additionally, live cells could be analyzed for the subcellular distribution of organelles, vesicular trafficking, protein translocation or calcium waves.

In fact, cell microarrays offer great versatility since numerous experimental parameters can be used in a combinatorial manner leading to a variety of potential applications. Variables amenable by cell arrays include the substance arrayed, cell line, cell culture conditions, external stimuli and assaying method [90].

Moreover, structure-function relationships of genes can be elucidated using cell arrays, simply expressing collections of mutants of a particular gene on a cell array. In fact, signal-transduction, cell adhesion, cell migration, and cellular chemotaxis studies take advantage of this technology. In the specific case of signal transduction pathways, cell arrays are a robust technique because signalling cannot be studied by DNA based methods due to the presence of post-translational modifications and *in vitro* cell-free systems [8, 90]. Cell arrays have also been used to study diseases and for drug screening [10, 90]. For instance, cell microarrays can express combinations of cDNA and siRNA constructs for candidate oncogenes and tumor-suppressor genes, in order to enlighten genetic criteria for tumor formation [90]. Relatively to drug screening, cell arrays are useful to evaluate potential drug targets and to characterize their effect in cells in a high-throughput manner [10].

1.4 *S. cerevisiae* as a model system

Model organisms are essential to study human diseases, in particular to discover the basic mechanisms underlying diseases, without ethical and experimental limitations [40, 66]. In this work, we have chosen *S. cerevisiae* as a model organism, because it is an eukaryote, its genome can be easily manipulated, grows rapidly as dispersed cells in culture, replica plating and mutant isolation are simple, has a well-defined genetic system, and an adaptable DNA transformation system. Yeasts are also suitable as model organisms for the study of basic molecular mechanism underlying human diseases, such as neurodegenerative diseases, because many of the cellular and biological processes are highly conserved from yeast to humans, such as cell division, DNA replication and recombination, mismatch repair, protein folding, intracellular transport, and metabolism [40, 66, 76]. Unlike most other organisms, strains of *S. cerevisiae* have both a stable haploid and diploid state, and so recessive mutations can be easily identified in haploid strains.

The *S. cerevisiae* genome was the first eukaryotic genome to be fully sequenced (1996), and its strains are viable with a large number of markers. *S. cerevisiae* contains 16 well-characterized chromosomes (haploid set), with 200 to 2200 kb in size. The complete genome sequence of *S. cerevisiae* includes about 5750 open reading frames (ORFs), which represent 72% of the total genome sequence. Additionally, the yeast genome contains some 120 ribossomal RNA genes (chromosome XII), 40 genes encoding small nuclear RNAs (smRNAs), and 262 tRNA genes. The yeast genome is highly compact, in contrast with those of its more complex relatives in the eukaryotic world. With this combination of properties, yeast allows one to perform genetic manipulations and to screen for induced phenotypes of relevance to human diseases. Furthermore, plasmids can be introduced into yeast cells as replicating molecules or to achieve DNA integration into the genome [24, 66, 76].

Many human genes related to disease have orthologues in yeast [40, 76], and many *S. cerevisiae* proteins share high amino acid sequence similarity with human proteins. Furthermore, several drugs act upon orthologous yeast proteins of human targets of specific diseases [66].

This model organism has been used with success by many researchers, to identify new genes and pathways involved in tolerance to radiation, oxidative stress, human mitochondrial disease, and to typify the effects of pharmacological agents, among others. In these studies, a collection of gene deletion mutants of *Saccharomyces cerevisiae*, developed by the *Saccharomyces* Genome Deletion Project, was used [66].

However, one must be aware that, at least in some studies, as in the study of neurodegenerative diseases, the use of yeast as a model organism may not be adequate. It so, the results obtained with yeast models of neurodegeneration have to be validated with human cells.

1.5 Principal objectives of this thesis

The objective of this thesis was to optimize a yeast cell array to identify new genes and environmental stressors that influence the formation of protein aggregates. We have tested various glass slides and reagents and we were able to produce high quality yeast arrays. These arrays were then used as a proof-of-principle to determine whether various chemicals and ribosomal errors would increase the formation of protein aggregates. The results obtained show that our methodology can be used to advance knowledge in the proteotoxic research field.

Chapter 2

Material and Methods

2.1 Yeast strains and growth conditions

S. cerevisiae strains used were BY4741 (MATa his3Δ0 leu2Δ0 met15Δ0 ura3Δ0), S288C (MATα SUC2 gal2 mal mel flo1 flo8-1 hap1 ho bio1 bio6), W303 (MATa/MATα leu2-3,112 trp1-1 can1-100 ura3-1 ade2-1 his3-11,15 [phi+]), BMA64 (MATa/MATα ura3-52/ura3-52; trp1Δ 2/trp1Δ 2; leu2-3,112/leu2-3,112; his3-11/his3-11; ade2-1/ade2-1; can1-100/can1-100), CEN.PK2 (MATa/α ura3-52/ura3-52 trp1-289/trp1-289 leu2-3_112/leu2-3_112 his3 Δ1/his3 Δ1 MAL2-8C/MAL2-8C SUC2/SUC2), EC1118 (Wine yeast HO/ho SUC/SUC MAL/MAL/ gal/gal), RM11-1a (MATa leu2Δ ura3Δ ho::Kan), BY4743 (MATa/MATα his3Δ1/his3Δ1 leu2Δ0/ leu2Δ0 met15Δ0/MET15 LYS2/lys2Δ0 ura3Δ0/ura3Δ0) and transformed BY4743 (with GFP fusion protein). All yeast strains were grown at 30 °C in YPD medium (glucose: 2% (w/v), yeast extract: 0.5% (w/v), and peptone: 1% (w/v)) (Formedium) and minimal medium (glucose: 2% (w/v), yeast nitrogen base without amino acids: 0.67% (w/v), each required amino acids (100 μg/ml)) (Formedium). BY4743 transformed cells were grown in MM-Leu-His and preserved at -80 °C in MM-Leu-His + 40% (v/v) glycerol. Solid media were performed by addiction of 2% agar (Formedium). All media were sterilized by heat in an autoclave.

2.2 Cell-arrays: protocol optimization

Yeast cell arrays were produced using coated glass-slides and contact high density printing. This technique was firstly described by Narayanaswamy and colleagues (2006), and we started replicating their protocol for yeast cell-array printing, but without acceptable results. We then decided to test all variables of the protocol in a systematic manner, in an attempt to optimize it for our working conditions. In the next 2 sections we describe in detail how each step was tested and the protocol optimized. Printing was carried out using a High Throughput Automated Microarrayer (Microgrid Compact II), using Whole Cell Microarray Printing Pins with 1.25 μl uptake loading volumes (Arrayit®), which were washed between printing runs. The resulting spots are ∼220 μm in diameter, spaced 0.7 mm apart. In a standard print run, the pins are washed in mQ water and dried 3 times by high velocity vacuum after each loading and printing step. All the slides were visualized using an epifluorescence up-right microscope Imager.Z1 (Zeiss), equipped with Brightfield filter and an oil-immersion objective, 63X.

2.2.1 Slides preparation

Cell arrays were tested on different glass microscope slides, namely poly-L-lysine and concanavalin-A coated slides prepared in the lab, Poly-prep™ slides (Sigma-Aldrich™), Menzel-Glaser Superfrost® Plus Gold (Thermo Scientific*), SuperEpoxy 2 (Arrayit® Corporation) and Hydrogel coated substrate − NEXTERION® Slide H.

For preparing poly-L-lysine coated slides we used 1 mg/ml and 10 mg/ml solutions of poly-L-lysine (Poly-L-lysine solution: 0.1% w/v, in water; Sigma-Aldrich™) in phosphate buffered saline 1X (1X PBS). Superfrost microscope slides (Cole-Parmer®), pre-cleaned, were immersed in each of the solutions and mixed on an orbital shaker (50 rpm) for 30 minutes. Then, slides were washed 3 times in fresh MilliQ water each time (plunging slides up and down 20 times), centrifuged at 200 rpm for 3 minutes, and dried in a 50 °C oven for 30 minutes. This protocol was adapted from several protocols for coating glass microscope slides with poly-L-lysine (http://cmgm.stanford.edu/pbrown/protocols/; http://www.sysbio.harvard.edu/csb/resources/resources/downloads/Bauer_Core_ Polylysine_Protocol.doc).

Concanavalin-A-coated slides were prepared by immersing pre-cleaned slides (Superfrost microscope slides; Cole-Parmer®) in a 0.1 mg/ml solution of ConA (Concanavalin A type VI (lectin), lyophilized powder; Sigma Aldrich™) in 1X PBS during 15 minutes. Then, slides were dried at room temperature for 1 hour, washed 2 times in fresh MilliQ water each time (plunging slides up and down 10 times), and dried at room temperature for a second time. This type of coated slides requires activation of ConA by adding $CaCl_2$ (20 mM) and $MnSO_4$ (20 mM) to cells prior to printing. This protocol was adapted from [62] and from other protocols (http://jura.wi.mit.edu/sabatini_public/fly_array/conA.htm).

2.2.2 Cell-arrays printing

Glass slides and cell preparation for printing

For printing cell-arrays, we tested different coated glass slides (see above). Besides that, we have also tested printing non-fixed and fixed cells, and different cell suspension solutions: MilliQ water, MilliQ water plus 7% glycerol, MilliQ water plus 17% glycerol, MilliQ water plus 27% glycerol, minimal medium (MM), MM plus 7% glycerol, MM plus 17% glycerol, MM plus 27% glycerol, 1X PBS, 1X PBS plus 7% glycerol, 1X PBS plus 17% glycerol, 1X PBS plus 27% glycerol, and sorbitol 0.5 M, 1 M and 1.5 M (Table 2.1). For fixation, cells were incubated in 3.7% formaldehyde for 1 hour at room temperature, and washed with the respective suspension solution.

Printing was performed using a High Throughput Automated Microarrayer (MicroGrid). Again, in order to promote the adherence of cells to the slide surface, the slides were centrifuged flat at 1500 x g during 5 minutes. We also tested whether variation in centrifugation temperature (4 °C, 12 °C and 20 °C) influenced the adherence of cells to the slide surface.

Before microscopy analysis slides were washed and definitive preparations were obtained using mounting media (Fluorshield™, Sigma-Aldrich). Washing is necessary to remove glycerol and sorbitol that inhibit evaporation and enhance the brightness of each spot during printing. Since we had spots with and without glycerol and sorbitol and cells suspended in different media, we tested the washing step with MilliQ water, 1X PBS and 95% ethanol.

Slides were visualized as described above and cells were counted manually. As routine practice, on average, 470 cells of 3 independent spots were analysed per experiment.

Table 2.1: **Conditions tested for the production of high density yeast cell-arrays.**

Coated Slides	Cells suspension	Slide washing
Poly-L-lysine	mQ water	mQ water
Concanavalin-A	mQ water + glycerol 7%	PBS 1X
SuperEpoxy 2	mQ water + glycerol 17%	Ethanol
Hydrogel	mQ water + glycerol 27%	
Superfrost plus gold	MM	
	MM + glycerol 7%	
	MM + glycerol 17%	
	MM + glycerol 27%	
	PBS 1X	
	PBS 1X + glycerol 7%	
	PBS 1X + glycerol 17%	
	PBS 1X + glycerol 27%	
	Sorbitol 0.5 M	
	Sorbitol 1 M	
	Sorbitol 1.5 M	

Effect of cell density on imaging

Cell density is critical to have spots where cells are not overlapped and are distributed over the entire area of the spot.

We started with 1.26×10^9 cells/ml (in MilliQ water) in the first well, followed for 7 serial dilutions of 1:2. For this, we used cells fixed as previously described and counted with the TC10™ Automated Cell Counter (BioRad).

After printing, poly-L-lysine (1 mg/ml) slides were centrifuged flat at 1500 x g for 5 minutes, washed with 1X PBS and mounted with mounting media (Fluoroshield™). The slides were visualized as described previously. Cells were counted manually. On average, 285 cells of 3 independent spots were analysed.

Aging of the cell arrays and fluorescence quality

The literature available about cell arrays does not clarify whether aging of the slides improves or degrades imaging quality [62, 60]. So, we perform an assay using a commercial poly-L-lysine slide (aged) and fresh coated poly-L-lysine (1 and 10 mg/ml) slides. After printing fixed cells in each slide, the array was treated as described above and analysed. We also tested coated-slides made in house after 8 and 30 days of coating. All slides were visualized on the day they were printed, as described previously. On average, 900 cells of 5 independent spots were analysed.

The yeast BY4743 strain used in this assay expresses a GFP fusion protein which allowed us to quantify cell fluorescence. The presence of fluorescent foci in cells was verified and the number of cells with such foci was counted manually. On average, 340 cells of 3 independent spots were analysed.

2.2.3 Effect of strain genotype and growth conditions on cell adhesion

Finally, we have tested whether the genotype of the yeast strains influenced binding to the glass slides. For this, we performed an assay with different yeast strains grown in 2 different media: rich (YPD) and minimal media. Yeast cells were fixed with 3.7% formaldehyde, and, then, printed onto poly-L-lysine-coated slides (1 mg/ml). After printing, slides were as described above and, on average, 350 cells of 3 independent spots were analysed.

2.3 Proteotoxic stress models

In order to check the reproducibility and feasibility of the cell-arrays technology to set up high throughput screens to identify genes involved in protein aggregation, we used ribosomal infidelity to destabilize the yeast proteome, which accelerates the formation of protein aggregates. Additionally, we have investigated the effect of various chemical stressors in promoting the formation of protein aggregates in yeast.

2.3.1 Plasmids

Previous studies in our laboratory have shown that misreading tRNAs can be used to destabilize the proteome [77]. We have taken advantage of such tRNAs cloned into the yeast single copy pRS315 vector, yielding the plasmid pUA261. New plasmids carrying mutant misreading tRNA genes were also constructed by site directed mutagenesis (SDM) so that a variety of codons can be mistranslated. The plasmids used are described in Table 2.2.

Table 2.2: **Description of the plasmids used.**

Plasmid	Description
pRS315	Plasmid of 6018 bp containing the Amp^R and LEU2 gene, allowing for selection of transformants in LB media with ampicilin or in yeast MM-Leu media, respectively. It is a single-copy vector.
pUA261	pRS315 plasmid containing one copy of *C. albicans* $tRNA_{UGA}^{Ser}$ gene cloned between BamHI and SalI restriction sites. For $tRNA_{UGA}^{Ser}$(Ser) expression in *S. cerevisae*.
pUA262	Plasmid constructed by SDM of the anticodon of $tRNA_{UGA}^{Ser}$ gene (pUA261) to originate $tRNA_{CAG(Leu)}^{Ser}$. For single-copy expression of mutant mistranslating $tRNA^{Ser}$(Leu) in *S. cerevisiae*.
pUA263	Plasmid constructed by SDM of the anticodon of $tRNA_{UGA}^{Ser}$ gene (pUA261) to originate $tRNA_{GUA(Tyr)}^{Ser}$. For single-copy expression of mutant mistranslating $tRNA^{Ser}$(Tyr) in *S. cerevisiae*.
pUA264	Plasmid constructed by SDM of the anticodon of $tRNA_{UGA}^{Ser}$ gene (pUA261) to originate $tRNA_{UUU(Lys)}^{Ser}$. For single-copy expression of mutant mistranslating $tRNA^{Ser}$(Lys) in *S. cerevisiae*.
pUA265	Plasmid constructed by SDM of the anticodon of $tRNA_{UGA}^{Ser}$ gene (pUA261) to originate $tRNA_{CGU(Thr)}^{Ser}$. For single-copy expression of mutant mistranslating $tRNA^{Ser}$(Thr) in *S. cerevisiae*.
pUA266	Plasmid constructed by SDM of the anticodon of $tRNA_{UGA}^{Ser}$ gene (pUA261) to originate $tRNA_{CAC(Val)}^{Ser}$. For single-copy expression of mutant mistranslating $tRNA^{Ser}$(Val) in *S. cerevisiae*.

Continued on next page

Table 2.2 – *Continued from previous page.*

Plasmid	Description
pUA267	Plasmid constructed by SDM of the anticodon of $tRNA_{UGA}^{Ser}$ gene (pUA261) to originate $tRNA_{UAU(Ile)}^{Ser}$. For single-copy expression of mutant mistranslating $tRNA^{Ser}$(Ile) in *S. cerevisiae*.
pUA268	Plasmid constructed by SDM of the anticodon of $tRNA_{UGA}^{Ser}$ gene (pUA261) to originate $tRNA_{UGC(Ala)}^{Ser}$. For single-copy expression of mutant mistranslating $tRNA^{Ser}$(Ala) in *S. cerevisiae*.
pUA269	Plasmid constructed by SDM of the anticodon of $tRNA_{UGA}^{Ser}$ gene (pUA261) to originate $tRNA_{UCC(Gly)}^{Ser}$. For single-copy expression of mutant mistranslating $tRNA^{Ser}$(Gly) in *S. cerevisiae*.
pUA801	Plasmid constructed by SDM of the anticodon of $tRNA_{UGA}^{Ser}$ gene (pUA261) to originate $tRNA_{CCU(Arg)}^{Ser}$. For single-copy expression of mutant mistranslating $tRNA^{Ser}$(Arg) in *S. cerevisiae*.
pUA802	Plasmid constructed by SDM of the anticodon of $tRNA_{UGA}^{Ser}$ gene (pUA261) to originate $tRNA_{AUG(His)}^{Ser}$. For single-copy expression of mutant mistranslating $tRNA^{Ser}$(His) in *S. cerevisiae*.
pUA803	Plasmid constructed by SDM of the anticodon of $tRNA_{UGA}^{Ser}$ gene (pUA261) to originate $tRNA_{CUC(Glu)}^{Ser}$. For single-copy expression of mutant mistranslating $tRNA^{Ser}$(Glu) in *S. cerevisiae*.
pUA804	Plasmid constructed by SDM of the anticodon of $tRNA_{UGA}^{Ser}$ gene (pUA261) to originate $tRNA_{GCA(Cys)}^{Ser}$. For single-copy expression of mutant mistranslating $tRNA^{Ser}$(Cys) in *S. cerevisiae*.
pUA805	Plasmid constructed by SDM of the anticodon of $tRNA_{UGA}^{Ser}$ gene (pUA261) to originate $tRNA_{AAA(Phe)}^{Ser}$. For single-copy expression of mutant mistranslating $tRNA^{Ser}$(Phe) in *S. cerevisiae*.
pUA806	Plasmid constructed by SDM of the anticodon of $tRNA_{UGA}^{Ser}$ gene (pUA261) to originate $tRNA_{CCA(Trp)}^{Ser}$. For single-copy expression of mutant mistranslating $tRNA^{Ser}$(Trp) in *S. cerevisiae*.
pUA807	Plasmid constructed by SDM of the anticodon of $tRNA_{UGA}^{Ser}$ gene (pUA261) to originate $tRNA_{AUU(Asn)}^{Ser}$. For single-copy expression of mutant mistranslating $tRNA^{Ser}$(Asn) in *S. cerevisiae*.
pUA808	Plasmid constructed by SDM of the anticodon of $tRNA_{UGA}^{Ser}$ gene (pUA261) to originate $tRNA_{CUG(Gln)}^{Ser}$. For single-copy expression of mutant mistranslating $tRNA^{Ser}$(Gln) in *S. cerevisiae*.

Continued on next page

Table 2.2 – *Continued from previous page.*

Plasmid	Description
pUA809	Plasmid constructed by SDM of the anticodon of $tRNA_{UGA}^{Ser}$ gene (pUA261) to originate $tRNA_{CAU(Met)}^{Ser}$. For single-copy expression of mutant mistranslating $tRNA^{Ser}$(Met) in *S. cerevisiae*.
pUA810	Plasmid constructed by SDM of the anticodon of $tRNA_{UGA}^{Ser}$ gene (pUA261) to originate $tRNA_{AGG(Pro)}^{Ser}$. For single-copy expression of mutant mistranslating $tRNA^{Ser}$(Pro) in *S. cerevisiae*.
pUA811	Plasmid constructed by SDM of the anticodon of $tRNA_{UGA}^{Ser}$ gene (pUA261) to originate $tRNA_{AUC(Asp)}^{Ser}$. For single-copy expression of mutant mistranslating $tRNA^{Ser}$(Asp) in *S. cerevisiae*.

2.3.2 Transformation of yeast cells

The transformation of yeast was performed using the LiAc/SS Carrier DNA/PEG method [22]. Yeast cells were inoculated onto minimal medium (MM-His) and incubated overnight at 30 °C, with 180 rpm shaking, until an OD_{600} of 0.4-0.5. Cells were then centrifuged (5000 rpm; 1 minute) in 1.5 ml microcentrifuge tubes. The supernatant was discarded and the transformation reagents were added to the pellet in the following order: 240 μl PEG 3500 (50% [w/v]), 36 μl 1.0 M LiAc, 50 μl boiled single-stranded carrier DNA (2.0 mg/ml), and 34 μl of an aqueous solution of the plasmid of interest (containing 0.5-4 μg plasmid). Microcentrifuge tubes were vortexed until a homogeneous suspension was obtained, followed by incubation at 42 °C for 40 minutes, in a Thermomixer comfort (Eppendorf). Cells were then centrifuged at maximum speed for 1 minute, the transformation mixture (supernatant) was discarded, and pellets were carefully resuspended in 200 μl of sterile mQ water. Each cell suspension was plated in selective medium plates (MM-His-Leu) and incubated at 30 °C, until isolated transformant colonies were visible (2-4 days).

2.3.3 Determination of protein aggregates

In order to visualize protein aggregates, we used a diploid BY4743 strain expressing an Hsp104-GFP fusion protein, constructed previously in our laboratory. For this, the GFP tag was fused inframe to the C-terminal coding region of the Hsp104 gene. The plasmid pKT128 (pFA6a-GFP(S65T)-His3MX) was used as a template for GFP amplification by PCR. This plasmid contains the *Schizosaccharomyces pombe* his5 gene as transformation marker and can be used in *Saccharomyces cerevisiae* for selecting positive clones. Cells containing the GFP fusion protein were transformed with the mutant misreading tRNAs using single-copy plasmids (Table 2.2), and positive transformants were selected in minimal medium lacking His and Leu. Yeast cells were grown up to middle exponential phase in 96-well plates and were then fixed with 3.7% formaldehyde for 1 hour at room temperature and washed (2x) in mQ water. These cells were printed onto a poly-L-lysine-coated slide (home made, with 1 mg/ml) using a High Throughput Automated Microarrayer (MicroGrid), and slides were centrifuged flat at 1500 x g and 12 °C for 5 minutes, washed in 1X PBS and mounting media (Fluoroshield™) was applied to them. Slides were then visualized using an epifluorescence up-right microscope Imager.Z1

(Zeiss) equipped with 38 HE GFP and Brightfield filters and an oil-immersion objective, 63X (Zeiss). The presence of fluorescent foci in cells was checked and their number was counted manually. On average, 950 cells of 5 independent spots were analysed.

2.3.4 Stress conditions

The effect of chemical stressor on the formation or mitigation of protein aggregates, was tested using the *Saccharomyces cerevisiae* BY4743 strain transformed with pRS315. Yeast cells grown overnight were transferred to a 96-well plate at an optical density of 0.25 and incubated with MM-Leu-His as a control or MM-Leu-His supplemented with the stressors indicated in Table 2.3. Cultures were incubated for 20 hours at 30 °C, or 37 °C (when high temperature was the stressor). For each condition, three clones of BY4743 strain with pRS315 were tested. After 20 h incubation, yeast cells were fixed with 3.7% formaldehyde for 1 hour at room temperature and washed (2x) in mQ water. The suspension of cells were printed onto a poly-L-lysine-coated slide (home made, with 1 mg/ml) using a High Throughput Automated Microarrayer (MicroGrid), and slides were centrifuged flat at 1500 x g and 12 °C for 5 minutes, washed in 1X PBS and mounting media (Fluoroshield™) was applied to them. Slides were visualized using an epifluorescence up-right microscope Imager.Z1 (Zeiss) equipped with 38 HE GFP and brightfield filters and an oil-immersion objective, 63X (Zeiss). The presence of brilliant dots in cells was checked and their number was counted manually. Moreover, total fluorescence of cells was quantified using Image J. On average, 290 cells of 4 independent spots for each of the three clones were analysed.

Table 2.3: **List of chemical stressors and respective concentrations used.**

Stress compound	**Concentration**
Arsenic trioxide	0.4 mM
Caffeine	2 mM and 10 mM
Calcium chloride	0.5 M and 0.75 M
Cadmium chloride	50 μM and 100 μM
Copper sulfate	2.5 mM
Chromium trioxide	0.2 mM and 0.5 mM
DTT	4 mM and 12 mM
Ethanol	2% and 5%
Geneticine	75 mg/l and 200 mg/l
Guanidine hydrochloride	3 mM
Hydrogen peroxide	5 mM and 10 mM
Lithium chloride	150 mM and 300 mM
Magnesium chloride	1 M
Menadione	10 μM, 90 μM and 150 μM
Paraquat	80 μg/ml
Potassium chloride	1 M
Sodium chloride	0.5 M and 1 M
SDS	0.01% and 0.015%
High temperature	37 °C

Chapter 3

Cell-arrays: Protocol optimization

3.1 Overview

We have optimized a method to print high density cell arrays which is based on contact printing technology developed for DNA and protein microarrays.

There is an increased need to miniaturization and parallelization of cell analysis methods, to achieve high throughput in the shortest and cheapest period of time. In this way cell arrays offer reduced assay volume and increased assay density. In fact, each spot of the array is treated as an independent experiment and, since typical spot sizes and spacings are hundreds of micrometers, this allows thousands of spots to be printed per slide. This high density of spots per slide is then quantified using automated microscopy and image-based analysis.

Since the first description of cell arrays, they have been applied to a wide variety of biological applications, as an experimental platform for miniaturizing and parallelizing genome wide gain- and loss-of-function studies. Therefore, this emerging technology offers opportunities to discover modulators of cellular function, identify genetic determinants of disease, and understand the complex and dynamic relationships between cells and their local environments [92].

In this chapter, we describe the optimization of a spotted cell array method based on the work of Narayanaswamy and colleagues (2006).

3.2 Results

3.2.1 Glass slides and cell preparation for printing

In order to optimize binding of yeast cells to coated glass slides, we have tested 5 different surfaces, namely: Poly-L-Lysine coated slide, Concanavalin-A-coated slide, SuperEpoxy Substrates; Hydrogel coated-Substrates and Gold substrates. These slides were tested simultaneously with fixed and non-fixed yeast cells, different cell suspension solutions and three different slide washing conditions (Material and Methods 2.2.2) (Figure 3.1 and Figures A.1-A.10, Appendix A).

Poly-L-lysine-coated glass slides are used to fabricate DNA and protein microarrays. In the latter case, proteins are immobilized non-covalently into the slides surface by printing proteins in PBS. For cell-arrays, poly-L-lysine promotes adherence of yeast cells to the slide surface by electrostatic interactions [62, 60].

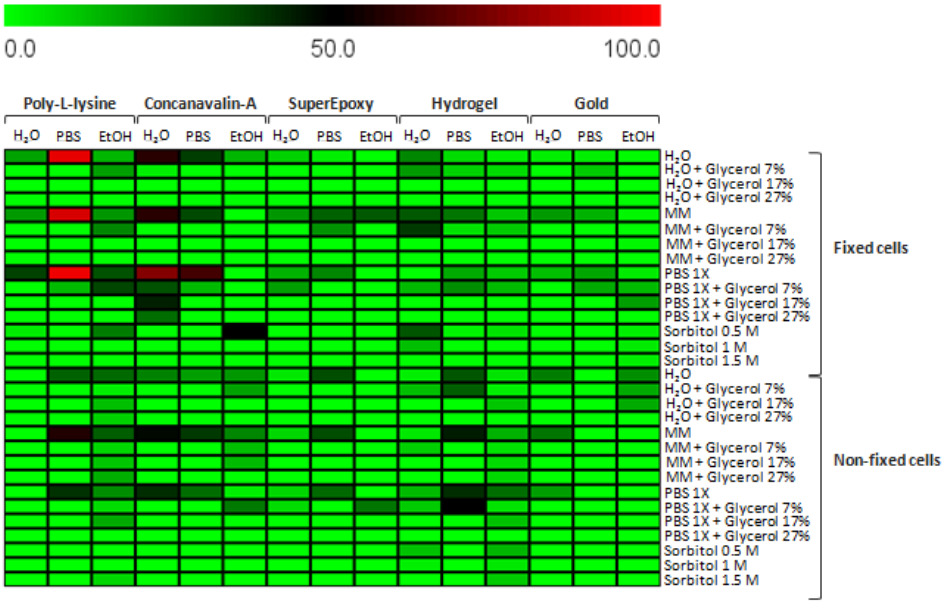

Figure 3.1: **Heat-map of the percentage of imageable cells obtained from the different conditions tested for the yeast cell-arrays protocol optimization.** In each column shows the percentage of imageable cells obtained with the different slide washing conditions (H_2O, PBS and EtOH − ethanol) and different coated glasse slides (Poly-L-lysine, Concanavalin-A, SuperEpoxy 2, Hydrogel, and Superfrost Plus Gold slides). Each row represents one of the different conditions used in the suspension of cells.

Our results show higher percentage of high quality imageable cells in poly-L-lysine-coated slides, but only when cells are fixed and suspended in media without glycerol or sorbitol prior to printing, and washed with 1X PBS (Figure 3.1). In contrast, almost all spots of cells treated with glicerol or sorbitol had few or no cells, or the percentage of imageable cells was very low. Printing of non-fixed yeast cells onto poly-L-lysine-coated slides showed higher percentages of imageable cells in spots corresponding to cells treated without glycerol or sorbitol, and slides washed with 1X PBS (Figure A.2, Appendix A).

Concanavalin-A-coated slides are also used to fabricate cell arrays, because lectin binds to mannose residues in the yeast cell wall [62]. We have also used concanavalin-A as a substrate for producing cell arrays (Figure 3.1 and Figures A.3 and A.4, Appendix A), however the percentage of imageable cells was lower than that obtained with poly-L-lysine slides. As with poly-L-lysine, several printing conditions were tested, but the general trend was lower adhesion of cells to the concavalin-A substrate.

SuperEpoxy slides were produced initially for protein-microarrays, because epoxy groups bind proteins covalently in several different ways and high number of amino acids reactive groups can be captured on this surface, namely primary amines, thiol and hydroxyl groups (http://arrayit.com/Products/Microarray_Slides/Epoxy_Slide/epoxy_slide). However, we were not able to identify binding conditions which would promote efficient adhesion of yeast cells to SuperEpoxy slides (Figure 3.1 and Figures A.5 and A.6, Appendix A).

NEXTERION® Slide H is used for printing protein microarrays by covalent immobilization of peptides and proteins. The coating of this slide consists of a cross-linked polymer layer ac-

tivated with N-Hydroxysuccinimide (NHS) esters to provide covalent immobilization of amine groups. The terminal amino of amino-modified nucleic acids and glycans react irreversibly with the NHS-ester groups to form a covalent bond. Proteins and other biomolecules bind *via* amine-groups exposed on their surfaces (http://www.us.schott.com/nexterion/english/products/coated_slides/thin_film.html). Our data showed that this is not a suitable substrate for production of yeast cell-arrays, because the percentage of imageable cells was low in all conditions tested (Figure 3.1 and Figures A.7 and A.8, Appendix A).

Gold substrates are also used to produce DNA and protein-microarrays. Thermo Scientific* Superfrost Plus Gold Slides are made with an advanced adhesive technology and are specifically designed for frozen tissue sections (http://www.menzel.de/Adhesion_Slides.678.0.html?L=1). However, our data showed that this substrate is not adequate for producing yeast cell arrays since binding of yeast cells to it was low in all conditions tested (Figure 3.1 and Figures A.9 and A.10, Appendix A).

Our data show differences between fixed and non-fixed cells. In particular, significant differences were observed in the percentage of localized GFP foci between fixed and non-fixed cells (Figure A.11-A.20, Appendix A), suggesting that the protocol used for slide definitive preparations could introduce stress in the cell and promote formation of protein aggregation. In order to verify this issue we have analysed GFP distribution in fixed and non-fixed cells in fresh slides (without mounting media) and in definitive preparations of the slides (Figure 3.2 and Figure 3.3). There was a significant increase in the percentage of imageable non-fixed cells, however it was attenuated in definitive preparations (with mounting) of fixed cells.

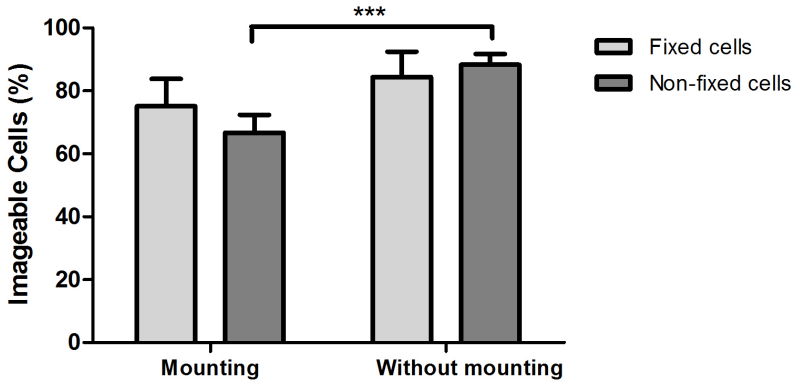

Figure 3.2: **Effect of cell fixation and mounting on the percentage of imageable yeast fixed and non-fixed cells.** Data represent the mean ± s. d. of 5 independent images (***p<0.001 Unpaired t test with CI 95%).

With respect to fluorescence distribution, the differences between fixed and non-fixed cells in definitive preparations (with mounting) was statistically significant, conversely to what was observed in fresh preparations (Figure 3.3), suggesting that the mounting media stressed live cells, leading to an increase of the presence of GFP foci and to decreased yeast cell survival.

We have also tested the effect of washing the glass slides with MilliQ water, 1X PBS and 95% ethanol prior to cell imaging, on the quality of the images. As the best results were obtained with fixed cells suspended in media without glycerol and sorbitol, it is possible to observe in detail the percentage of imageable cells in cells suspended in MilliQ water, 1X PBS

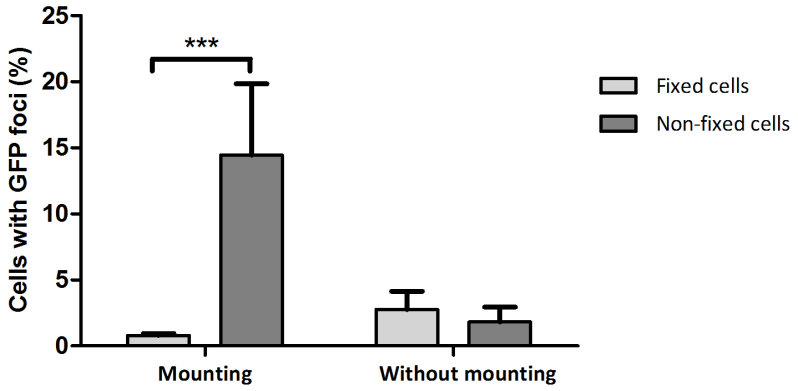

Figure 3.3: **Percentage of fixed and non-fixed yeast cells with GFP foci.** Data represent the mean ± s. d. of 5 independent images (***p<0.001 Two-way RM ANOVA post Bonferroni's test with CI 95%). Means are significantly different using or no mounting media (Unpaired t test with CI 95%).

and MM, Figure 3.1 and in Figures A.21 to A.23, Appendix A.

The higher percentage of imageable cells was obtained with poly-L-lysine slides and fixed cells resuspended in MilliQ water and 1X PBS, after slide washing with 1X PBS. The other types of slides had a mean of percentages of imageable cells lower than 90% ($p<0.05$, Wilcoxon Signed Rank Test with CI 95%).

Slides washing with MilliQ water produced the best results in concanavalin-A coated slides with fixed cells resuspended in PBS. However, the mean of imageable cells was below 90% ($p=0.0495$, Wilcoxon Signed Rank Test with CI 95%). In the other slide types, the mean of imageable cells was below 60% ($p<0.05$, Wilcoxon Signed Rank Test with CI 95%).

Using ethanol as wash solution, in all slides, the mean of percentages of imagebale cells was below 60% ($p<0.05$, Wilcoxon Signed Rank Test with CI 95%), indicating that ethanol washing should be avoid.

Another parameter tested in this assay was temperature of array centrifugation (4, 12 and 20 °C) (Figure 3.4). The best imaging results were obtained with a centrifugation temperature step of 12 °C. Other temperatures, in particular 20 °C, reduced the percentage of imageable cells.

The above data indicated therefore that cells fixed in 3.7% formaldehyde for 1 hour at room temperature, washed in MilliQ water or 1X PBS, and printed onto poly-L-lysine-coated slides using a High Throughput Automated Microarrayer (MicroGrid) produced the best imaging results. Imaging could be improved by centrifuging the slides at 1500 x g and 12 °C for 5 minutes, washing in 1X PBS, and mounting in appropriate media. This produces definitive slide preparations that can be imaged by fluorescence microscopy multiple times.

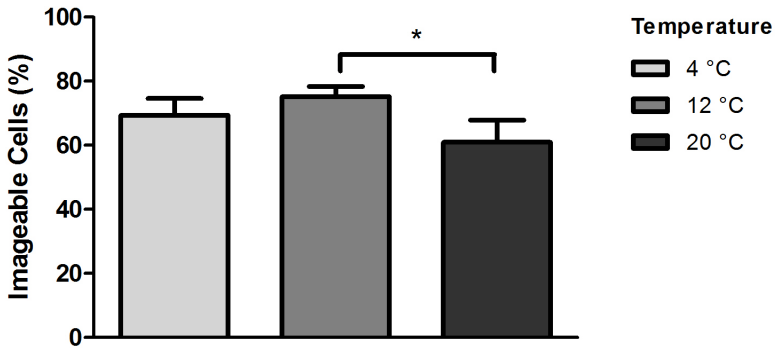

Figure 3.4: **Effect of the temperature of array centrifugation on cell imaging quality.** Data represent the mean ± s. d. of 5 independent spots (*p<0.05 One-way analysis of variance post Tukey's Multiple Comparison test with CI 95%).

3.2.2 Effect of cell density on imaging

In order to optimize the printing process we have also tested the density of cells in the printing master plates. For this, we used multiwell plates (384 wells) and 1.26x10^9 cells/ml (in MilliQ water) as the starting printing solution, followed for 7 serial 1:2 dilutions.

Only the spots printed from wells containing 1.26x10^9 cells/ml and 5.14x10^8 cells/ml produced imageable cells on the array (Figure 3.5). The percentage of imageable cells printed from 1.26x10^9 cells/ml or 5.14x10^8 cells/ml stocks was similar, but the number of cells in each printed spot was lower in the latter case (Figure 3.6). This suggested that cell density should be approximately 10^9 to obtain the best results (Figure 3.7).

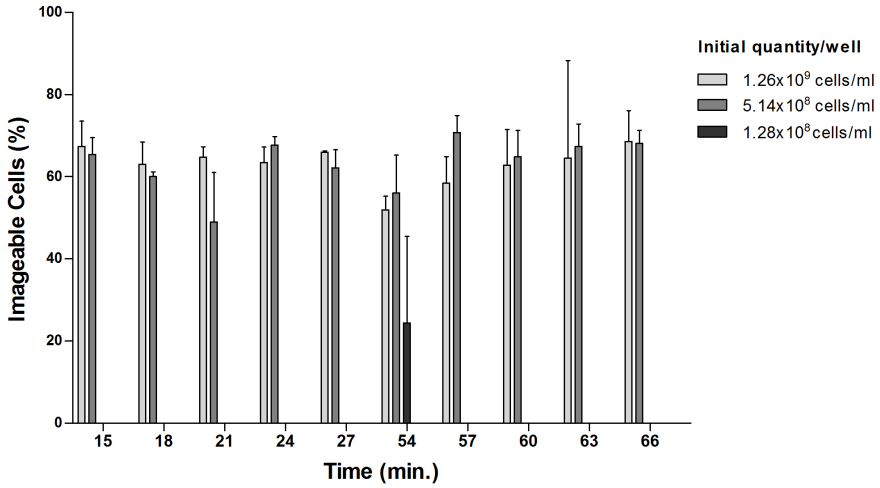

Figure 3.5: **Effect of cell density on the percentage of imageable cells on the array.** For printing purposes, cell stocks were prepared in 384-well plates at various densities and printed directly onto the glass slides. Data represent the mean ± s. d. of 3 independent spots. The medians do not vary significantly in each initial well (Kruskal-Wallis post Dunn's Multiple Comparison test with CI 95%).

Starting with stocks of 10^9 cells/ml allowed us to obtain an average of 500 cells per spot on the array (Figure 3.6). Increased spot cell density resulted in overlapping of cells, which reduced the number of cells that could be imaged.

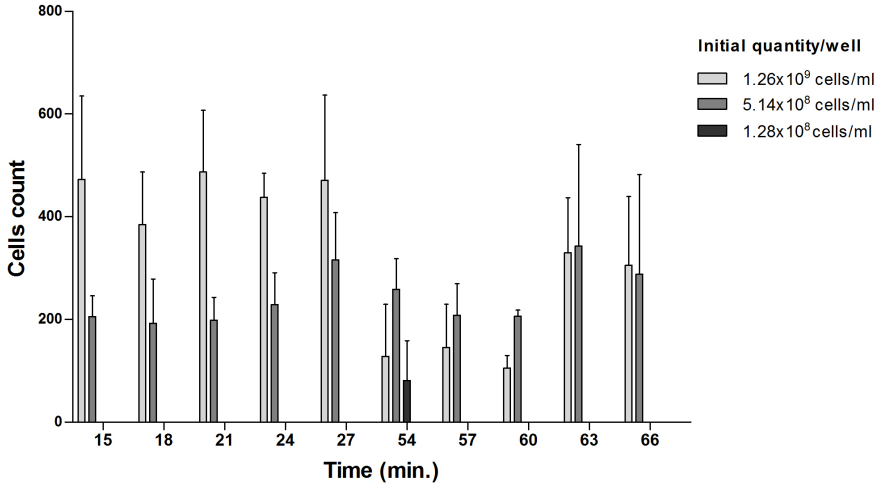

Figure 3.6: **Effect of cell density on the total number of imageable cells on the array.** For printing purposes, cell stocks were prepared in 384-well plates at various densities and printed directly onto the glass slides. Data represent the mean ± s. d. of 3 independent spots. The medians do not vary significantly in each initial quantity of well (Kruskal-Wallis post Dunn's Multiple Comparison test with CI 95%).

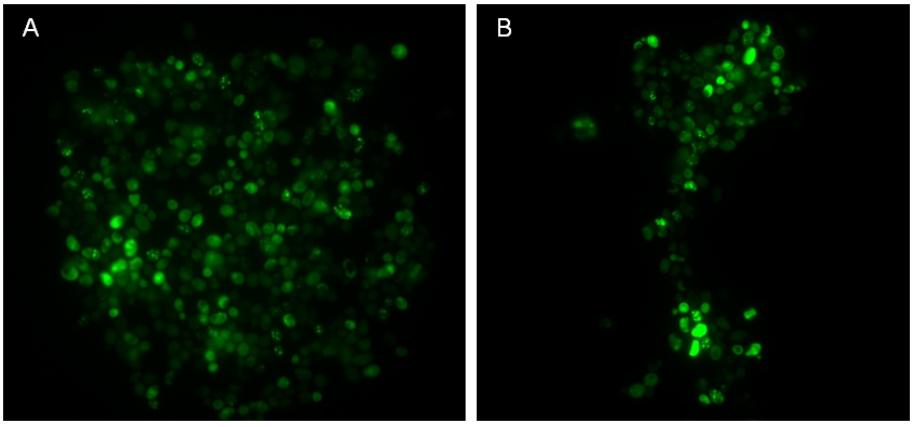

Figure 3.7: **Effect of cell density on imaging quality.** For printing purposes, cell stocks were prepared in 384-well plates at various densities and printed directly onto the glass slides. A) Image of a spot printed from a 1.26x10^9 cells/ml stock; B) Image of a spot printed from a 5.14x10^8 cells/ml stock.

3.2.3 Aging of the cell arrays and fluorescence quality

In routine DNA-microarrays, poly-L-lysine coated slides are used after 2 weeks to 1 month post-coating, to allow the surface to become sufficiently hydrophobic [60]. In contrast, for cells-arrays, Narayanaswamy and colleagues (2006) suggested that only freshly prepared slides can be used for each printing run. Since the hydrophobicity is also important to promote electrostatic interactions between poly-L-lysine and the yeast cell wall, we performed an assay using commercial poly-L-lysine slides (aged) and freshly coated poly-L-lysine (1 and 10 mg/ml) slides (Figure 3.8). Our data showed higher percentage of imageable cells in aged (8 days) slides, and the difference was statistically significant for slides coated with 1 mg/ml of poly-L-lysine.

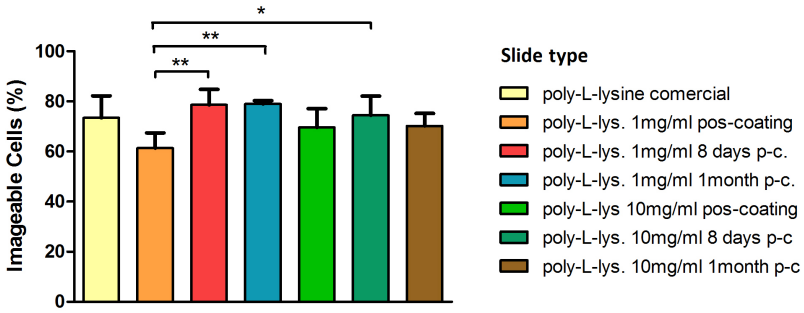

Figure 3.8: **Effect of aging of slides coating on cell imaging.** Data represent the mean ± s. d. of 5 independent spots. ($^{*}p<0.05$ and $^{**}p<0.01$ One-way analysis of variance post Tukey's Multiple Comparison test with CI 95%).

We have also tested the effect of aging on the fluorescence of printed slides (8 days, 3 weeks, and/or 1 month after printing) (Figures 3.9-3.13). The fluorescence in 3 types of poly-L-lysine slides was compared and in all cases there was a decrease in fluorescence over time.

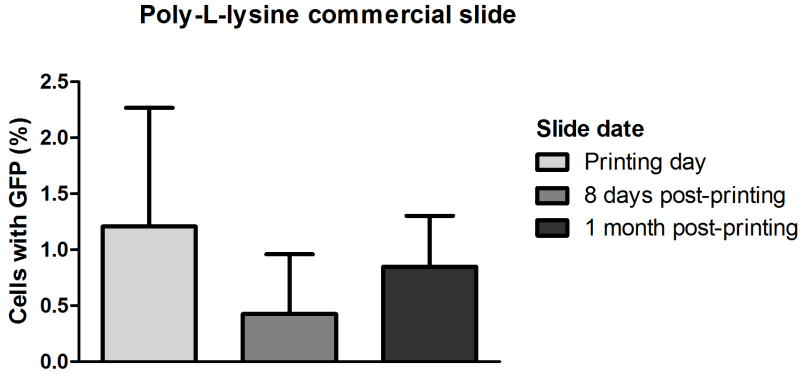

Figure 3.9: **Effect of aging on the fluorescence of printed slides. Commercial poly-L-lysine was used for this assay.** Data represent the mean ± s. d. of 3 independent spots. For statistical analysis, Kruskal-Wallis post Dunn's Multiple Comparison test with CI 95% was performed and medians don't vary significantly (Printing day: s. d. = 1.060; 8 days post-printing: s. d. = 0.5327; 1 month post-printing: s. d. = 0.4561).

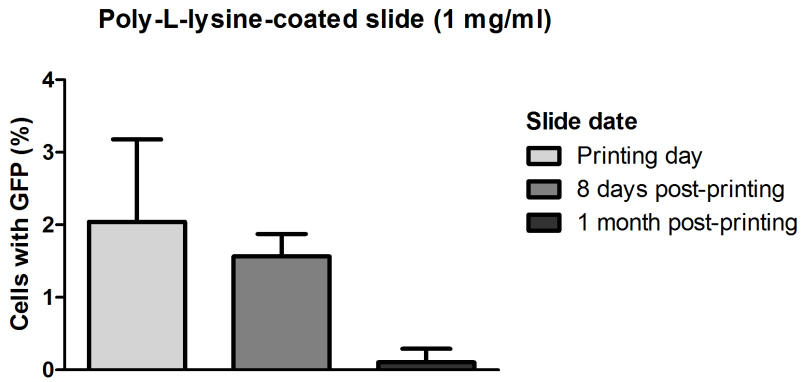

Figure 3.10: **Effect of aging on the fluorescence of printed slides. Slides coated with 1 mg/ml of poly-L-lysine were used in this assay.** The printing and coating were done in the same day. Data represent the mean ± s. d. of 3 independent spots. For statistical analysis, Kruskal-Wallis post Dunn's Multiple Comparison test with CI 95% was performed and medians don't vary significantly (Printing day: s. d. = 1.138; 8 days post-printing: s. d. = 0.3075; 1 month post-printing: s. d. = 0.1848).

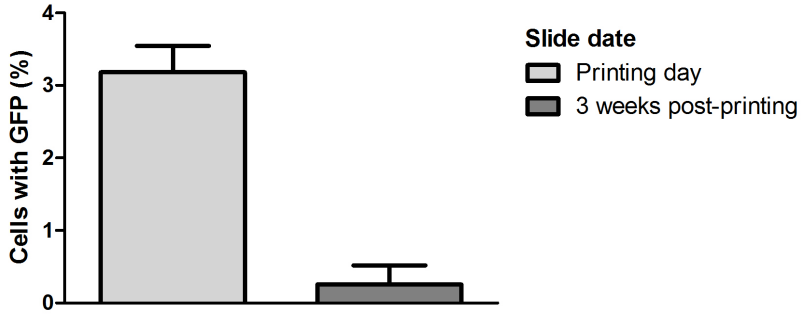

Figure 3.11: **Effect of aging on the fluorescence of printed slides. Slides coated with 1 mg/ml of poly-L-lysine were used in this assay.** Printing step was done 8 days post-coating. Data represent the mean ± s. d. of 3 independent spots. For statistical analysis, Mann Whitney test with CI 95% and the medians are significantly different (Printing day: s. d. = 0.3636; 3 weeks post-printing: s. d. = 0.2601).

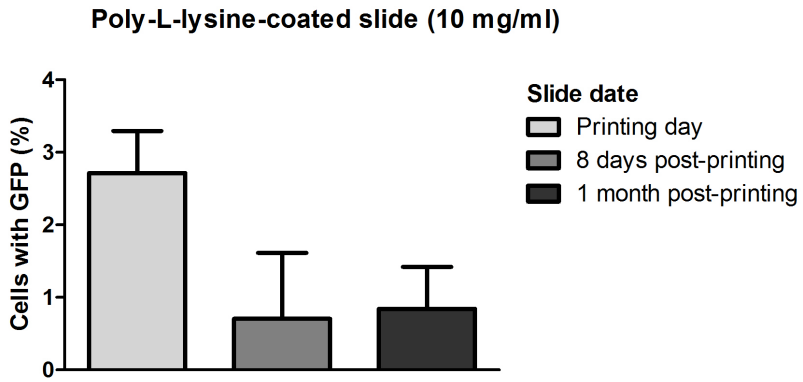

Figure 3.12: **Effect of aging on the fluorescence of printed slides. Slides coated with 10 mg/ml of poly-L-lysine are used in this assay.** The printing and coating were done in the same day. Data represent the mean ± s. d. of 3 independent spots. For statistical analysis, Kruskal-Wallis post Dunn's Multiple Comparison test with CI 95% was performed and medians vary significantly (Printing day: s. d. = 0.5801; 8 days post-printing: s. d. = 0.9074; 1 month post-printing: s. d. = 0.5813).

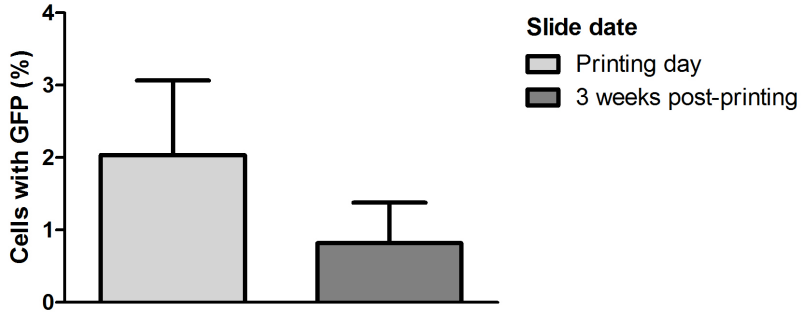

Figure 3.13: **Effect of aging on the fluorescence of printed slides. Slides coated with 10 mg/ml of poly-L-lysine are used in this assay.** Printing step was done 8 days post-coating. Data represent the mean ± s. d. of 3 independent spots. For statistical analysis, Mann Whitney test with CI 95% and the medians aren't significantly different (Printing day: s. d. = 1.030; 3 weeks post-printing: s. d. = 0.5576).

3.2.4 Effect of strain genotype and growth conditions on cell adhesion

In order to clarify if the strain genotype was relevant for the efficient production of yeast arrays we have carried out an assay using different yeast strains grown in 2 different media: rich (YPD) and minimal medium (Figure 3.14). Imageable cell spots were obtained with all strains tested (Figure 3.14), however significant differences in the percentage of cells per spot were observed. This suggests that for optical imaging printing conditions may have to be optimized for each strain and growth medium.

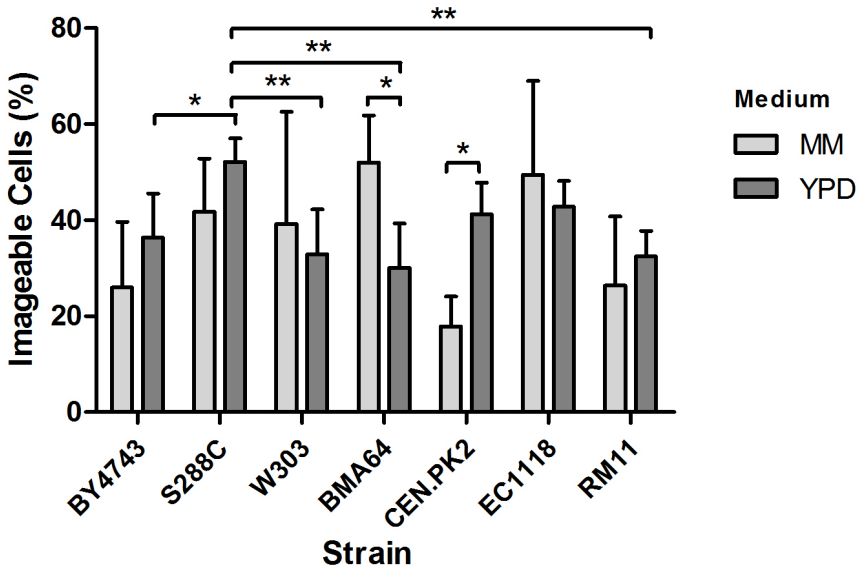

Figure 3.14: **Effect of strain genotype and growth media on cell printing.** Data represent the mean ± s. d. of 5 independent spots for each medium ($^{*}p<0.05$ Two-way RM ANOVA post Bonferroni's test with CI 95% and $^{*}p<0.05$ and $^{**}p<0.01$ One-way analysis of variance post Tukey's Multiple Comparison test with CI 95% to compare strains in YPD medium).

3.3 Discussion

As for DNA and proteins, cell-arrays are being developed for high content genetic screens, whose applications range from basic research to biomedicine. The starting point for these techniques is the ability to immobilize cells, cell lysates and molecules on solid surfaces. For DNA and protein microarrays, there is a rising number of slides surfaces. However, the immobilization of cells is more complex and less developed due to difficulties associated to the complexity of the cell membrane and cell wall that contain many types of molecules, namely, proteins, lipids, sugars, etc. [60]. Indeed, the yeast cell wall represents 15 to 30% of the cell dry weight and is formed by three main groups of polysaccharides: polymers of glucose (β-glucan, 60% of the cell wall dry mass), polymers of mannose (mannoproteins, 40% of the cell dry mass) and polymers of N-acetylglucosamine (chitin, 2% of the cell dry mass) [2]. Moreover, the linkage of the other constituents of the cell wall (inner and outer walls) occurs through branched β-1,6 glucan. The β-1,3 glucan-chitin complex is the major component of the inner wall, while mannoproteins are on the outer surface of the wall and are extensively O and N glycosilated. In other words, the yeast cell walls has an anionic surface due to the presence of negatively charged phosphate groups in the carbohydrate side-chains, and these glycans form helical (β-1,3 glucan) and ribbon-like (chitin) structures that have non-hydrogen ring constituents in an equatorial position [49].

For the production of yeast cell-arrays, the substrates described in the literature are poly-L-lysine and concanavalin-A. The first substrate promotes adherence of yeast cells by electrostatic interactions [62, 60], while the second takes advantage of the binding of lectin to mannose residues in the yeast cell wall [62]. We have tested 3 additional substrates that are normally used for the production of protein microarrays: Thermo Scientific* Superfrost Plus Gold Slides, SuperEpoxy 2 slide and Hydrogel-coated substrate.

Superfrost Plus Gold Slides are specifically designed for frozen tissue sections, but our results showed that this surface does not bind yeast cells efficiently (Figure 3.1 and Figures A.9 and A.10, Appendix A). Even when using different cells suspension buffers and different solutions to wash the slides after printing.

SuperEpoxy Substrates and NEXTERION® Slide H are usually used for printing protein-microrrays due to their capacity to bind proteins covalently. In the first case, epoxy groups bind to primary amines, thiol and/or hydroxyl groups of proteins. In the second case, slides are coated with a cross-linked polymer layer activated with N-Hydroxysuccinimide (NHS) esters, which react irreversibly with the terminal amino of amino-modified nucleic acids and glycans. Our data showed poor binding of yeast cells to these slides (Figure 3.1 and Figures A.5-A.8, Appendix A). However, hydrogel-coated slides were slightly better than the others, probably because this substrate can also react with glycans that are abundant in the yeast cell wall, whereas SuperEpoxy substrates only react with proteins.

Our best results were obtained with Concanavalin-A and Poly-L-Lysine-coated slides prepared in house (Figure 3.1 and Figures A.1-A.4, Appendix A). For concanavalin-A-coated slides, efficient cell binding was obtained by washing the slides with MilliQ water, whereas the best results with poly-L-lysine-coated slides were the obtained by washing slides with 1X PBS. This was somewhat expected because the concanavalin-A lectin binds to mannose, which is abundant in the yeast cell wall, while poly-L-lysine is a positively charged amino acid polymer and the yeast cell wall has an anionic surface, allowing for strong electrostatic interactions to occur between the two surfaces [2, 49, 62, 60].

Conversely to what is described in the literature [62], glycerol and sorbitol produced poor

binding results in all slides and conditions tested (Figure 3.1 and Figures A.1-A.10, Appendix A), while MilliQ water, PBS and MM produced the best results. Glycerol increased viscosity and lowered evaporation producing spots with regular shape, but decreased binding strongly due to its hydrophobic properties.

Considering all variables, including the price of commercial slides (Figure 3.15), we conclude that the poly-L-lysine-coated slides (1 mg/ml) produced in house are the best for producing cell-arrays.

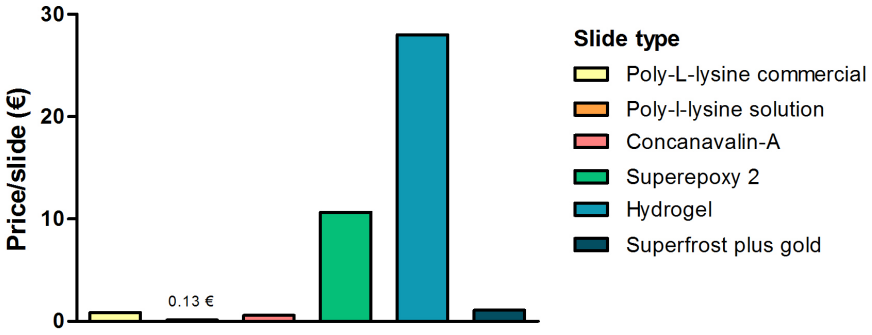

Figure 3.15: **Comparative analysis of the price of microarrays slides.**

The higher percentages of imageable cells was obtained when slides were washed with PBS, which is isotonic and non-toxic to the cells (Figure A.22, Appendix A). In contrast, lower percentages of imageable cells were obtained when the slides were washed with 95% ethanol (Figure A.23, Appendix A).

Cell-arrays are a high-throughput technique to perform large scale genetic screens. We have used a GFP-Hsp104 reporter to test whether we could use our cell arrays to detect protein aggregates. Fixed or non-fixed yeast cells were used and our data clearly shows that live cells displayed a higher percentage of GFP labelled foci in definitive preparations (Figure 3.3). This was not observed in live cells in fresh preparations, without mounting media, suggesting that the mounting media stressed cells and promoted formation of protein aggregates. In other words, one should be careful when preparing the yeast cell arrays for proteotoxic stress analysis to avoid introducing artefacts due to the cell preparation protocol.

The overall data shows that the best protocol for producing yeast cell-arrays is the following: yeast cells grown in MM/YPD at 30 °C until culture reaches 10^9 cells/ml; yeast cells should be fixed with 3.7% formaldehyde for 1 hour at room temperature and washed (2x) in MilliQ water. Cells should be printed onto poly-L-lysine-coated slides (1 mg/ml) using a High Throughput Automated Microarrayer (MicroGrid). After printing slides should be centrifuged at 1500 x g and 12 °C for 5 minutes, washed in 1X PBS and mounted using Fluoroshield™ mounting media.

Chapter 4

Proteotoxic Stress

4.1 Overview

Cells respond to changes in environmental conditions that disturb their normal physiology or threaten their survival. The response and adaptation to stress involves complex mechanisms that lead to regulation of cell growth and proliferation, adjustments of gene expression and metabolic activity. These adaptations are necessary to protect cells from the detrimental effects of stress and to allow for repairing damaged cellular components [32].

Some stressors induce accumulation of aggregated proteins that trigger a proteotoxic stress response [27, 54].

Cells respond to protein aggregation by inducing and/or up-regulating the expression of molecular chaperones which help refolding or degrading aggregated proteins [32]. The chaperone genes induced as part of the environmental stress response include small heat shock proteins (HSP12, HSP26, and HSP48), members of the Hsp70 family of chaperones (SSA4, SSE2, HSP78), and Hsp104. The latter is an ATPase that dissociate aggregated proteins (disaggregase), allowing Hsp70 chaperones to bind and refold them back into native and functional conformations [17, 30, 32, 63, 72]. Denatured proteins that cannot be refolded are targeted for degradation through the ubiquitin-proteasome pathway [30, 32], which also plays a role in the alteration of the cellular protein content during stress adaptation. The efficient elimination of potentially toxic proteins is an important selective advantage, and the inability to do so can lead to disease, in particular to neurodegenerative diseases [54].

Many studies have already been carried out on the yeast stress response to understand mechanisms of stress adaptation. In this chapter, we investigate the role of various chemical stressors in the formation of protein aggregates in yeast. We also use ribosomal infidelity to destabilize the proteome in order to accelerate the formation of protein aggregates in the absence of environmental stress.

4.2 Results

4.2.1 Mistranslation induces protein aggregation

In order to destabilize the yeast proteome we have used a series of mutant tRNAs that misincorporate serine at 19 non-cognate codons. This mutagenises proteins on a global scale, decreasing their stability and folding rate. We then compared the toxicity of the mutant

tRNAs *in vivo* in yeast BY4743 strain co-transformed with a GFP-Hsp104 reporter system. As mentioned before, Hsp104 is a disaggregase and its induction and cellular distribution are indicative of increased protein aggregation in the cell [17, 83]

Yeast cells expressing the Hsp104-GFP reporter system and transformed with the mutant tRNAs genes were printed onto an array, using the optimized protocol of cell-arrays production described previously. The slide array was analyzed by epifluorescence microscopy in order to detect protein aggregates (Figure 4.1). The number of cells containing GFP fluorescence foci was quantified and data showed significant increase in localized Hsp104-GFP in cells expressing $tRNA^{Ser}$ (Gln) (*), $tRNA^{Ser}$ (Glu) (**), $tRNA^{Ser}$ (Ser), $tRNA^{Ser}$ (Leu), $tRNA^{Ser}$ (Thr), $tRNA^{Ser}$ (Val), $tRNA^{Ser}$ (Ala), $tRNA^{Ser}$ (Gly), $tRNA^{Ser}$ (Arg), $tRNA^{Ser}$ (His), $tRNA^{Ser}$ (Asn), $tRNA^{Ser}$ (Met), and $tRNA^{Ser}$ (Pro) (***) relative to control (pRS315) (Figure 4.2).

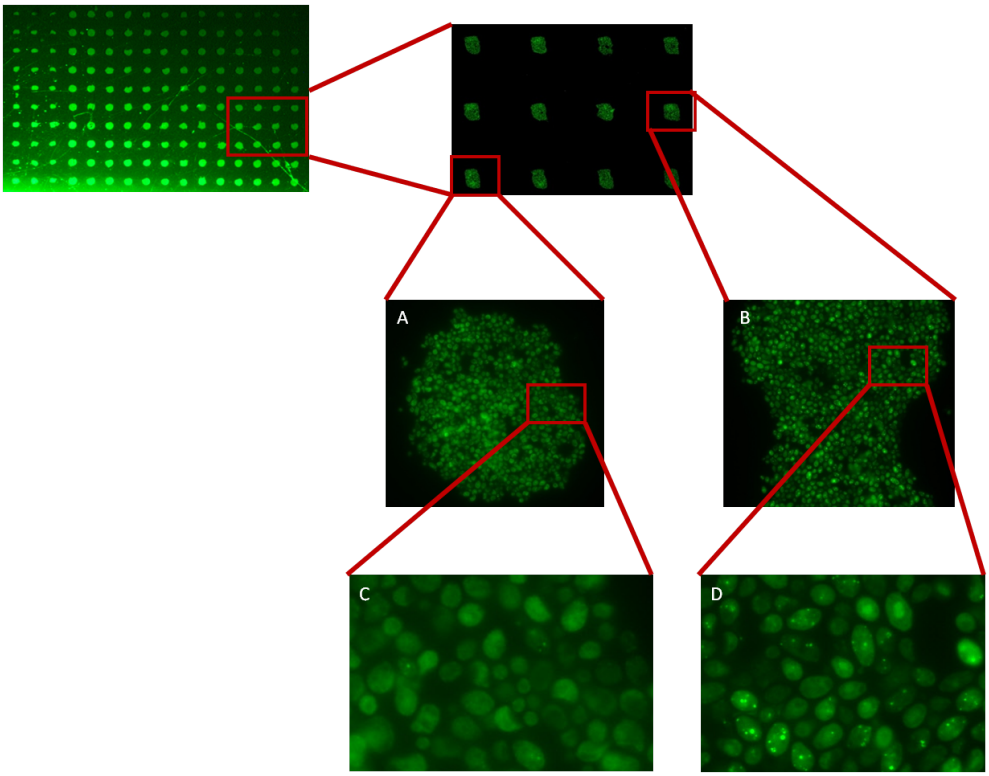

Figure 4.1: **Gene mistranslations induce formation of protein aggregates.** Yeast cells expressing the Hsp104-GFP reporter protein were transformed with pRS315 (A and C), $tRNA_{UGA(Ser)}{}^{Ser}$ and mistranslating $tRNA^{Ser}$ (B and D: $tRNA_{CAG(Leu)}{}^{Ser}$). Cells were allowed to grow to middle exponential phase, were fixed with 3.7% formaldehyde, printed on an array and were observed by fluorescence microscopy (63X objective). Cells expressing the $tRNA_{CAG(Leu)}{}^{Ser}$ showed localized Hsp104-GFP fluorescence, indicating the presence of protein aggregates.

Besides the total number of cells with protein aggregates in each array spot, other characteristics were studied, namely, the size of the aggregates and the number of aggregates per cell. The data show that each type of mistranslation has slightly different phenotypes in terms of protein aggregation (Figures 4.3 and 4.4).

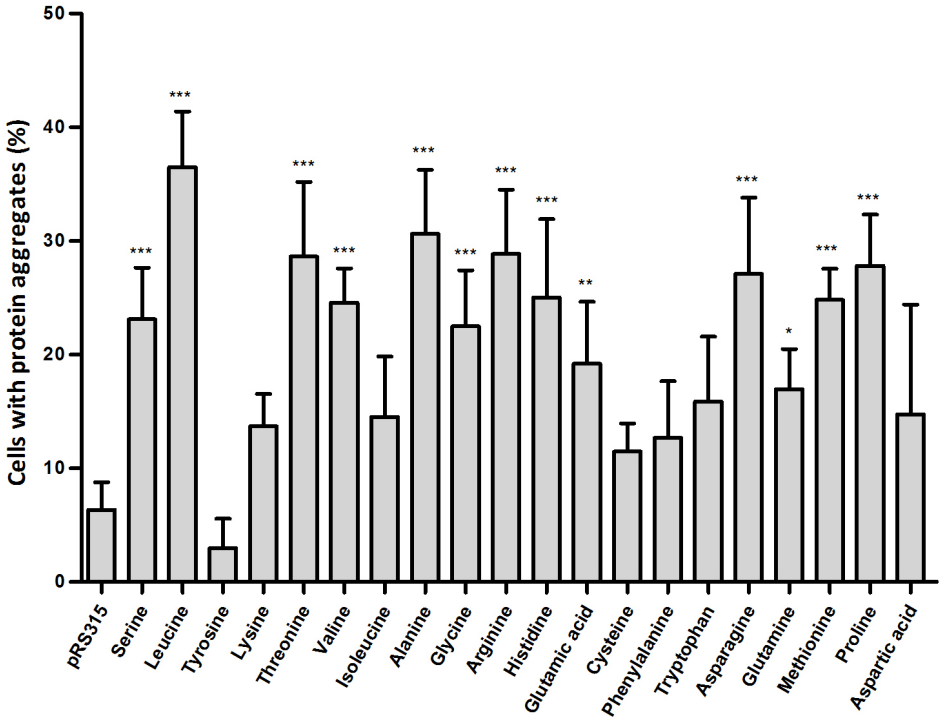

Figure 4.2: **Effect of mistranslation on the formation of protein aggregates.** The plots show the percentage of yeast cells containing localized Hsp104-GFP fluorescence foci. Results are expressed as the percentage of positive cells (with Hsp104-GFP foci) per cell array spot. Data represent the mean ± s. d. of three independent spots from arrays ($^{***}p<0.001$, $^{**}p<0.01$, $^{*}p<0.05$ one-way Anova post Dunnett's multiple comparison test with CI 95% relative to pRS315).

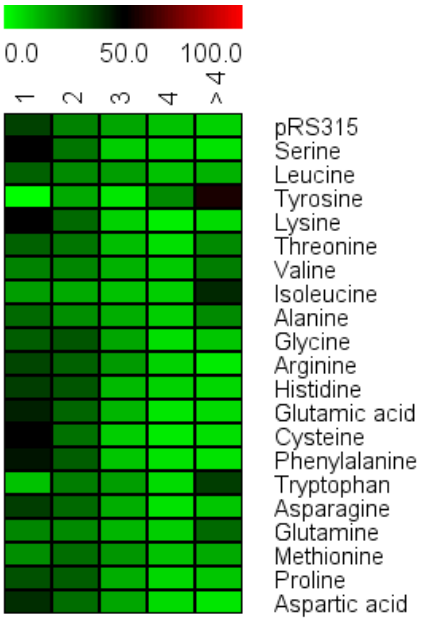

Figure 4.3: **Heat-map representing the number of protein aggregates per cell.** Yeast cells containing localized Hsp104-GFP fluorescence foci were counted and differentiated according to the number of localized Hsp104-GFP fluorescence foci per cell. Results are expressed as the percentage of positive cells (with Hsp104-GFP foci) relative to the total number of cells with protein aggregates per spot. Data represent the mean of three independent spots from arrays.

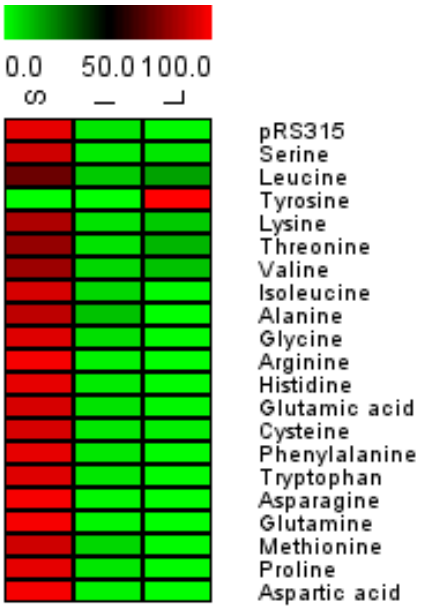

Figure 4.4: **Heat-map representing the different types of aggregates produced by misreading.** Yeast cells containing localized Hsp104-GFP fluorescence foci were counted and differentiated according to the size of localized Hsp104-GFP fluorescence foci per cell. Results are expressed as the percentage of positive cells (with Hsp104-GFP foci) relative the total number of cells with protein aggregates per array spot. Data represent the mean of three independent spots from arrays. S – small protein aggregates; I – intermediate protein aggregates; L – large protein aggregates.

4.2.2 Chemical stressors induce protein aggregation

In order to better understand the effects of known chemical stressors in the cell, we performed an assay where yeast cells (BY4743 *S. cerevisiae* strain) were exposed to specific stressors. Protein aggregation was then monitored using the Hsp104-GFP reporter protein described above. Cells were grown in presence of different stress conditions (Table 2.3), during 20 hours, and were then printed onto a cell array, according to the optimized protocol of cell-arrays described previously. The slide array was analyzed by epifluorescence microscopy in order to detect protein aggregates (Figure 4.5). The data showed significant increase in localized Hsp104-GFP in cells grown in presence of calcium chloride (0.5 M), cadmium chloride (100 μM), chromium trioxide (0.5 mM), geneticine (75 mg/l and 200 mg/l), lithium chloride (150 mM and 300 mM), magnesium chloride (1 M), menadione (150 μM) and high temperature (37 °C). Our data showed that cells exposed to different chemical stressors produce different types of aggregates (Figures 4.7 and 4.8).

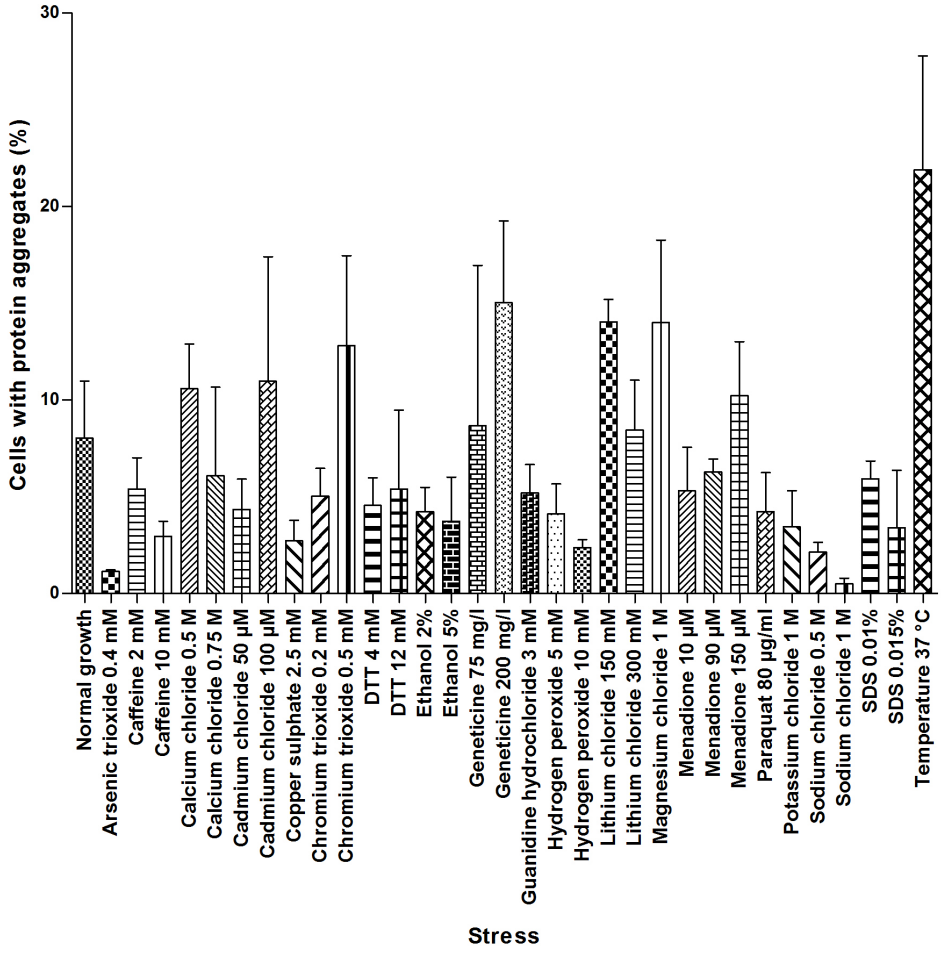

Figure 4.5: **Effect of chemical stressors on protein aggregation.** The plots show the percentage of yeast cells with protein aggregates (localized Hsp104-GFP fluorescence foci) that were exposed to 32 different chemical conditions. Results are expressed as the percentage of positive cells (with Hsp104-GFP foci) relative to the total number of cells per spot. Data represent the mean ± s. d. of three independent clones, obtained from three different spots from arrays. For statistical analysis, One-way analysis of variance test was performed and means are significantly different from control (normal growth), $p<0.0001$.

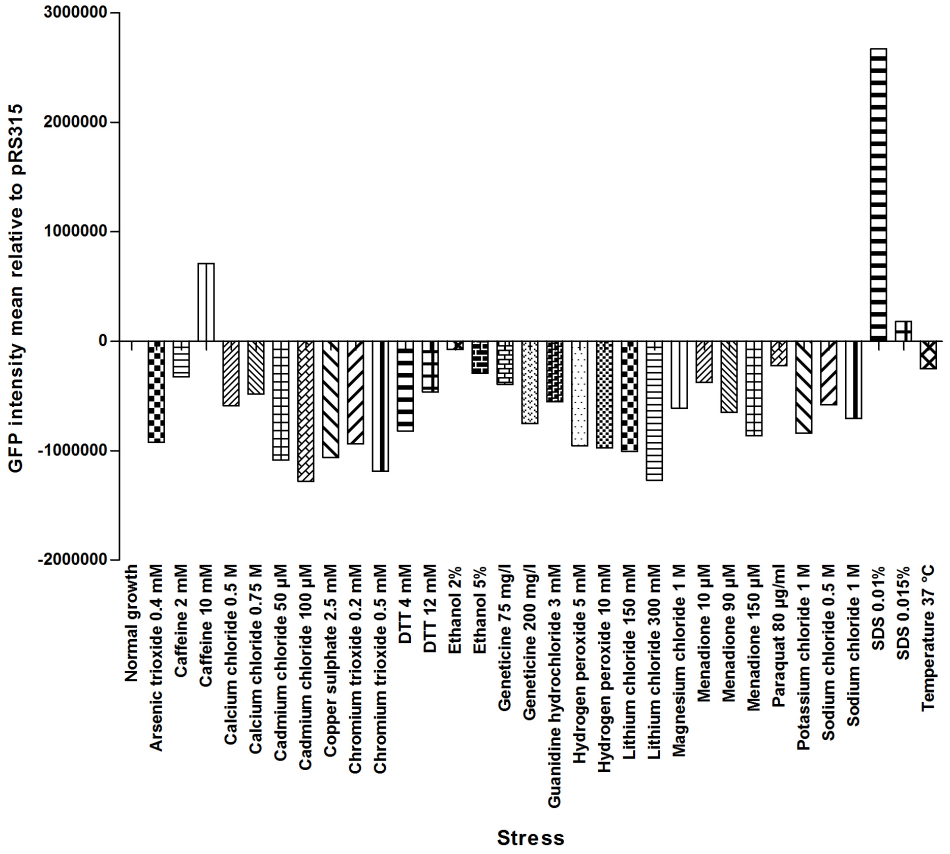

Figure 4.6: **Relative quantification of total fluorescence in cells exposed to different chemical stressors.** Total fluorescence of Hsp104-GFP fusion protein expressed in yeast cells exposed to 32 different chemical conditions was quantified using Image J. Data represent the mean of three independent clones relative to the control (intensity = 0; normal growth condition). One-way analysis of variance test was performed and means are significantly different from control (normal growth), $p<0.0001$.

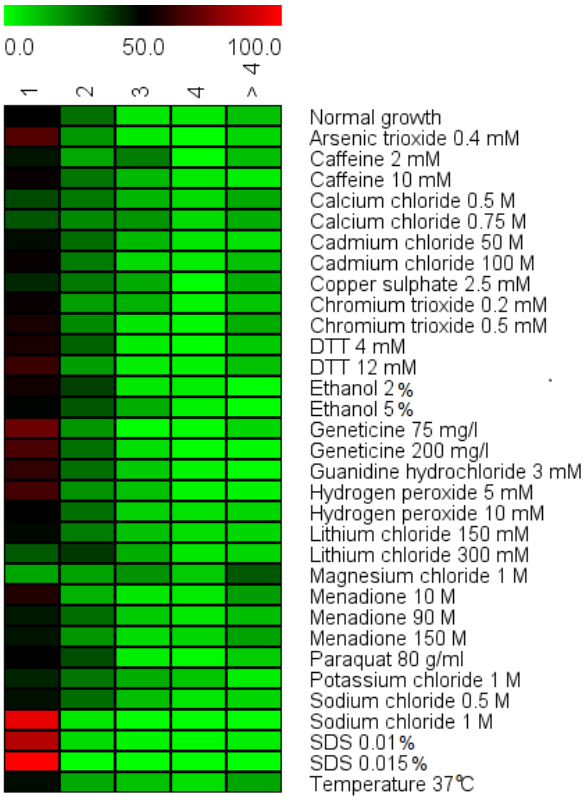

Figure 4.7: **Heat-map representing the number of protein aggregates per cell exposed to chemical stressors.** Yeast cells containing localized Hsp104-GFP fluorescence foci were counted and differentiated according to the number of localized Hsp104-GFP fluorescence foci per cell. Results are expressed as the percentage of positive cells (with Hsp104-GFP foci) relative to the total number of cells with protein aggregates per spot. Data represent the mean of three independent clones, obtained from three different array spots.

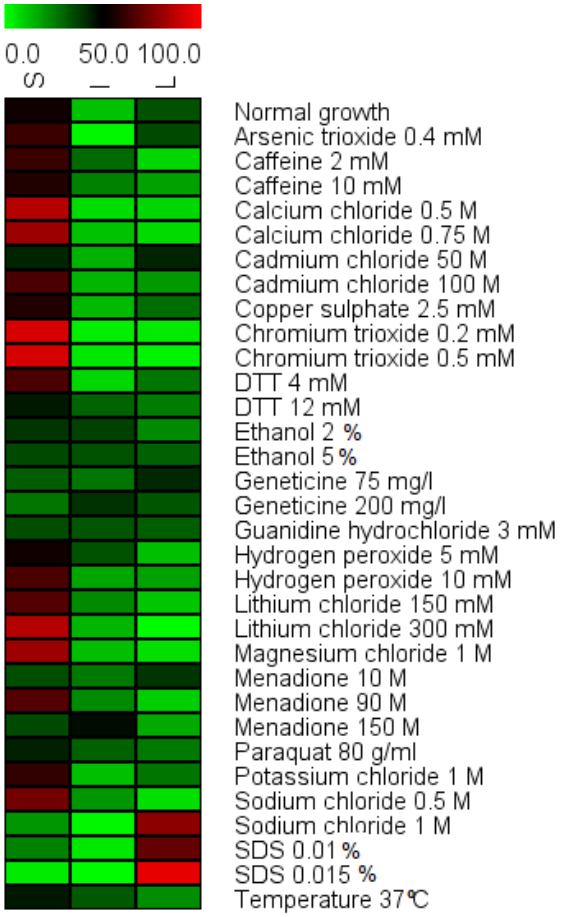

Figure 4.8: **Heat-map representing different types of aggregates in yeast cells exposed to chemical stressors.** Yeast cells containing localized Hsp104-GFP fluorescence foci were counted and differentiated according to the size of localized Hsp104-GFP fluorescence foci. Results are expressed as the percentage of positive cells (with Hsp104-GFP foci) relative to the total number of cells with protein aggregates per array spot. Data represent the mean of three independent clones, obtained from three different array spots. S – small protein aggregates; I – intermediate protein aggregates; L – large protein aggregates.

4.3 Discussion

Our data show that mistranslation induces formation of protein aggregates. In particular tRNAs that misincorporated serine at leucine, threonine, valine, alanine, glycine, arginine, histidine, glutamic acid, asparagine, glutamine, methionine, and proline codons had a strong impact on protein aggregation (Figure 4.2). In fact, the misincorporation of serine in general destabilizes protein structure and should have promoted the synthesis of misfolded or unfolded proteins that aggregated. Depending on the properties of the substituted amino acid (Figure 4.9), the misincorporations of serine likely lead to more or less extensive protein aggregation.

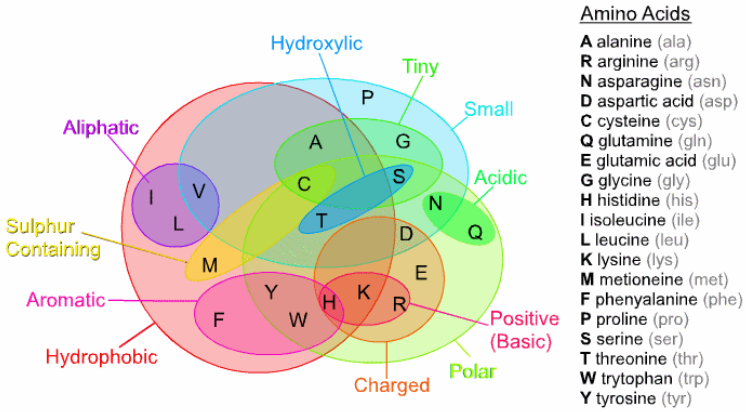

Figure 4.9: **Venn diagram with the classification of the physical and chemical properties of amino based on [82].** Adapted from [51].

From a theoretical point of view the amino acids substitution matrix BLOSUM 62 [31] (Figure 4.10) provides important information regarding the likelyhood of protein aggregation. This matrix classifies amino acids according to their tendency to be exchanged by other amino acid in proteins. This matrix was built from large sets of protein alignments sequences by counting the number of times that a specific substitution occurs and comparing this to what would be expected by random substitutions. In this way, high values indicate that a substitution occurs often in nature and so is favorable, and vice versa [7].

Substitution of aliphatic amino acids (Leu, Ile, and Val) for Ser has a value of -2, indicating that this is a rare event. This is expected because these amino acids have a hydrophobic nature and non-reactive side chains and are normally buried in protein hydrophobic cores, while Ser is a small polar amino acid containing a reactive hydroxyl group and is located on proteins surface [7]. In other words, it is likely that misincorporation of Ser at Leu, Ile and Val codons will disrupt protein structure, leading to misfolding and protein aggregation. Indeed, the misincorporation of Ser at Leu codons produced the highest percentage of protein aggregates in our assay (Figure 4.2). The misincorporation of Ser at Ile and Val codons also produced protein aggregates, but at lower level than Leu. However, the misincorporation of Ser at Ile and Val codons promoted the formation of more than four protein aggregates per cell (Figure 4.3). These data are in line with previous studies which show that Val/Thr substitutions cause protein denaturation [61].

The substitution of Phe and Tyr have a value of -2 and Trp has a value of -3 in the substitution matrix BLOSUM 62. These amino acids have an aromatic side chain and are buried in protein hydrophobic cores [7]. Therefore, one expected that misincorporation of Ser

	Ala	Arg	Asn	Asp	Cys	Gln	Glu	Gly	His	Ile	Leu	Lys	Met	Phe	Pro	Ser	Thr	Trp	Tyr	Val
Ala	4																			
Arg	-1	5																		
Asn	-2	0	6																	
Asp	-2	-2	1	6																
Cys	0	-3	-3	-3	9															
Gln	-1	1	0	0	-3	5														
Glu	-1	0	0	2	-4	2	5													
Gly	0	-2	0	-1	-3	-2	-2	6												
His	-2	0	1	-1	-3	0	0	-2	8											
Ile	-1	-3	-3	-3	-1	-3	-3	-4	-3	4										
Leu	-1	-2	-3	-4	-1	-2	-3	-4	-3	2	4									
Lys	-1	2	0	-1	-3	1	1	-2	-1	-3	-2	5								
Met	-1	-1	-2	-3	-1	0	-2	-3	-2	1	2	-1	5							
Phe	-2	-3	-3	-3	-2	-3	-3	-3	-1	0	0	-3	0	6						
Pro	-1	-2	-2	-1	-3	-1	-1	-2	-2	-3	-3	-1	-2	-4	7					
Ser	1	-1	1	0	-1	0	0	0	-1	-2	-2	0	-1	-2	-1	4				
Thr	0	-1	0	-1	-1	-1	-1	-2	-2	-1	-1	-1	-1	-2	-1	1	5			
Trp	-3	-3	-4	-4	-2	-2	-3	-2	-2	-3	-2	-3	-1	1	-4	-3	-2	11		
Tyr	-2	-2	-2	-3	-2	-1	-2	-3	2	-1	-1	-2	-1	3	-3	-2	-2	2	7	
Val	0	-3	-3	-3	-1	-2	-2	-3	-3	3	1	-2	1	-1	-2	-2	0	-3	-1	4

Figure 4.10: **Amino acids substitutions matrix: BLOSUM 62.** Adapted and modified from [31].

at Phe, Tyr and Trp codons would also increase misfolding and protein aggregation. However, our data showed that Ser misincorporation at these codons did not result in significant protein aggregation (Figure 4.2). Interestingly, the substitution of Tyr and Trp for Ser lead to the formation of more than four protein aggregates per cell, in most of the cells. Additionally, the substitution of Tyr for Ser produced large protein aggregates occupying most of the cell cytoplasm (Figures 4.3 e 4.4).

A value of -1 in the substitution matrix BLOSUM 62 is also indicative of rare substitutions and represents misincorporation of Ser at Arg, Cys, His, Met and Pro codons. Our data showed that substitution of these amino acids with Ser, except for Cys with Ser, resulted in higher percentage of cells with aggregates relative to control (Figure 4.2). Although, arginine and serine are polar amino acids, arginine is positively-charged and is frequently involved in salt-bridges. It also forms hydrogen bonds with negatively charged amino acids that can be important for protein stability [7]. In other words the substitution of Arg with Ser decreases protein stability, leading to unfolded or misfolded proteins and protein aggregation. Similarly, histidine is a polar amino acid whose substitution by other amino acids is problematic, in particular because it has a pK_a near physiological pH and may alter the charge of the side chain from neutral to positive in response to small alterations in intracellular pH [7]. Proline also has unique chemical properties and its replacement normally leads to protein instability. Its side chain is crucial for the native secondary structure of proteins. So, replacement of both His and Pro with Ser are likely to unfold proteins, promoting their aggregation. Methionine, like the other hydrophobic amino acids referred before, is normally buried in protein hydrophobic cores and, so, it is likely that misincorporation of Ser at Met positions leads to protein misfolding and aggregation. Interestingly, cells tolerate relatively well substitutions of Cys with other small amino acids, namely serine [7], which explains the lack of protein aggregation in cells misincorporating Ser at Cys codon in our assay.

The misincorporation of Ser at Gly, Glu and Gln codons has a BLOSUM 62 matrix value of zero, indicating that these substitutions occur often in nature and have little impact on protein structure. However, our data indicates that these replacements increase protein aggregation, but to a lesser extent than the replacements described before (Figure 4.2). Interestingly, our data show that misincorporation of Ser at Lys and Asp codons has little impact on protein

aggregation, which is in agreement with the value (0) given by the BLOSUM 62 matrix (Figures 4.2 e 4.10), and with their shared polar properties (Figure 4.9).

Substitution of Ala with Ser has value BLOSUM 62 of 1 and is generally viewed as having little impact on protein structure [26, 74]. However, mischarged Ser-tRNA^{Ala} and Gly-tRNA^{Ala} up-regulate cytoplasmatic chaperones and induce the unfolded protein response [26, 74], which is in line with our GFP-Hsp104 fluorescence data (Figure 4.2). Finally, replacement of Thr and Asn with Ser are common in nature and have a BLOSUM 62 matrix value of 1. But, our data indicates that they cause proteotoxic stress in yeast cells (Figure 4.2) and more studies are needed to explain the toxicity produced by these amino acids substitutions.

The role of environmental stress on protein aggregation is still poorly understood [32], however some stressors such as heat and ethanol have a strong effect on protein misfolding and aggregation. For example, ethanol is known to bind protein sites, displace water molecules and alter protein structure, leading to protein aggregation [19]. In our study exposure to 2% and 5% of ethanol resulted in lower levels of protein aggregation than those observed in control cells grown without ethanol (Figure 4.5). This may be explained by the natural resistance of yeast to ethanol since the latter is a natural product of glucose fermentation.

Toxic metals are environmental pollutants which are linked to a broad range of degenerative conditions in humans [33]. The effect of these metals in growth and metabolic activities is well documented [81], however the molecular mechanisms of metals toxicity is still poorly understood. We have tried to understand the effect of arsenic, cadmium, copper, chromium, lithium, magnesium on protein aggregation.

Chromium is an environmental pollutant that can cause genotoxicity, carcinogenicity and allergenicity. How it does so is not yet clear but one hypothesis is that Cr toxicity is caused by increased production of reactive oxygen species (ROS) and protein oxidation [33, 81], leading to accumulation of toxic protein aggregates [33]. Our data support this hypothesis since protein aggregates increased significantly in cells exposed to chromium (Figure 4.5).

Cadmium inhibits enzymes involved in detoxification of ROS, with consequent cellular accumulation of ROS [44, 54]. Cadmium can also replace Fe^{+2} in proteins, producing oxygen radicals due to the release of Fe^{+2} [54]. This can lead to protein structure destabilization, and our data showed that the percentage of cells with protein aggregates increased in the presence of cadmium chloride (100 μM) (Figure 4.5).

Copper toxicity is associated with oxidative stress in neurodegenerative diseases and there is some evidence that it may impair hsp70 function, which is critical for protecting cells from proteotoxicity [84]. Our data shows that cells exposed to copper sulfate have lower levels of protein aggregates and expression of hsp104 is lower than that observed in control cells (normal growth conditions) (Figure 4.5).

Similarly, arsenite may also destabilise proteins through increased ROS production [84]. But, our data showed that cells exposed to arsenic trioxide produced lower levels of protein aggregates than the control cells (normal growth conditions) (Figure 4.5). Therefore, additional studies are required to clarify the association of ROS and protein aggregation mediated through arsenite ions.

Our data showed that lithium and magnesium chloride increased the percentage of cells containing protein aggregates (Figure 4.5). To our knowledge this is the first time that lithium and magnesium chloride have been shown to increase formation of protein aggregates. The only indirect evidence for a role of Li^{2+} and Mg^{2+} in protein aggregation is the up-regulation

of the expression of Hsp26 in cells exposed to Li^{2+} and the up-regulation of SSA1 and SSA2 in cells exposed to Mg^{2+} [34]. Additionally, cells exposed to magnesium chloride showed more than one protein aggregation foci per cell, in more than 80% of the cases (in normal growth conditions cells had one aggregate per cell in 50% of the cases, only) (Figure 4.7).

Guanidine hydrochloride (GuHCl) is a chaotropic salt that promotes protein denaturation [17, 27, 63]. High concentration of this denaturant unfolds almost all proteins through disruption of intra- and inter-molecular interactions [27]. Additionally, GuHCl promote the expression of the stress protein Hsp104 [17]. However, our data showed that cells exposed to guanidine hydrochloride had lower levels of protein aggregates and hsp104 than the control cells (normal growth conditions) (Figure 4.5). GuHCl can also have adverse effects on the ATPase activity of Hsp104 [17, 63]. Since our system to quantify protein aggregation was based on the interaction of the molecular chaperone hsp104 with the aggregates one cannot exclude the hypothesis that GuHCl inhibits hsp104 activity. Interestingly, in cells exposed to GuHCl, protein aggregates were larger that in the other stressors (Figure 4.8).

DTT is a reducing agent that promotes reductive stress and can increase the cellular levels of misfolded proteins [69]. Our results show however that DTT reduces the relative percentage of cells with protein aggregates (Figure 4.5). However, reductive stress due to DTT can lead to accumulation of misfolded proteins in the ER which triggers the unfolded protein response (UPR) [69], with consequent up-regulation of BiP; an ER protein involved in the translocation, folding, and assembly of secretory and transmembrane proteins [42].

Oxidative stress is known to increase protein aggregation, we have exposed our yeast cells to menadione, hydrogen peroxide and paraquat and we could confirm increased protein aggregation in presence of menadione (150 μM), but we could not confirm the presence of protein aggregates in cells exposed to H_2O_2 (Figure 4.5), suggesting that H_2O_2 may increase the breakdown of unfolded or misfolded proteins preventing them from entering the aggregation pathway.

Paraquat is a bipyridinium salt used as an herbicide, but with toxic effects on microorganisms, animals and humans. It is a superoxide generator and its toxicity as been linked to ROS accumulation with consequent damage of proteins [54]. Inhibition of yeast growth has also been reported [28], but very little is known about its effects on protein aggregation. Nevertheless, paraquat has been shown to cause aggregation of α-synuclein and formation of Lewy bodies [52], which are characteristic of Parkinson's disease. We were not able to confirm the increased production of protein aggregates in cells exposed to paraquat (Figure 4.5).

The effect of ionic/osmotic stress in protein aggregation was also tested in this study using calcium, sodium, and potassium chloride. Although, at low concentrations, they can stabilize proteins *via* non-specific electrostatic interactions, at high concentrations, salts can stabilize or destabilize proteins, or even denature proteins, depending on the types and concentration of the salts [27]. In fact, high concentration of inorganic ions, such K^+, Na^+, and Cl^-, disrupt enzyme activity and destabilize protein secondary structure, leading to protein aggregate formation due to non-native protein-protein interactions [11]. High salt concentrations, mainly Na^+ and K^+, elicits the osmostress response, which is similar to the general stress/heat shock protein responses, induced by accumulation of misfolded or improperly assembled proteins in the ER [46]. Again, our cells exposed to NaCl and KCl did not show an increase in the percentage of protein aggregates relative to non-stressed cells (Figure 4.5), probably because the concentration used was too low to trigger protein aggregation.

Calcium-induced aggregation has been described and it can have a role in the storage of regulated secretory proteins in secretory granules [36]. Our data confirms previous studies

since cells exposed to calcium chloride (0.5 M) produced higher levels of protein aggregates than control cells (Figure 4.5).

Finally, caffeine (1,3,7-trimethylzanthine) was also tested. Caffeine is an analogue of purine bases and has pleiotropic effects in the cell [45]. Our results show that cells exposed to caffeine have lower percentage of protein aggregates than the control cells (Figure 4.5). Interestingly, GFP-Hsp104 total fluorescence was higher in cells exposed to caffeine than in control cells (Figure 4.6), indicating that caffeine may promote formation of small aggregates that are dispersed in the cytoplasm. Additional studies are therefore needed to clarify this interesting observation. Similarly, cells exposed to SDS (or sodium dodecyl sulfate) showed lower percentage of protein aggregates (Figure 4.5), but increased level of total fluorescence (Figure 4.6). Since SDS is an anionic detergent that binds to hydrophobic regions of polypeptides, it helps solubilizing denaturated proteins dispersing them in the cytoplasm [27].

4.4 Conclusion and Future Work

Our main goal was to develop a yeast cell-array for high-throughput genetic screens. We have optimized the technology for producing high density cell arrays and, as a proof-of-principle, used them to screen chemical and genetic cues that promote the formation of protein aggregates. As one would expect, our data showed that mistranslation and various chemical stressors induce protein aggregation, as monitored by increased expression and localization of the Hsp104 disaggregase.

Our technology is robust, but it will be necessary to automate acquisition of images and establish a computational pipeline for analysis. Simultaneously, integration of robotic tools must be done to produce large-scale data sets for setting up genetic screens. Such tools would allow us to use our cell array technology to identify chemical stressors that cause proteotoxic stress, which is relevant to understand the role of environmental factors in protein conformational diseases.

Since *Saccharomyces cerevisiae* proteins have high homology with higher eukaryotic proteins, yeast can be used to elucidate the molecular biology of proteotoxic stress. Our technology can therefore be applied to study the molecular mechanisms of human diseases associated to protein misfolding and aggregation, using yeast cell arrays.

Bibliography

[1] P. F. Agris. Decoding the genome: a modified view. *Nucleic acids research*, 32(1):223–38, Jan. 2004.

[2] B. Aguilar-Uscanga and J. M. François. A study of the yeast cell wall composition and structure in response to growth conditions and mode of cultivation. *Letters in Applied Microbiology*, 37:268–274, 2003.

[3] C. Anfinsen. Principles that Govern the Folding of Protein Chains. *Science*, 181(4096): 223–230, 1973.

[4] J. M. Barral, S. a. Broadley, G. Schaffar, and F. U. Hartl. Roles of molecular chaperones in protein misfolding diseases. *Seminars in cell & developmental biology*, 15(1):17–29, Feb. 2004.

[5] S. Belkin. Microbial whole-cell sensing systems of environmental pollutants. *Current Opinion in Microbiology*, 6(3):206–212, June 2003.

[6] S. J. S. Berke and H. L. Paulson. Protein aggregation and the ubiquitin proteasome pathway: gaining the UPPer hand on neurodegeneration. *Current Opinion in Genetics & Development*, 13:253–261, 2003.

[7] M. J. Betts and R. B. Russell. Amino Acid Properties and Consequences of Substitutions. In M. R. Barnes and I. C. Gray, editors, *Bioinformatics for Geneticists*, volume 4, chapter 14, pages 289–316. John Wiley & Sons, Ltd., 2003. ISBN 0470843934.

[8] B. Blagoev and A. Pandey. Microarrays go live – new prospects for proteomics. *TRENDS in Biochemical Sciences*, 26(11):639–641, 2001.

[9] A. Buchberger, B. Bukau, and T. Sommer. Protein quality control in the cytosol and the endoplasmic reticulum: brothers in arms. *Molecular cell*, 40(2):238–52, Oct. 2010.

[10] D. Castel, A. Pitaval, M.-A. Debily, and X. Gidrol. Cell microarrays in drug discovery. *Drug discovery today*, 11(13-14):616–22, July 2006.

[11] K. P. Choe and K. Strange. Genome-wide RNAi screen and in vivo protein aggregation reporters identify degradation of damaged proteins as an essential hypertonic stress response. *American journal of physiology. Cell physiology*, 295(6):C1488–98, Dec. 2008.

[12] T. E. Dever. Translation initiation: adept at adapting. *Trends in biochemical sciences*, 24(10):398–403, Oct. 1999.

[13] T. E. Dever. Gene-specific regulation by general translation factors. *Cell*, 108(4):545–56, Feb. 2002.

[14] C. M. Dobson. The structural basis of protein folding and its links with human disease. *Philosophical transactions of the Royal Society of London. Series B, Biological sciences*, 356(1406):133–45, Feb. 2001.

[15] C. M. Dobson. Principles of protein folding, misfolding and aggregation. *Seminars in cell & developmental biology*, 15(1):3–16, Feb. 2004.

[16] T. K. V. A. N. Dyk, E. J. D. E. Rose, and G. E. Gonye. LuxArray, a High-Density, Genomewide Transcription Analysis of Escherichia coli Using Bioluminescent Reporter Strains. *Journal of Bacteriology*, 183(19):5496–5505, 2001.

[17] S. S. Eaglestone, L. W. Ruddock, B. S. Cox, and M. F. Tuite. Guanidine hydrochloride blocks a critical step in the propagation of the prion-like determinant [PSI+] of Saccharomyces cerevisiae. *PNAS*, 97(1):240–244, 2000.

[18] E. W. Eldred and P. R. Schimmel. Rapid Deacylation by Isoleucyl Transfer Ribonucleic Acid Synthetase of Isoleucine-specific Transfer Ribonucleic Acid Aminoacylated with Valine. *The Journal of biological chemistry*, 274(9), 1972.

[19] J. E. Ferns, C. S. Theisen, E. E. Fibuch, and N. W. Seidler. Protection Against Protein Aggregation by Alpha-Crystallin as a Mechanism of Preconditioning. *Neurochem Res*, 2011.

[20] A. Fiebitz, L. Nyarsik, B. Haendler, Y.-h. Hu, F. Wagner, S. Thamm, H. Lehrach, M. Janitz, and D. Vanhecke. High-throughput mammalian two-hybrid screening for protein-protein interactions using transfected cell arrays. *BMC Genomics*, 9(68), 2008.

[21] A. L. Fink. Protein aggregation: folding aggregates, inclusion bodies and amyloid. *Folding & Design*, 3(1):9–23, 1998.

[22] R. D. Gietz and R. A. Woods. Yeast Transformation by the LiAc/SS Carrier DNA/PEG Method. In W. Xiao, editor, *Yeast Protocols*, volume 313, chapter 12, pages 107–120. Humana Press, New Jersey, second edition, Sept. 2006. ISBN 1-59259-958-3.

[23] A. Gnirke, U. Geigenmuller, H.-J. Rheinberger, and K. H. Nierhaus. The Allosteric Three-site Model for the Ribosomal Elongation Cycle. *The Journal of Biological Chemistry*, 264 (May 5):7291–7301, 1989.

[24] A. Goffeau, B. G. Barrell, H. Bussey, R. W. Davis, B. Dujon, H. Feldmann, F. Galibert, J. D. Hoheisel, C. Jacq, M. Johnston, E. J. Louis, H. W. Mewes, Y. Murakami, P. Philippsen, H. Tettelin, and S. G. Oliver. Life with 6000 Genes. *Science*, 274(Genome), 1996.

[25] E. Goldman. Transfer RNA, 2008.

[26] M. Guo, Y. E. Chong, R. Shapiro, K. Beebe, X.-L. Yang, and P. Schimmel. Paradox of mistranslation of serine for alanine caused by AlaRS recogniton dilemma. *Nature*, 462 (7274):808–812, 2010.

[27] H. Hamada, T. Arakawa, and K. Shiraki. Effect of additives on protein aggregation. *Current pharmaceutical biotechnology*, 10(4):400–7, June 2009.

[28] L. Hansson and M. H. Hafiggstrom. Metabolic Effects of Paraquat on Saccharomyces cerevisiae. *Current Microbiology*, 13:81–83, 1986.

[29] T. Hart, A. Zhao, A. Garg, S. Bolusani, and E. M. Marcotte. Human cell chips: adapting DNA microarray spotting technology to cell-based imaging assays. *PloS one*, 4(10), Jan. 2009.

[30] M. Haslbeck, A. Miess, T. Stromer, S. Walter, and J. Buchner. Disassembling protein aggregates in the yeast cytosol. The cooperation of Hsp26 with Ssa1 and Hsp104. *The Journal of biological chemistry*, 280(25):23861–8, June 2005.

[31] S. Henikoff and J. G. Henikoff. Amino acid substitution matrices from protein blocks. *Proceedings of the National Academy of Sciences of the United States of America*, 89(22): 10915–9, Nov. 1992.

[32] S. Hohmann and W. H. Mager. *Yeast Stress Responses*. 2003. ISBN 3540439269.

[33] S. Holland, E. Lodwig, T. Sideri, T. Reader, I. Clarke, K. Gkargkas, D. C. Hoyle, D. Delneri, S. G. Oliver, and S. V. Avery. Application of the comprehensive set of heterozygous yeast deletion mutants to elucidate the molecular basis of cellular chromium toxicity. *Genome Biology*, 8(12), 2007.

[34] Y. Hu, G. Wang, G. Y. J. Chen, X. Fu, and S. Q. Yao. Proteome analysis of Saccharomyces cerevisiae under metal stress by two-dimensional differential gel electrophoresis. *Electrophoresis*, 24(9):1458–70, May 2003.

[35] W.-p. Huang and D. J. Klionsky. Autophagy in Yeast: A Review of the Molecular Machinery. *Cell Structure and Function*, 27:409–420, 2002.

[36] R. K. Jain, P. B. M. Joyce, and S.-U. Gorr. Aggregation Chaperones Enhance Aggregation and Storage of Secretory Proteins in Endocrine Cells *. *The Journal of Biological Chemistry*, 275(35):27032–27036, 2000.

[37] H. Jakubowski. Quality control in tRNA charging. *Wiley interdisciplinary reviews. RNA*, 3(3):295–310, 2012.

[38] M. Jansen, C. H. de Moor, J. S. Sussenbach, and J. L. van den Brande. Translational control of gene expression. *Pediatric research*, 37(6):681–6, June 1995.

[39] L. D. Kapp and J. R. Lorsch. The molecular mechanics of eukaryotic translation. *Annual review of biochemistry*, 73:657–704, Jan. 2004.

[40] H. Karathia, E. Vilaprinyo, A. Sorribas, and R. Alves. Saccharomyces cerevisiae as a model organism: a comparative study. *PloS one*, 6(2):e16015, Jan. 2011.

[41] S. H. Kim, G. Quigley, F. L. Suddath, A. McPherson, D. Sneden, J. J. Kim, J. Weinzierl, P. Blattmann, and A. Rich. The Three-Dimensional Structure of Yeast Phenylalanine Transfer RNA: Shape of the Molecule at 5.5-A Resolution. *Proc. Natl. Acad. Sci. USA*, 69(12):3746–3750, 1972.

[42] K. Kohno, K. Normington, J. Sambrook, M. J. Gething, and K. Mori. The promoter region of the yeast KAR2 (BiP) gene contains a regulatory domain that responds to the presence of unfolded proteins in the endoplasmic reticulum. *Molecular and cellular biology*, 13(2):877–90, Feb. 1993.

[43] R. R. Kopito. Aggresomes, inclusion bodies and protein aggregation. *TRENDS in Cell Biology*, 10(2000):524–530, 2000.

[44] U. Kruegel, B. Robison, T. Dange, G. Kahlert, J. R. Delaney, S. Kotireddy, M. Tsuchiya, S. Tsuchiyama, C. J. Murakami, J. Schleit, G. Sutphin, D. Carr, K. Tar, G. Dittmar, M. Kaeberlein, B. K. Kennedy, and M. Schmidt. Elevated proteasome capacity extends replicative lifespan in Saccharomyces cerevisiae. *PLoS genetics*, 7(9), Sept. 2011.

[45] K. Kuranda, V. Leberre, S. Sokol, G. Palamarczyk, and J. François. Investigating the caffeine effects in the yeast Saccharomyces cerevisiae brings new insights into the connection between TOR , PKC and Ras / cAMP signalling pathways. *Molecular Microbiology*, 61(5):1147–1166, 2006.

[46] R. Lahav, A. Nejidat, and A. Abeliovich. Alterations in protein synthesis and levels of heat shock 70 proteins in response to salt stress of the halotolerant yeast Rhodotorula mucilaginosa. *Antonie van Leeuwenhoek*, 85(4):259–69, May 2004.

[47] A. B. Lindner and A. Demarez. Protein aggregation as a paradigm of aging. *Biochimica et Biophysica Acta*, 1790(10):980–996, 2009.

[48] J. Ling, N. Reynolds, and M. Ibba. Aminoacyl-tRNA synthesis and translational quality control. *Annual review of microbiology*, 63:61–78, Jan. 2009.

[49] P. N. Lipke and R. Ovalle. Cell Wall Architecture in Yeast: New Structure and New Challenges. *Journal of Bacteriology*, 180(15):3735–3740, 1998.

[50] H. F. Lodish. Translational control of protein synthesis. *Annual review of biochemistry*, 45:39–72, Jan. 1976.

[51] T.-D. Luu, A. Rusu, V. Walter, B. Linard, L. Poidevin, R. Ripp, L. Moulinier, J. Muller, W. Raffelsberger, N. Wicker, O. Lecompte, J. D. Thompson, O. Poch, and H. Nguyen. KD4v: Comprehensible Knowledge Discovery System for Missense Variant. *Nucleic acids research*, 40(Web Server issue):W71–5, July 2012.

[52] A. B. Manning-Bog, A. L. McCormack, J. Li, V. N. Uversky, A. L. Fink, and D. A. D. Monte. The Herbicide Paraquat Causes Up-regulation and Aggregation of alpha-Synuclein in Mice. *Journal of Biological Chemistry*, 277(3):1641–1644, Nov. 2001.

[53] P. Matula, A. Kumar, I. Wörz, H. Erfle, R. Bartenschlager, R. Eils, and K. Rohr. Single-cell-based image analysis of high-throughput cell array screens for quantification of viral infection. *Cytometry. Part A : the journal of the International Society for Analytical Cytology*, 75(4):309–18, Apr. 2009.

[54] B. Medicherla and A. L. Goldberg. Heat shock and oxygen radicals stimulate ubiquitin-dependent degradation mainly of newly synthesized proteins. *The Journal of cell biology*, 182(4):663–73, Aug. 2008.

[55] I. Miranda, R. Rocha, M. C. Santos, D. D. Mateus, G. R. Moura, L. Carreto, and M. A. S. Santos. A Genetic Code Alteration Is a Phenotype Diversity Generator in the Human Pathogen Candida albicans. *PLoS ONE*, (10), 2007.

[56] R. I. Morimoto. Proteotoxic stress and inducible chaperone networks in neurodegenerative disease and aging. *Genes & Development*, 22:1427–1438, 2008.

[57] G. R. Moura, L. C. Carreto, and M. A. S. Santos. Genetic code ambiguity: an unexpected source of proteome innovation and phenotypic diversity. *Current Opinion in Microbiology*, 12:1–7, 2009.

[58] G. R. Moura, J. P. Lousado, M. Pinheiro, L. Carreto, R. M. Silva, J. L. Oliveira, and M. A. S. Santos. Codon-triplet context unveils unique features of the Candida albicans protein coding genome. *BMC Genomics*, 8(444), 2007.

[59] G. R. Moura, J. a. A. Paredes, and M. A. S. Santos. Development of the genetic code: Insights from a fungal codon reassignment. *FEBS Letters*, 584:334–341, 2010.

[60] U. R. Muller and D. V. Nicolau. *Microarray Technology and Its Applications*. 2005. ISBN 3540229310.

[61] L. a. Nangle, C. M. Motta, and P. Schimmel. Global effects of mistranslation from an editing defect in mammalian cells. *Chemistry & biology*, 13(10):1091–100, Oct. 2006.

[62] R. Narayanaswamy, W. Niu, A. D. Scouras, G. T. Hart, J. Davies, A. D. Ellington, V. R. Iyer, and E. M. Marcotte. Systematic profiling of cellular phenotypes with spotted cell microarrays reveals mating-pheromone response genes. *Genome biology*, 7(1):R6, Jan. 2006.

[63] F. Ness, P. Ferreira, B. S. Cox, and M. F. Tuite. Guanidine Hydrochloride Inhibits the Generation of Prion "Seeds" but Not Prion Protein Aggregation in Yeast. *Molecular and Cellular Biology*, 22(15):5593–5605, 2002.

[64] N. Neznanov, A. P. Komarov, L. Neznanova, P. Stanhope, and A. V. Gudkov. Proteotoxic stress targeted therapy (PSTT): induction of protein misfolding enhances the antitumor effect of the proteasome inhibitor bortezomib. *Oncotarget*, 2(3):209–221, 2011.

[65] W. Niu. *Development of imaging-based high-throughput genetic assays and genomic evaluation of yeast gene function in cell cycle progression*. PhD thesis, University of Texas at Austin, 2007.

[66] T. F. d. O. Outeiro. *Yeast as a model organism to study diseases of protein misfolding*. PhD thesis, Universidade do Porto, 2004.

[67] K. Papp, Z. Szittner, and J. Prechl. Life on a microarray: assessing live cell functions in a microarray format. *Cellular and molecular life sciences: CMLS*, 69(16):2717–2725, Aug. 2012.

[68] L. R. D. Pouplana and P. Schimmel. Aminoacyl-tRNA synthetases: potential markers of genetic code development. *TRENDS in Biochemical Sciences*, 26(10):591–596, 2001.

[69] J. D. Rand and C. M. Grant. The Thioredoxin System Protects Ribosomes against Stress-induced Aggregation. *Molecular Biology of the Cell*, 17(January):387–401, 2006.

[70] M. V. Rodnina, M. Beringer, and W. Wintermeyer. Mechanism of peptide bond formation on the ribosome. *Quarterly reviews of biophysics*, 39(3):203–25, Aug. 2006.

[71] F. A. Salomons, V. Mene, C. Bo, B. A. Mccray, J. P. Taylor, and N. P. Dantuma. Selective Accumulation of Aggregation-Prone Proteasome Substrates in Response to Proteotoxic Stress. *Molecular and cellular Biology*, 29(7):1774–1785, 2009.

[72] Y. Sanchez, J. Taulien, K. A. Borkovich, and S. Lindquist. Hspl104 is required for tolerance to forms of stress many. *The EMBO journal*, 1(6):2357–2364, 1992.

[73] M. A. S. Santos, C. Cheesman, V. Costa, P. Moradas-ferreira, and M. F. Tuite. Selective advantages created by codon ambiguity allowed for the evolution of an alternative genetic code in Candida spp. *Molecular Microbiology*, 31(3):937–947, 1999.

[74] P. Schimmel. An editing activity that prevents mistranslation and connection to disease. *The Journal of biological chemistry*, 283(43):28777–82, Oct. 2008.

[75] P. R. Schimmel. Aminoacyl-tRNA Synthetases: General Features and Recodnition of Transfer RNAs. *Annual review of biochemistry*, 48:601–648, 1979.

[76] F. Sherman. Getting Started with Yeast. *Methods in Enzymology*, 350:3–41, 2002.

[77] R. M. Silva, I. Miranda, G. Moura, and M. A. S. Santos. Yeast as a model organism for studying the evolution of non-standard genetic codes. *Briefings in functional genomics & proteomics*, 3(1):35–46, Apr. 2004.

[78] R. M. Silva, J. a. A. Paredes, G. R. Moura, B. Manadas, T. Lima-costa, R. Rocha, I. Miranda, A. C. Gomes, M. J. G. Koerkamp, M. Perrot, F. C. P. Holstege, H. Boucherie, and M. A. S. Santos. Critical roles for a genetic code alteration in the evolution of the genus Candida. *The EMBO Journal*, pages 1–11, 2007.

[79] C. So. Aging and molecular chaperones. 38:1037–1040, 2003.

[80] M. Stefani. Protein misfolding and aggregation: new examples in medicine and biology of the dark side of the protein world. *Biochimica et Biophysica Acta*, 1739:5–25, 2004.

[81] E. R. Sumner, A. Shanmuganathan, T. C. Sideri, S. A. Willetts, J. E. Houghton, and S. V. Avery. Oxidative protein damage causes chromium toxicity in yeast. *Microbiology*, 151:1939–1948, 2005.

[82] W. R. Taylor. The Classification of Amino Acid Conservation. *J. theor. Biol.*, 119: 205–218, 1986.

[83] E. W. Trotter, C. M.-F. Kao, L. Berenfeld, D. Botstein, G. a. Petsko, and J. V. Gray. Misfolded proteins are competent to mediate a subset of the responses to heat shock in Saccharomyces cerevisiae. *The Journal of biological chemistry*, 277(47):44817–25, Nov. 2002.

[84] M. Valko, H. Morris, and M. T. D. Cronin. Metals, toxicity and oxidative stress. *Current medicinal chemistry*, 12(10):1161–208, Jan. 2005.

[85] C. Voisine, J. S. n. Pedersen, and R. I. Morimoto. Chaperone networks : Tipping the balance in protein folding diseases. *Neurobiology of Disease*, 40(1):12–20, 2010.

[86] S. Walter and J. Buchner. Molecular Chaperones – Cellular Machines for Protein Folding. *Angewandte Chemie Int. Ed.*, 41:1098–1113, 2002.

[87] D. B. Wheeler, A. E. Carpenter, and D. M. Sabatini. Cell microarrays and RNA interference chip away at gene function. *Nature genetics*, 37 Suppl(June):S25–30, June 2005.

[88] D. N. Wilson and K. H. Nierhaus. The E-site story: the importance of maintaining two tRNAs on the ribosome during protein synthesis. *Cellular and molecular life sciences : CMLS*, 63(23):2725–37, Dec. 2006.

[89] C. R. Woese, G. J. Olsen, M. Ibba, and D. Söll. Aminoacyl-tRNA Synthetases, the Genetic Code, and the Evolutionary Process. *Microbiology and Molecular Biology Reviews*, 64(1), 2000.

[90] R. Z. Wu, S. N. Bailey, and D. M. Sabatini. Cell-biological applications of transfected-cell microarrays. *TRENDS in Cell Biology*, 12(10):485–488, 2002.

[91] S. S. Yadavalli and M. Ibba. Quality control in aminoacyl-tRNA synthesis its role in translational fidelity. In *Advances in protein chemistry and structural biology*, volume 86, pages 1–43. Jan. 2012. ISBN 9780123864970.

[92] M. L. Yarmush and K. R. King. Living-cell microarrays. *Annual review of biomedical engineering*, 11:235–57, Jan. 2009.

[93] M. Yarus. Phenylalanyl-tRNA Synthetase and Isoleucyl-tRNAPhe: A Possible Verification Mechanism for Aminoacyl-tRNA. *Proc. Natl. Acad. Sci. USA*, 69(7):1915–1919, 1972.

[94] J. Zhao, W. Niu, J. Yao, S. Mohr, E. M. Marcotte, and A. M. Lambowitz. Group II intron protein localization and insertion sites are affected by polyphosphate. *PLoS biology*, 6(6): e150, June 2008.

[95] J. Ziauddin and D. M. Sabatini. Microarrays of cells expressing defined cDNAs. *Nature*, 411, 2001.

Appendix A

Cell-arrays protocol optimization extra data

Table A.1: **Summary table of the percentage of imageable cells obtained in the protocol optimization for producing yeast cell-arrays.**

		Poly-L-lysine			Concanavalin A			SuperEpoxy 2			Hydrogel			Gold		
		H_2O	PBS	EtOH	H2O	PBS	EtOH	H_2O	PBS	EtOH	H_2O	PBS	EtOH	H_2O	PBS	EtOH
Fixed cells	H_2O	18,60%	95,30%	14,09%	59,23%	37,58%	14,48%	9,17%	3,62%	0,00%	24,09%	7,43%	3,57%	3,23%	3,63%	1,00%
	H_2O+Glyc. 7%	0,00%	0,00%	18,63%	3,57%	0,00%	0,00%	0,00%	0,00%	0,00%	20,14%	8,60%	7,28%	0,00%	10,50%	0,00%
	H_2O+Glyc. 17%	0,00%	0,00%	0,00%	0,00%	0,00%	0,00%	0,00%	0,00%	0,00%	0,00%	0,00%	0,00%	0,00%	0,00%	0,00%
	H_2O+Glyc. 27%	0,00%	0,00%	0,00%	0,00%	0,00%	0,00%	0,00%	0,00%	0,00%	0,00%	0,00%	0,00%	0,00%	0,00%	0,00%
	MM	19,60%	92,10%	20,21%	58,08%	35,14%	0,00%	20,69%	30,71%	32,20%	32,62%	26,62%	11,12%	19,61%	15,25%	1,69%
	MM+Glyc. 7%	0,00%	0,00%	23,63%	0,00%	0,00%	0,00%	0,00%	21,59%	0,00%	38,38%	5,32%	10,77%	0,00%	0,00%	0,00%
	MM+Glyc. 17%	0,00%	0,00%	0,00%	0,00%	0,00%	0,00%	0,00%	0,00%	0,00%	0,00%	0,00%	0,00%	0,00%	0,00%	1,79%
	MM+Glyc. 27%	0,00%	0,00%	0,00%	0,00%	0,00%	0,00%	0,00%	0,00%	0,00%	0,00%	0,00%	0,00%	0,00%	0,00%	0,00%
	PBS	36,79%	95,74%	34,28%	76,28%	64,26%	0,00%	15,32%	23,35%	0,00%	0,00%	16,33%	10,12%	12,76%	17,46%	3,79%
	PBS+Glyc. 7%	0,00%	13,49%	36,41%	33,77%	13,26%	0,00%	19,18%	0,00%	0,00%	13,19%	21,97%	13,87%	0,00%	16,43%	13,24%
	PBS+Glyc. 17%	0,00%	0,00%	0,00%	43,56%	0,00%	0,00%	0,00%	0,00%	0,00%	0,00%	0,00%	0,00%	0,00%	0,00%	19,23%
	PBS+Glyc. 27%	0,00%	0,00%	0,00%	28,07%	0,00%	0,00%	0,00%	0,00%	0,00%	0,00%	0,00%	0,00%	0,00%	0,00%	0,00%
	Sorbitol 0,5 M	3,81%	0,00%	25,44%	0,00%	0,00%	49,79%	0,00%	0,00%	0,00%	33,51%	2,56%	5,30%	0,00%	0,00%	3,32%
	Sorbitol 1 M	0,00%	0,00%	0,00%	0,00%	0,00%	0,00%	0,00%	0,00%	0,00%	12,47%	0,00%	0,00%	0,00%	0,00%	3,81%
	Sorbitol 1,5 M	0,00%	0,00%	0,00%	0,00%	0,00%	0,00%	0,00%	0,00%	0,00%	0,00%	0,00%	0,00%	0,00%	0,00%	3,61%
Non-fixed cells	H_2O	0,00%	30,54%	28,87%	24,83%	18,79%	20,47%	4,57%	34,98%	0,00%	3,19%	32,81%	5,97%	25,16%	0,00%	22,39%
	H_2O+Glyc. 7%	0,00%	0,00%	3,51%	0,00%	0,00%	18,06%	0,00%	0,00%	0,00%	12,80%	31,88%	3,47%	0,00%	0,00%	16,58%
	H_2O+Glyc. 17%	0,00%	0,00%	12,89%	0,00%	0,00%	0,00%	0,00%	0,00%	0,00%	0,00%	0,00%	10,95%	0,00%	0,00%	16,53%
	H_2O+Glyc. 27%	0,00%	0,00%	8,99%	0,00%	0,00%	0,00%	0,00%	0,00%	0,00%	0,00%	0,00%	0,00%	0,00%	0,00%	0,00%
	MM	0,00%	57,02%	31,18%	48,26%	38,98%	23,99%	8,06%	35,00%	0,00%	4,95%	43,90%	15,35%	26,73%	0,00%	0,00%
	MM+Glyc. 7%	0,00%	0,00%	8,25%	0,00%	0,00%	12,48%	0,00%	0,00%	0,00%	9,22%	0,00%	5,32%	0,00%	0,00%	0,00%
	MM+Glyc. 17%	0,00%	0,00%	11,40%	0,00%	0,00%	13,72%	0,00%	0,00%	0,00%	0,00%	0,00%	6,95%	0,00%	0,00%	0,00%
	MM+Glyc. 27%	0,00%	0,00%	15,83%	0,00%	0,00%	0,00%	0,00%	0,00%	0,00%	0,00%	0,00%	7,77%	0,00%	0,00%	0,00%
	PBS	0,00%	39,93%	21,92%	41,24%	28,82%	3,16%	7,98%	28,91%	0,00%	13,35%	41,20%	28,24%	19,34%	0,00%	0,00%
	PBS+Glyc. 7%	0,00%	0,00%	7,36%	0,00%	0,00%	26,05%	7,14%	0,00%	26,89%	10,35%	50,94%	5,72%	0,00%	0,00%	0,00%
	PBS+Glyc. 17%	0,00%	0,00%	16,41%	0,00%	0,00%	0,00%	0,00%	0,00%	0,00%	0,00%	0,00%	11,72%	0,00%	0,00%	0,00%
	PBS+Glyc. 27%	0,00%	0,00%	0,00%	0,00%	0,00%	0,00%	0,00%	0,00%	0,00%	0,00%	0,00%	0,00%	0,00%	0,00%	0,00%
	Sorbitol 0,5 M	0,00%	0,00%	0,00%	0,00%	0,00%	0,00%	0,00%	0,00%	0,00%	12,24%	0,00%	14,35%	0,00%	0,00%	0,00%
	Sorbitol 1 M	0,00%	0,00%	0,00%	0,00%	0,00%	0,00%	0,00%	0,00%	0,00%	3,63%	0,00%	4,69%	0,00%	0,00%	0,00%
	Sorbitol 1,5 M	0,00%	0,00%	8,30%	0,00%	0,00%	0,00%	0,00%	0,00%	0,00%	0,00%	0,00%	10,38%	0,00%	0,00%	0,00%

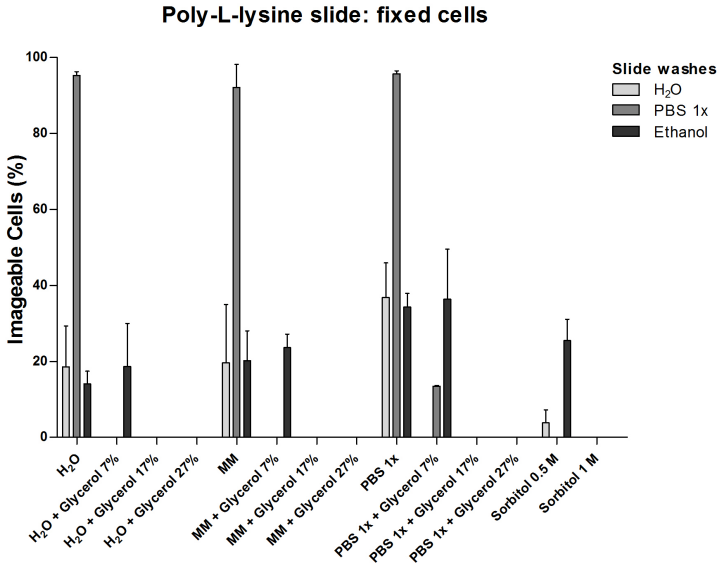

Figure A.1: **Percentage of imageable cells printed on poly-L-lysine coated slides.** Cells were fixed with 3.7% prior to printing. Data represent the mean ± s. d. of 3 independent spots. The medians were calculated using the Kruskal-Wallis post Dunn's Multiple Comparison test with CI 95%.

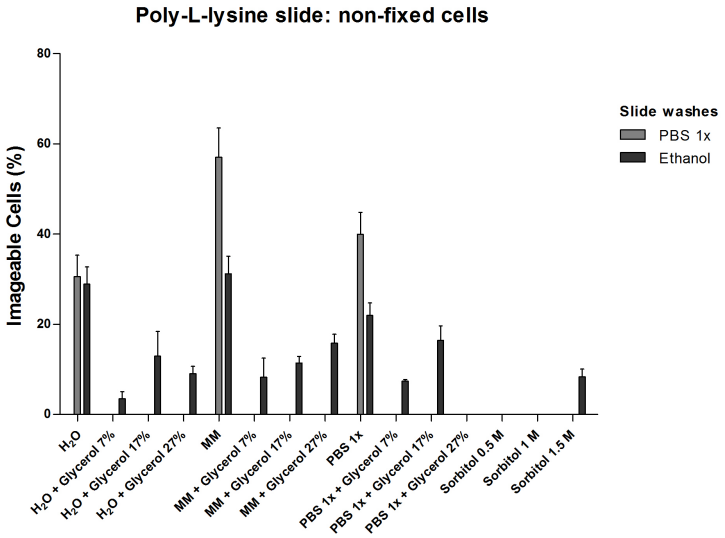

Figure A.2: **Percentage of imageable cells printed on poly-L-lysine coated slides.** Cells were not fixed prior to printing. Data represent the mean ± s. d. of 3 independent spots. The medians were calculated using the Kruskal-Wallis test with CI 95%.

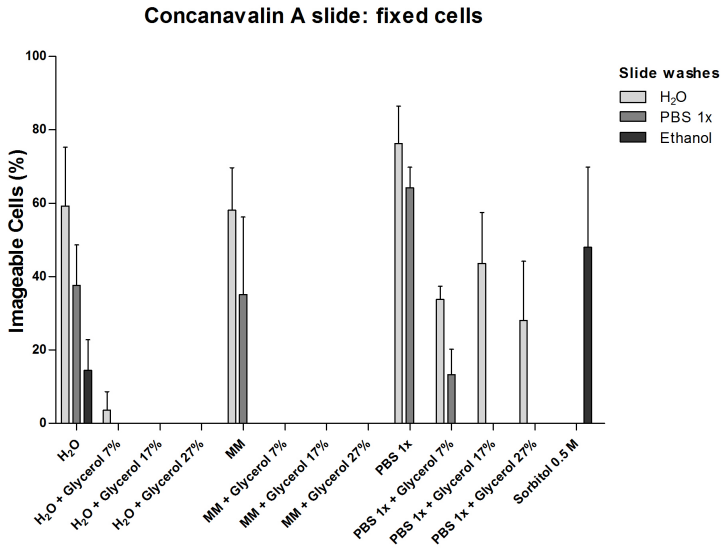

Figure A.3: **Percentage of imageable cells printed on concanavalin-A coated slides.** Cells were fixed prior to printing. Data represent the mean ± s. d. of 3 independent spots. The medians were calculated using the Kruskal-Wallis test with CI 95%.

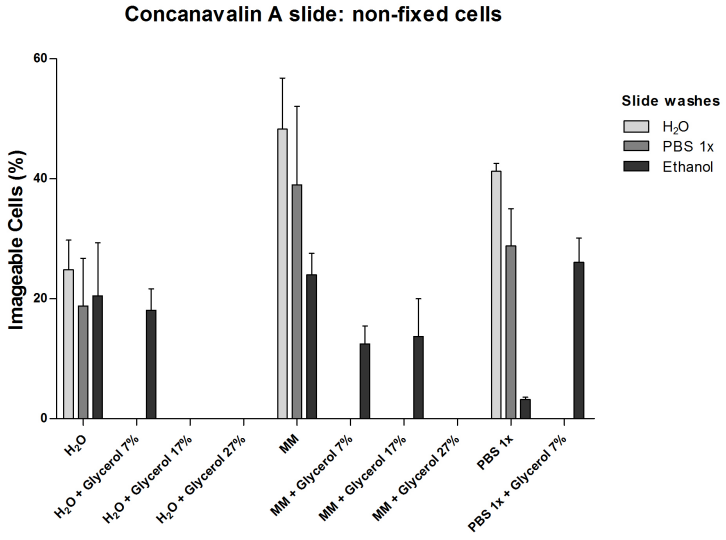

Figure A.4: **Percentage of imageable cells printed on concanavalin-A glass slides.** Cells were not fixed prior to printing. Data represent the mean ± s. d. of 3 independent spots. The medians were calculated using the Kruskal-Wallis post Dunn's Multiple Comparison test with CI 95%.

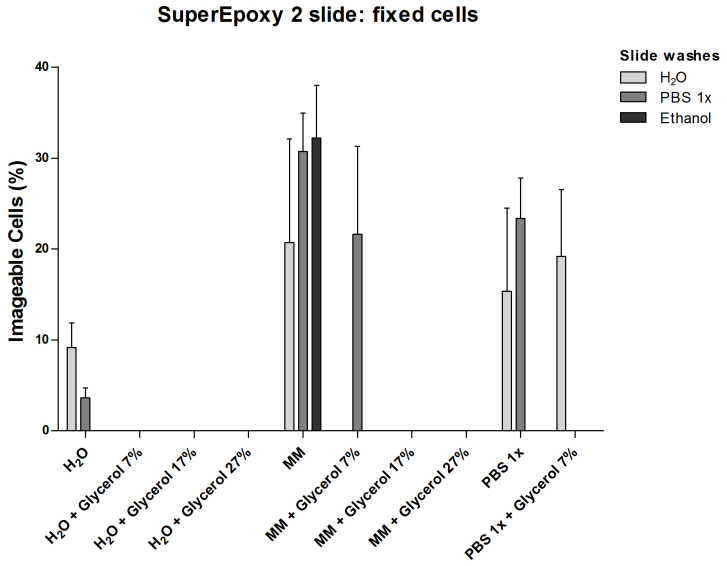

Figure A.5: **Percentage of imageable cells printed on SuperEpoxy 2 coated slides.** Cells were fixed prior to printing. Data represent the mean ± s. d. of 3 independent spots. The medians were calculated using the Kruskal-Wallis test with CI 95%.

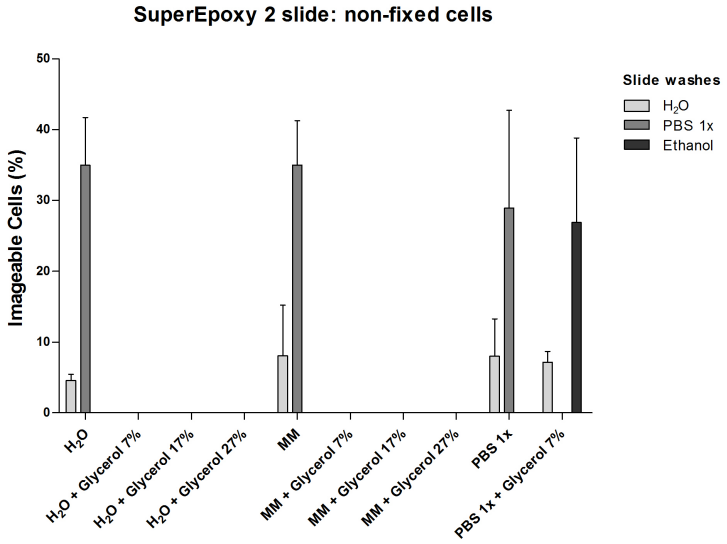

Figure A.6: **Percentage of imageable cells printed on SuperEpoxy 2 glass slides.** Cells were not fixed prior to printing. Data represent the mean ± s. d. of 3 independent spots. The medians were calculated using the Kruskal-Wallis test with CI 95%.

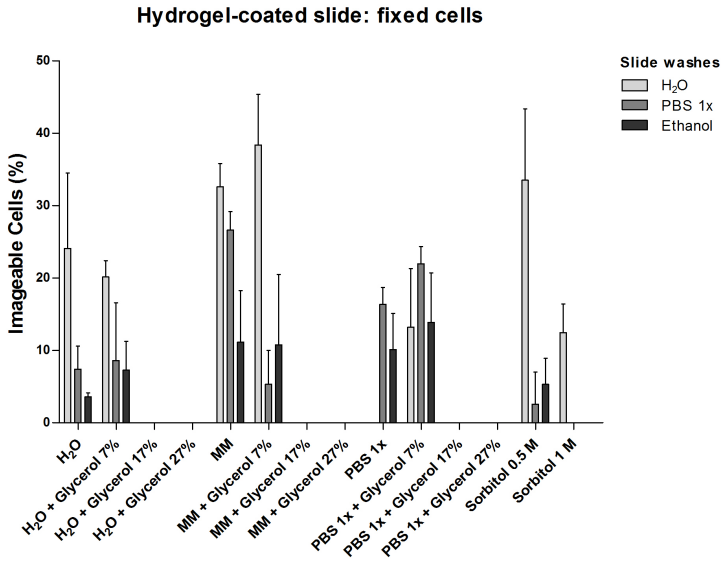

Figure A.7: **Percentage of imageable cells printed on Hydrogel-coated slides.** Cells were fixed prior to printing. Data represent the mean ± s. d. of 3 independent spots. The medians were calculated using the Kruskal-Wallis post Dunn's Multiple Comparison test with CI 95%.

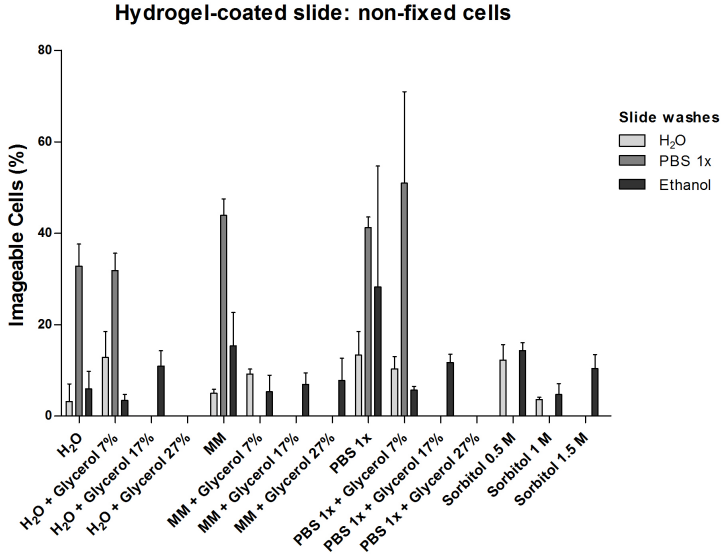

Figure A.8: **Percentage of imageable cells printed on Hydrogel glass slides.** Cells were not fixed prior to printing. Data represent the mean ± s. d. of 3 independent spots. The medians were calculated using the Kruskal-Wallis post Dunn's Multiple Comparison test with CI 95%.

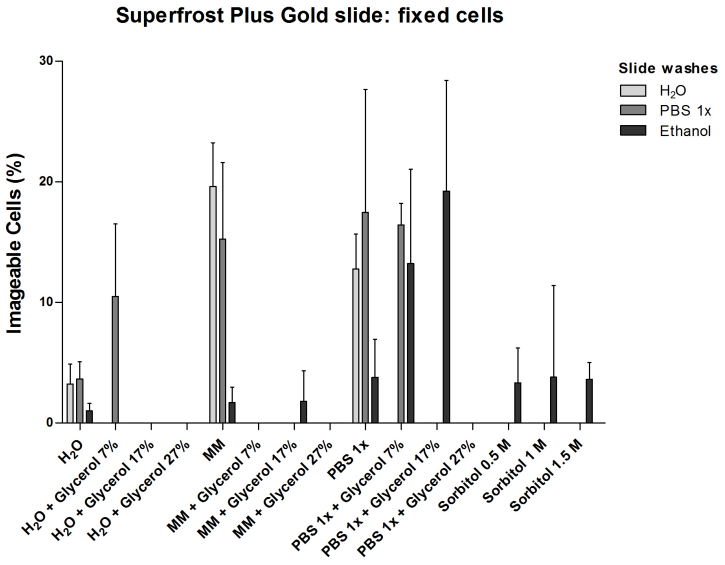

Figure A.9: **Percentage of imageable cells printed on Superfrost Plus Gold slides.** Cells were fixed prior printing. Data represent the mean ± s. d. of 3 independent spots. The medians were calculated using the Kruskal-Wallis test with CI 95%.

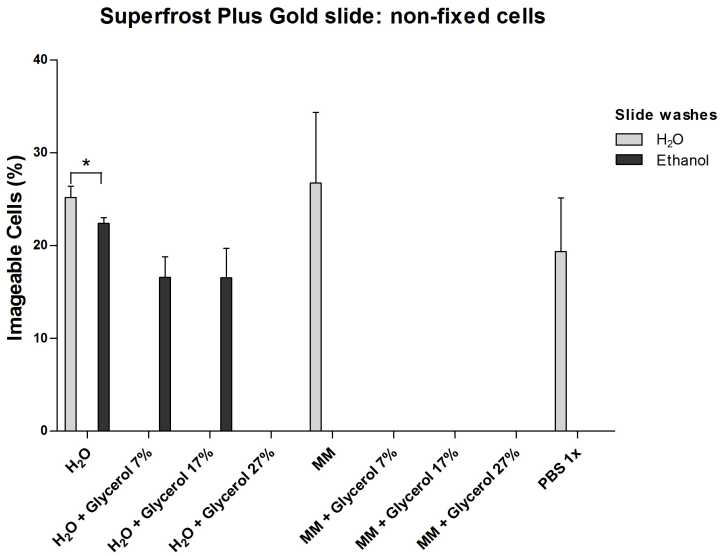

Figure A.10: **Percentage of imageable cells printed on Superfrost Plus Gold glass slides.** Cells were not fixed prior printing. Data represent the mean ± s. d. of 3 independent spots (*p<0.05 Kruskal-Wallis post Dunn's Multiple Comparison test with CI 95%). The medians were calculated using the Kruskal-Wallis post Dunn's Multiple Comparison test with CI 95%.

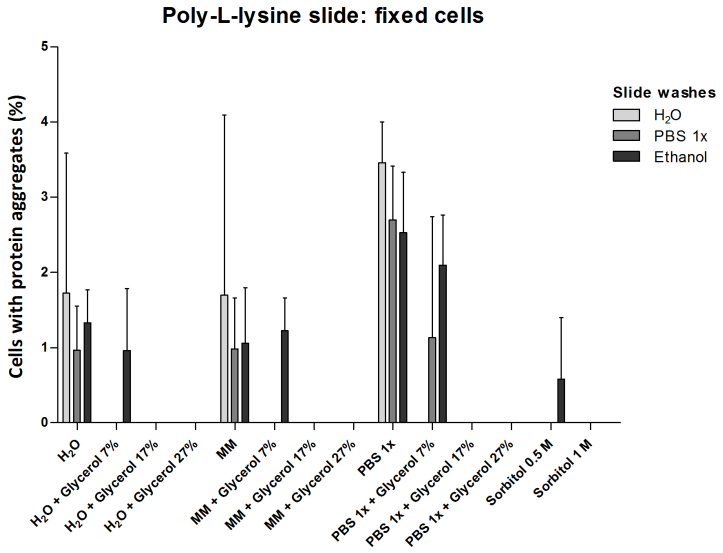

Figure A.11: **Percentage of cells with protein aggregates (localized Hsp104-GFP fluorescence foci) printed on poly-L-lysine coated slides.** Cells were fixed with 3.7% prior to printing. Data represent the mean ± s. d. of 3 independent spots. The medians were calculated using the Kruskal-Wallis post Dunn's Multiple Comparison test with CI 95%.

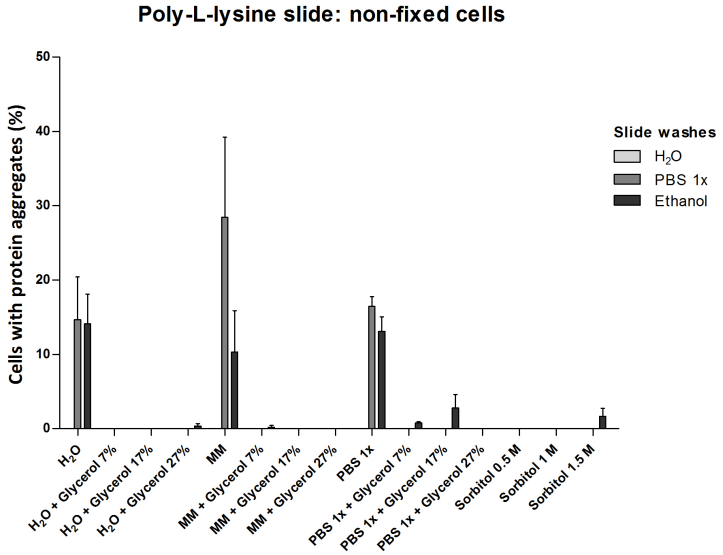

Figure A.12: **Percentage of cells with protein aggregates (localized Hsp104-GFP fluorescence foci) printed on poly-L-lysine coated slides.** Cells were not fixed prior to printing. Data represent the mean ± s. d. of 3 independent spots. The medians were calculated using the Kruskal-Wallis test with CI 95%.

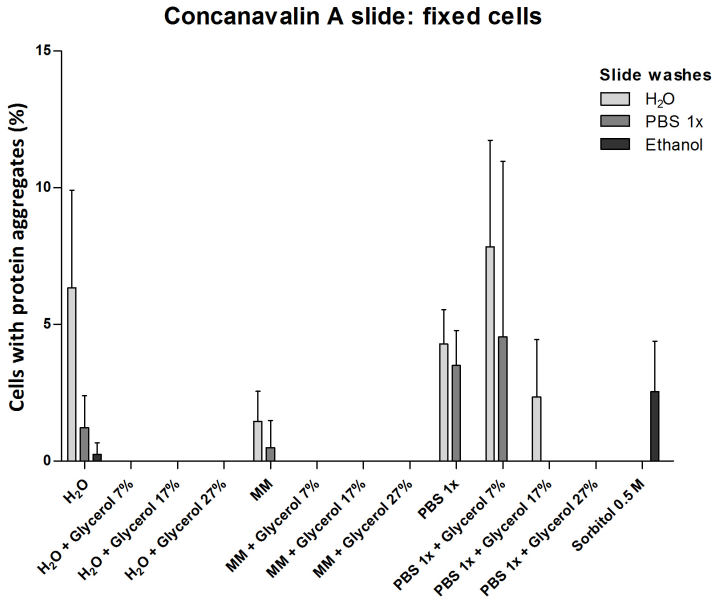

Figure A.13: **Percentage of cells with protein aggregates (localized Hsp104-GFP fluorescence foci) printed on concanavalin-A coated slides.** Cells were fixed prior to printing. Data represent the mean ± s. d. of 3 independent spots. The medians were calculated using the Kruskal-Wallis test with CI 95%.

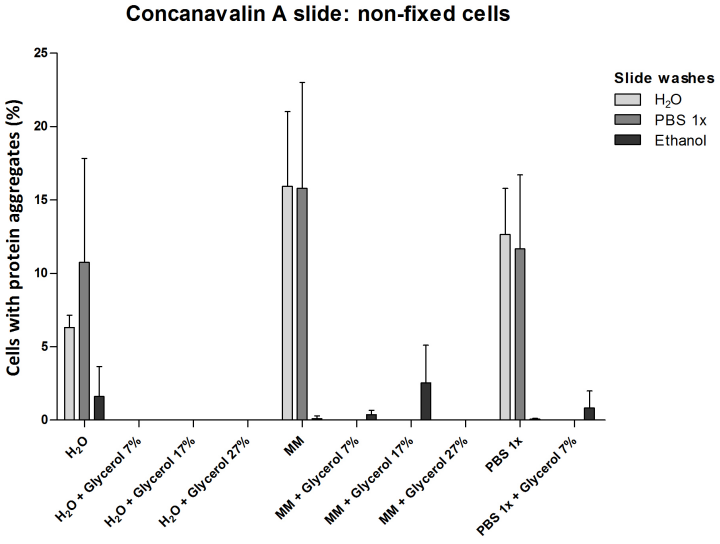

Figure A.14: **Percentage of cells with protein aggregates (localized Hsp104-GFP fluorescence foci) printed on concanavalin-A glass slides.** Cells were not fixed prior to printing. Data represent the mean ± s. d. of 3 independent spots. The medians were calculated using the Kruskal-Wallis post Dunn's Multiple Comparison test with CI 95%.

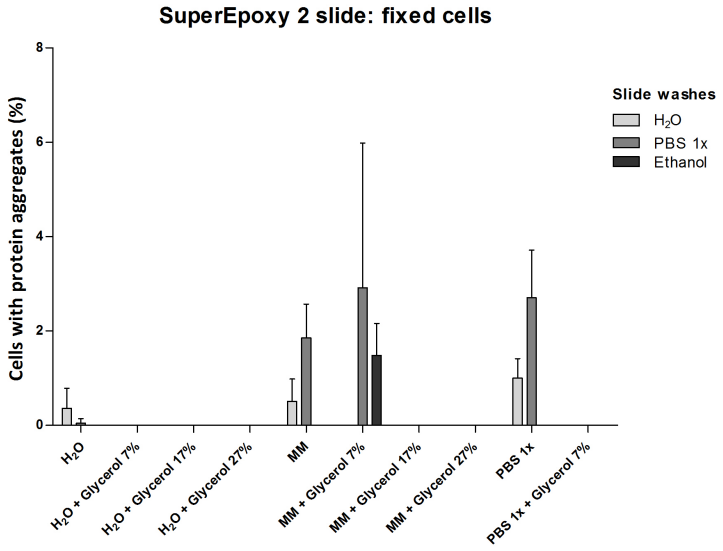

Figure A.15: **Percentage of cells with protein aggregates (localized Hsp104-GFP fluorescence foci) printed on SuperEpoxy 2 coated slides.** Cells were fixed prior to printing. Data represent the mean ± s. d. of 3 independent spots. The medians were calculated using the Kruskal-Wallis test with CI 95%.

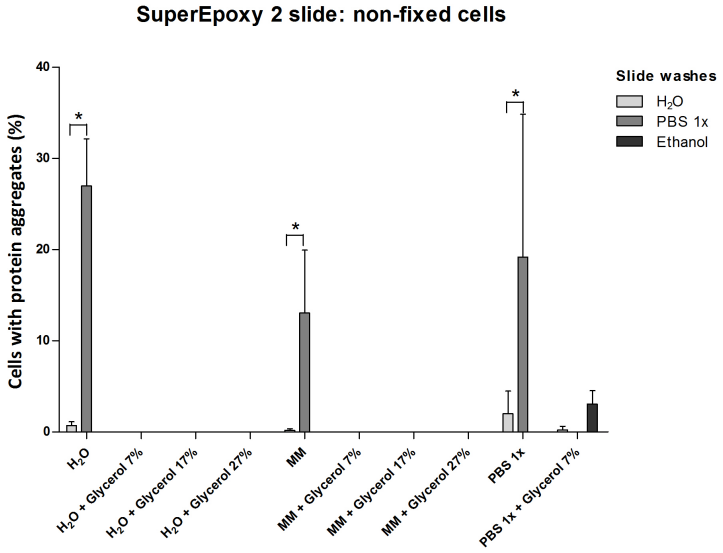

Figure A.16: **Percentage of cells with protein aggregates (localized Hsp104-GFP fluorescence foci) printed on SuperEpoxy 2 glass slides.** Cells were not fixed prior to printing. Data represent the mean ± s. d. of 3 independent spots (*p<0.05 Kruskal-Wallis post Dunn's Multiple Comparison test with CI 95%). The medians were calculated using the Kruskal-Wallis post Dunn's Multiple Comparison test with CI 95%.

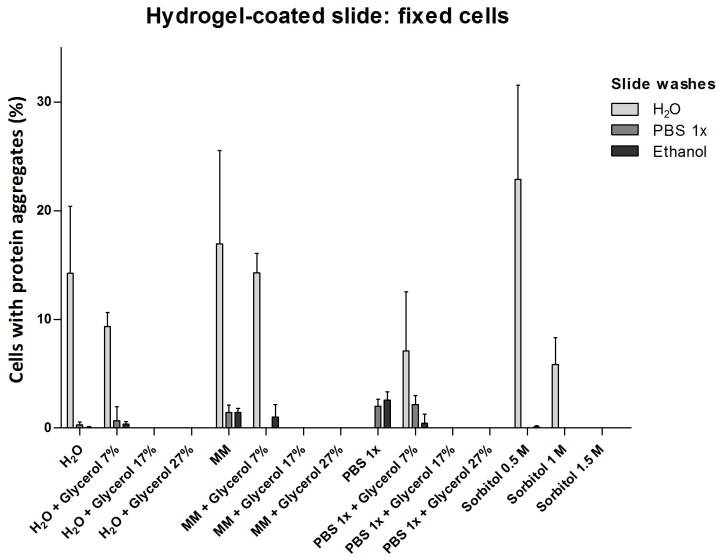

Figure A.17: **Percentage of cells with protein aggregates (localized Hsp104-GFP fluorescence foci) printed on Hydrogel-coated slides.** Cells were fixed prior to printing. Data represent the mean ± s. d. of 3 independent spots. The medians were calculated using the Kruskal-Wallis post Dunn's Multiple Comparison test with CI 95%.

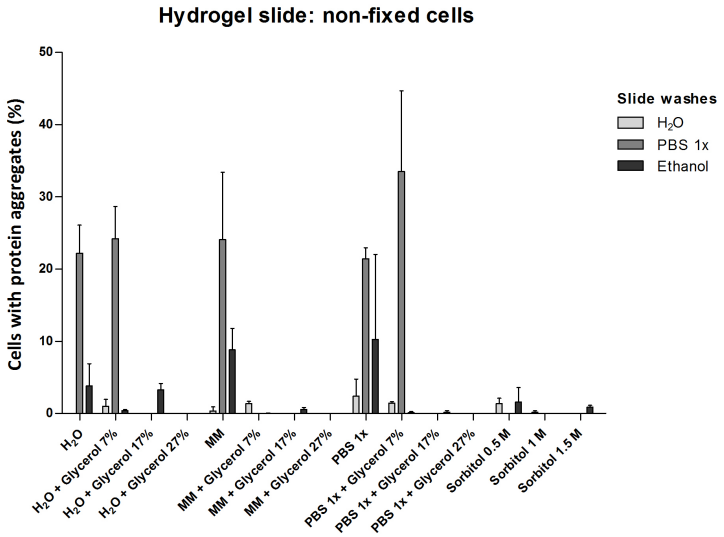

Figure A.18: **Percentage of cells with protein aggregates (localized Hsp104-GFP fluorescence foci) printed on Hydrogel glass slides.** Cells were not fixed prior to printing. Data represent the mean ± s. d. of 3 independent spots. The medians were calculated using the Kruskal-Wallis post Dunn's Multiple Comparison test with CI 95%.

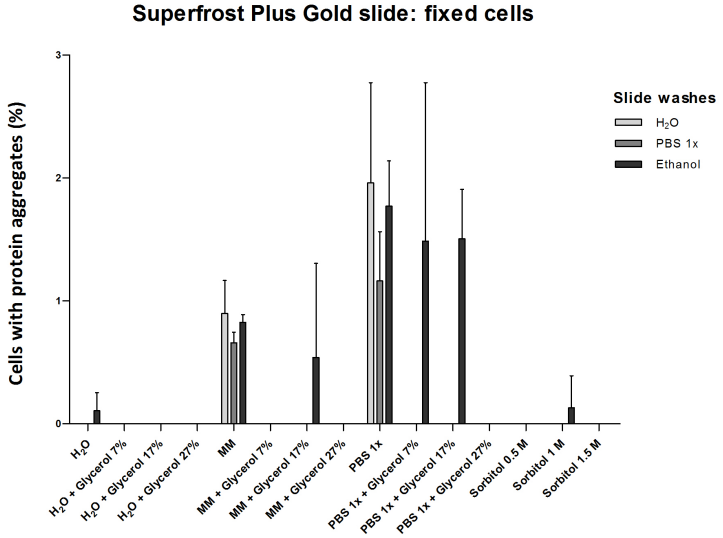

Figure A.19: **Percentage of cells with protein aggregates (localized Hsp104-GFP fluorescence foci) printed on Superfrost Plus Gold slides.** Cells were fixed prior printing. Data represent the mean ± s. d. of 3 independent spots. The medians were calculated using the Kruskal-Wallis test with CI 95%.

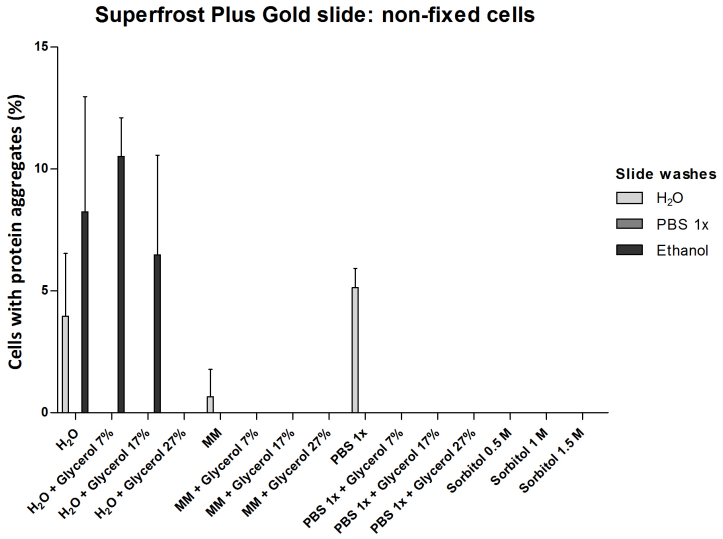

Figure A.20: **Percentage of cells with protein aggregates (localized Hsp104-GFP fluorescence foci) printed on Superfrost Plus Gold slides.** Cells were not fixed prior printing. Data represent the mean ± s. d. of 3 independent spots. The medians were calculated using the Kruskal-Wallis test with CI 95%.

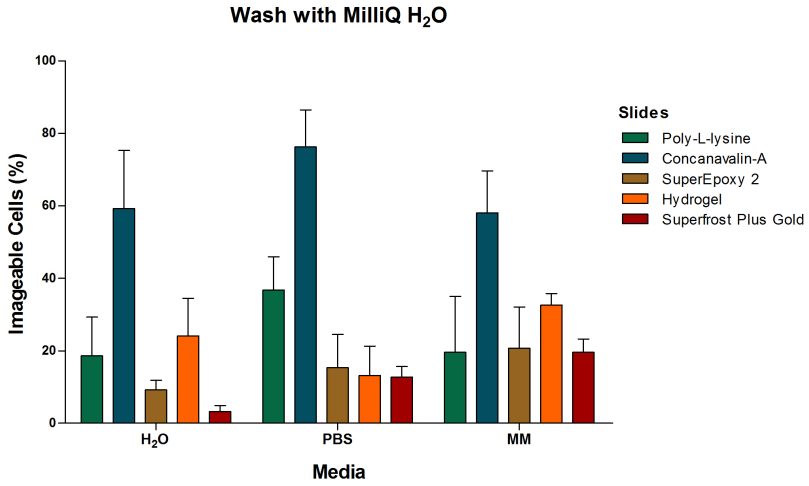

Figure A.21: **Effect of slide washing with MilliQ water on imaging of fixed yeast cells.** Data represent the mean ± s. d. of 3 independent spots. The medians vary significantly (Kruskal-Wallis test with CI 95%).

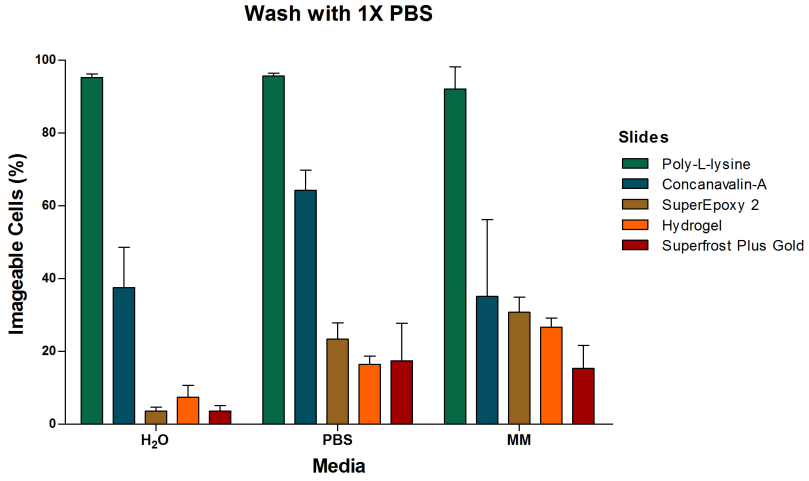

Figure A.22: **Effect of slide washing with 1X PBS on imaging of fixed yeast cells.** Data represent the mean ± s. d. of 3 independent spots. The medians vary significantly (Kruskal-Wallis test with CI 95%).

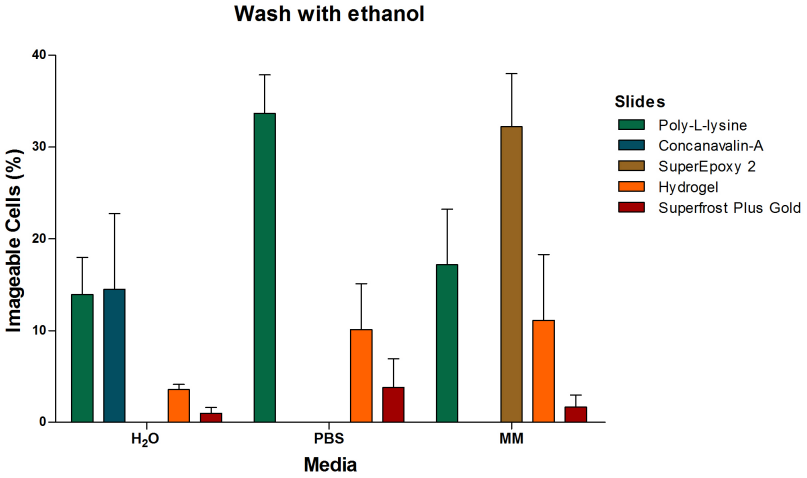

Figure A.23: **Effect of slide washing with ethanol on imaging of fixed yeast cells.** Data represent the mean ± s. d. of 3 independent spots. The medians vary significantly (Kruskal-Wallis test with CI 95%).

Appendix B

Proteotoxic stress extra data

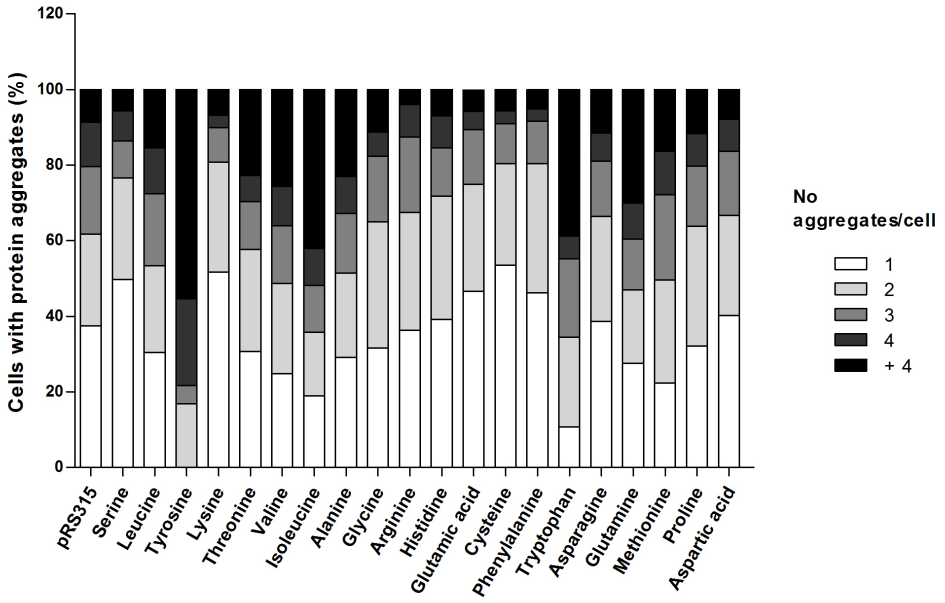

Figure B.1: **Number of protein aggregates per cell.** Yeast cells containing localized Hsp104-GFP fluorescence foci were counted and differentiated according to the number of localized Hsp104-GFP fluorescence foci per cell. Results are expressed as the percentage of positive cells (with Hsp104-GFP foci) relative to the total number of cells with protein aggregates per spot. Data represent the mean of three independent spots from arrays.

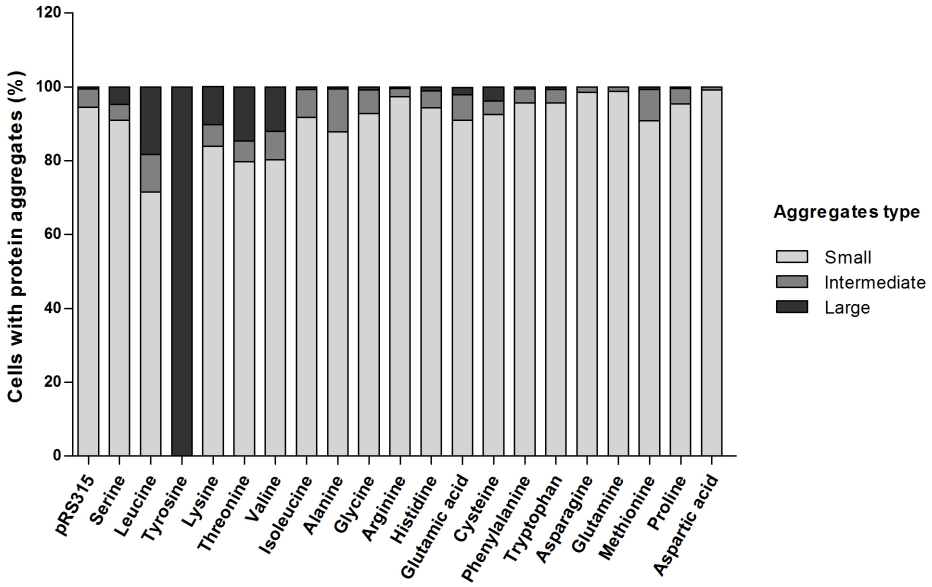

Figure B.2: **Misreading produces different types of aggregates.** Yeast cells containing localized Hsp104-GFP fluorescence foci were counted and differentiated according to the size of localized Hsp104-GFP fluorescence foci per cell. Results are expressed as the percentage of positive cells (with Hsp104-GFP foci) relative the total number of cells with protein aggregates per array spot. Data represent the mean of three independent spots from arrays.

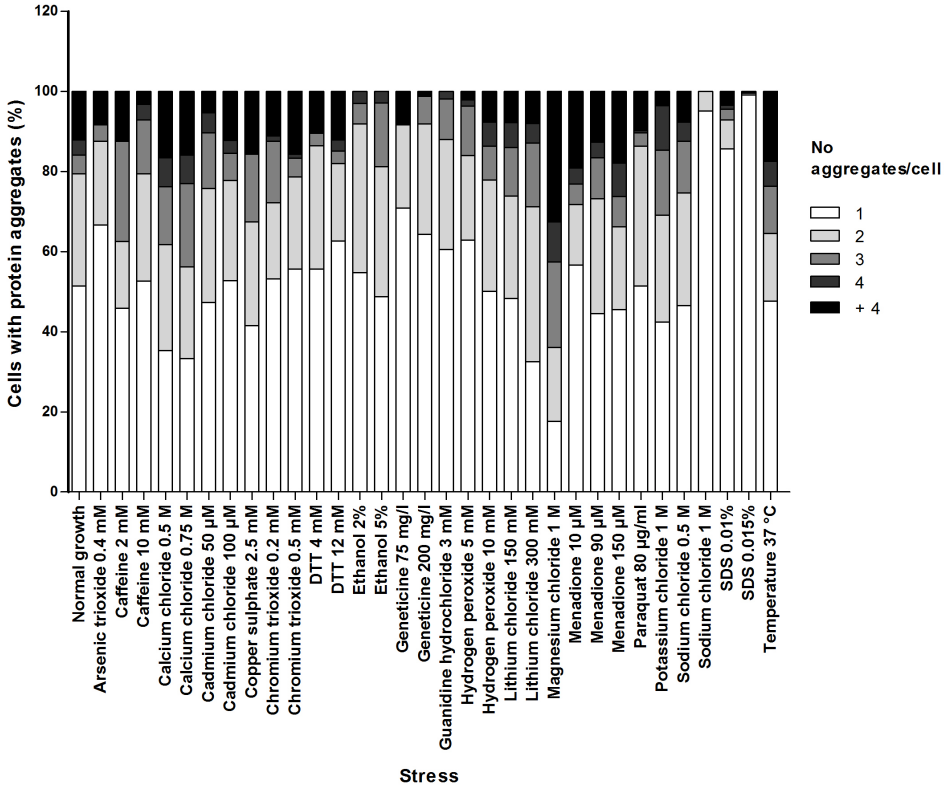

Figure B.3: **Number of protein aggregates per cell exposed to chemical stressors.** Yeast cells containing localized Hsp104-GFP fluorescence foci were counted and differentiated according to the number of localized Hsp104-GFP fluorescence foci per cell. Results are expressed as the percentage of positive cells (with Hsp104-GFP foci) relative to the total number of cells with protein aggregates per spot. Data represent the mean of three independent clones, obtained from three different array spots.

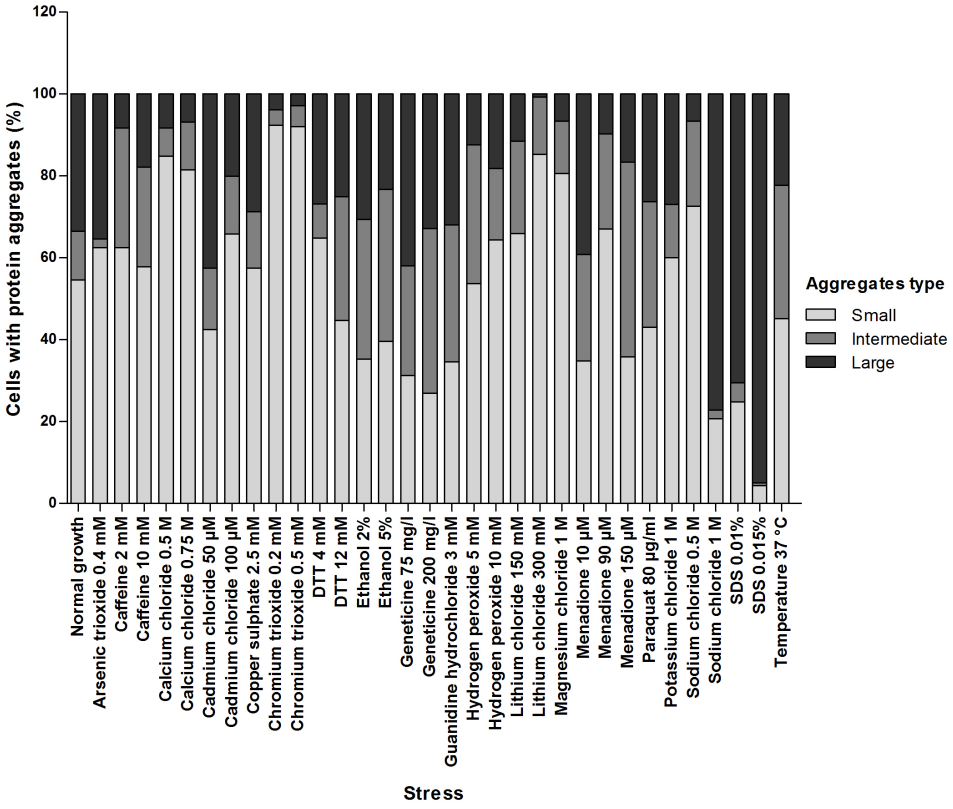

Figure B.4: **Different chemical stressors induce formation of different types of aggregates in yeast cells.** Yeast cells containing localized Hsp104-GFP fluorescence foci were counted and differentiated according to the size of localized Hsp104-GFP fluorescence foci. Results are expressed as the percentage of positive cells (with Hsp104-GFP foci) relative to the total number of cells with protein aggregates per array spot. Data represent the mean of three independent clones, obtained from three different array spots.